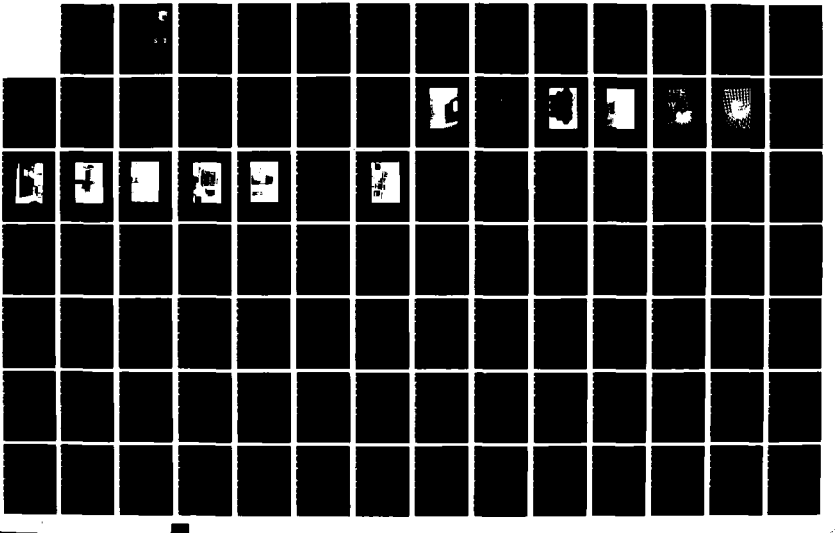
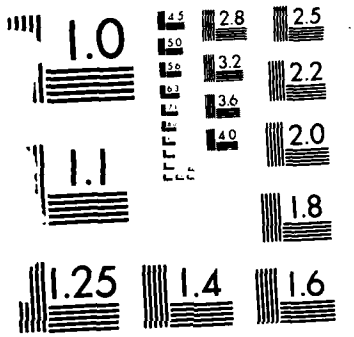
AD-A165 275 EXPERIMENTAL VERIFICATION OF THE FAR FIELD CRITERIA FOR AFWAL'S COMPACT R (U) AIR FORCE WRIGHT AERONAUTICAL LABS WRIGHT-PATTERSON AFB OH H M CHIZEVER ET AL. 1/2

UNCLASSIFIED OCT 85 AFWAL-TR-85-1080 F/G 20/14 NL





MICROCOPY RESOLUTION TEST CHART
NATIONAL BUREAU OF STANDARDS 1963-A

AFWAL-TR-85-1080

(2)

AD-A165 275



EXPERIMENTAL VERIFICATION OF THE FAR FIELD CRITERIA FOR AFWAL'S COMPACT RANGE IN THE QUIET ZONE REGION (8-26 GHZ)

Hirsch M. Chizever
Brian M. Kent, Ph.D.

Passive ECM Branch
Electronic Warfare Division

DTIC
ELECTE
MAR 1 8 1986
S D
D

October 1985

Interim Report for Period June 1983 - July 1984

DTIC FILE COPY

Approved for public release, distribution unlimited.

AVIONICS LABORATORY
AIR FORCE WRIGHT AERONAUTICAL LABORATORIES
AIR FORCE SYSTEMS COMMAND
WRIGHT-PATTERSON AIR FORCE BASE, OHIO 45433

86 3 18 099

NOTICE

When Government drawings, specifications, or other data are used for any purpose other than in connection with a definitely related Government procurement operation, the United States Government thereby incurs no responsibility nor any obligation whatsoever; and the fact that the government may have formulated, furnished, or in any way supplied the said drawings, specifications, or other data, is not to be regarded by implication or otherwise as in any manner licensing the holder or any other person or corporation, or conveying any rights or permission to manufacture use, or sell any patented invention that may in any way be related thereto.

This report has been reviewed by the Office of Public Affairs (ASD/PA) and is releasable to the National Technical Information Service (NTIS). At NTIS, it will be available to the general public, including foreign nations.

This technical report has been reviewed and is approved for publication.

Brian M. Kent

BRIAN M. KENT, Ph.D., Elec Engr
Passive ECM Branch, EW Division
Avionics Laboratory

Hirsch M. Chizever

Hirsch M. Chizever, Elec Engr
Passive ECM Branch, EW Division
Avionics Laboratory

FOR THE COMMANDER

Dave Niebauer

DAVID J. NIEBAUER, Colonel, USAF
Chief, Electronic Warfare Division
Avionics Laboratory

William F. Bahret

WILLIAM F. BAHRET, Chief
Passive ECM Br, EW Division
Avionics Laboratory

If your address has changed, if you wish to be removed from our mailing list, or if the addressee is no longer employed by your organization please notify AFWAL/AAWP-3 *W-PAFB, OH 45433 to help us maintain a current mailing list.*

Copies of this report should not be returned unless return is required by security considerations, contractual obligations, or notice on a specific document.

DISCLAIMER NOTICE

THIS DOCUMENT IS BEST QUALITY PRACTICABLE. THE COPY FURNISHED TO DTIC CONTAINED A SIGNIFICANT NUMBER OF PAGES WHICH DO NOT REPRODUCE LEGIBLY.

UNCLASSIFIED

SECURITY CLASSIFICATION OF THIS PAGE

REPORT DOCUMENTATION PAGE

1a. REPORT SECURITY CLASSIFICATION UNCLASSIFIED	1b. RESTRICTIVE MARKINGS
2a. SECURITY CLASSIFICATION AUTHORITY	3. DISTRIBUTION/AVAILABILITY OF REPORT Approved for public release; distribution unlimited.
2b. DECLASSIFICATION/DOWNGRADING SCHEDULE	
4. PERFORMING ORGANIZATION REPORT NUMBER(S) AFWAL-TR-85-1080	5. MONITORING ORGANIZATION REPORT NUMBER(S)
6a. NAME OF PERFORMING ORGANIZATION U.S. AIR FORCE AVIONICS LABORATORY 6b. OFFICE SYMBOL (If applicable) AFWAL/AAWP-3	7a. NAME OF MONITORING ORGANIZATION
6c. ADDRESS (City, State and ZIP Code) AFWAL/AAWP-3 Wright-Patterson AFB OH 45433-6543	7b. ADDRESS (City, State and ZIP Code)
8a. NAME OF FUNDING/SPONSORING ORGANIZATION 8b. OFFICE SYMBOL (If applicable)	9. PROCUREMENT INSTRUMENT IDENTIFICATION NUMBER
8c. ADDRESS (City, State and ZIP Code)	10. SOURCE OF FUNDING NOS. PROGRAM ELEMENT NO.: 62204F PROJECT NO.: 7633 TASK NO.: 13 WORK UNIT NO.: 09
11. TITLE (Include Security Classification) (SEE BACK)	
12. PERSONAL AUTHOR(S) Hirsch M. Chizever and Brian M. Kent	
13a. TYPE OF REPORT Interim	13b. TIME COVERED FROM Jun 83 TO Jul 84
14. DATE OF REPORT (Yr., Mo., Day) 85 October	15. PAGE COUNT 66
16. SUPPLEMENTARY NOTATION	

17 COSATI CODES		
FIELD	GROUP	SUB GR
17	04	
20	03	

18. SUBJECT TERMS (Continue on reverse if necessary and identify by block number)

Radar cross section measurement techniques, Compact range, Aperture field probe

19. ABSTRACT (Continue on reverse if necessary and identify by block number)

In past years, the radiation and scattering properties of aerospace components have been tested on large outdoor measurement ranges. The distance between the transmitting and receiving antenna (for radiation measurements) or target (for scattering measurements) is normally dictated by the far field criteria. Recent interest in the millimeter wavelength region and the need to measure larger targets requires longer distances between source and target to satisfy the far field condition.

This report documents an alternative method of creating a "space limited" far field environment for radiation and scattering measurements using the compact range approach. However, some questions concerning the planarity of the aperture field have been raised by the scientific community. Field probe data is presented here which unquestionably verifies the planarity of the aperture field. This data

(continued)

20. DISTRIBUTION/AVAILABILITY OF ABSTRACT UNCLASSIFIED/UNLIMITED ☒ SAME AS RPT. ☐ DTIC USERS ☐	21. ABSTRACT SECURITY CLASSIFICATION UNCLASSIFIED
22a. NAME OF RESPONSIBLE INDIVIDUAL Dr Brian M. Kent	22b. TELEPHONE NUMBER (Include Area Code) 513-255-5076 22c. OFFICE SYMBOL AFWAL/AAWP-3

DD FORM 1473, 83 APR EDITION OF 1 JAN 73 IS OBSOLETE.

UNCLASSIFIED

SECURITY CLASSIFICATION OF THIS PAGE

19. Continued

demonstrates that the amplitude and phase distribution across the measurement zone (5 ft. X 5 ft.) meets or exceeds the far field criteria, (+/- 0.5 dB amplitude taper and +/- 22.5 degrees phase taper) from 8.2 to 26.0 GHz.

Block II. (Title) "Experimental Verification of the Far Field Criteria for AFWAL'S Compact Range in the Quiet Zone Region (8-26 GHz) (U)"

FOREWORD

This interim report describes a series of field probe measurements made on AFWAL's Compact Radar Cross Section Range located in Building 821. These measurements were performed to verify that the plane wave (far field) criteria is met in the aperture of the reflector. These measurements are an integral part of evaluating the compact RCS measurement technique.

The research was performed from June 1983 to July 1984, in support of AFWAL Work Unit 76331309. This work was performed by Dr. Brian M. Kent and Mr. Hirsch M. Chizever of the Passive ECM Branch, Electronic Warfare Division, Avionics Laboratory, Air Force Wright Aeronautical Laboratories, Wright-Patterson Air Force Base, Ohio 45433.

The authors wish to extend their sincere gratitude to the following persons who assisted in the completion of this research effort. First, we would like to thank co-workers Dr. Robert Puskar, Mr. James Kelly, and Mr. James Common who performed measurements in support of this effort. Also, we would like to recognize Dr. Walter Burnside and Dr. Leon Peters of The Ohio State Electro-Science Laboratory who supplied many helpful suggestions.

Second, a special thanks is also extended to our secretary Ms George Ann Thompson who assisted in the completion of this report.

QUALITY INSPECTED 3

Accesion For
NTIS CRA&I
DTIC TAB
Unannounced
Justification
By
Distribution /
Availability Codes
Dist | Avail a d/or Special
A-1 | 23

TABLE OF CONTENTS

SECTION		PAGE
I	INTRODUCTION	1
II	MEETING THE FAR FIELD CRITERIA: HARDWARE AND METHODS	3
III	THE TEST MATRIX	19
IV	CONCLUSIONS	42
	REFERENCES	43
	APPENDIX COMPLETE TEST MATRIX OF FIELD PROBE MEASUREMENTS	45

LIST OF ILLUSTRATIONS

FIGURE		PAGE
1	Planewave Approximation to Diverging Spherical Wavefront (Far Field)	2
2	Schematic Diagram of the Compact Radar Cross Section Measurement Range	4
3	Photograph of the Compact Radar Cross Section Measurement Range	5
4	Section of Paraboloid Shown in Original Radio Telescope	6
5	Compact Range Reflector Prior to Installation of Lower Edge Treatment	7
6	Compact Range Reflector After Installation of Lower Edge Treatment	8
7	X-Band (8.2 - 12.4 GHz) Feed Antenna Positioner	9
8	Ku (12.4 - 18.0 GHz) Band Dual Feed Antenna Positioner	10
9	Microwave Synthesizer Used During Experiments (Lower Left)	12
10	Near Field Two Axis Probe Scanner	13
11	Field Probes Used During Experiments (Horn Probe - Left) (Waveguide - Right)	14
12	Computer Controlled Motor Positioners	15
13	Mainframe Computer Used to Control Motor Positioners and Store Field Probe Amplitude and Phase Information	16
14	Principle Plane Measurements as Seen by the Field Probe	17
15	Microwave Receiver Used During Experiments	18
16	X-Plane Amplitude and Phase Field Proble Plot Taken at 12.0 GHz, V-Polarization, Using the Horn Probe	22
17	Y-Plane Amplitude and Phase Field Probe Plot Taken at 12.0 GHz, V-Polarization, Using the Horn Probe	23

LIST OF ILLUSTRATIONS

FIGURE		PAGE
18	(Top) Y-Plane Amplitude Field Probe Plot, 13.0 GHz, V-Polarization (Bottom) Full "Quiet Zone" Y-Plane Field Probe Plot, 13.0 GHz, V-Polarization (Untreated Bottom Edge)	24
19	Unsymmetrical Amplitude Distribution Due to Incorrect Feed Antenna Positioning (Azimuth or Elevation)	25
20	Slanted Phase Profile Due to Incorrect Feed Antenna Positioning	26
21	Curved Phase Profile Due to Incorrect Feed Antenna Positioning	28
22	Radiation Patterns for the Selected Horn Probe (Right) and Waveguide Probe (Left)	29
23	X-Plane Amplitude and Phase Field Probe Plot Taken at 12.0 GHz, V-Polarization, Using the Waveguide Probe	30
24	Y-Plane Amplitude and Phase Field Probe Plot Taken at 12.0 GHz, V-Polarization, Using the Waveguide Probe	31
25	3D Amplitude Field Probe Plot Taken at 12.0 GHz, V-Polarization, Using the Horn Probe (X - Y Layover at Bottom)	32
26	3D Phase Field Probe Plot Taken at 12.0 GHz, V-Polarization, Using the Horn Probe (X - Y Layover at Bottom)	33
27	X-Plane Amplitude and Phase Field Probe Plot Taken at 8.2 GHz, V-Polarization, Using the Horn Probe	35
28	Y-Plane Amplitude and Phase Field Probe Plot Taken at 8.2 GHz, V-Polarization, Using the Horn Probe	36
29	3D X-Plane Phase Field Probe Plot Taken at 18.0 GHz, H-Polarization, Using the Horn Probe (Note Phase Discontinuities)	37
30	Side View of Elliptical Curved Edge Treatments for the OSU and NASA Compact Range Reflector Antenna	38
31	Amplitude Field Probe Taken Across an Exposed Reflector Rim (Measurements are Compared to Moment Method Calculations at 10. GHz)	39
32	Amplitude Field Probe Taken Across a Modified Curved Edge Treatment (Measurements Compared to Moment Method Calculations at 10. GHz)	40

LIST OF ILLUSTRATIONS (Cont'd)

FIGURE		PAGE
A.1	X-Plane Amplitude and Phase Field Probe Plot Taken at 8.2 GHz, V-Polarization, Using the Horn Probe	46
A.2	Y-Plane Amplitude and Phase Field Probe Plot Taken at 8.2 GHz, V-Polarization, Using the Horn Probe	47
A.3	X-Plane Amplitude and Phase Field Probe Plot Taken at 8.2 GHz, V-Polarization, Using the Waveguide Probe	48
A.4	Y-Plane Amplitude and Phase Field Probe Plot Taken at 8.2 GHz, V-Polarization, Using the Waveguide Probe	49
A.5	3D X-Plane Amplitude and Phase Field Probe Plot Taken at 8.2 GHz, V-Polarization, Using the Horn Probe	50
A.6	3D Y-Plane Amplitude and Phase Field Probe Plot Taken at 8.2 GHz, V-Polarization, Using the Horn Probe	51
A.7	X-Plane Amplitude and Phase Field Probe Plot Taken at 8.2 GHz, H-Polarization, Using the Horn Probe	52
A.8	Y-Plane Amplitude and Phase Field Probe Plot Taken at 8.2 GHz, H-Polarization, Using the Horn Probe	53
A.9	X-Plane Amplitude and Phase Field Probe Plot Taken at 8.2 GHz, H-Polarization, Using the Waveguide Probe	54
A.10	Y-Plane Amplitude and Phase Field Probe Plot Taken at 8.2 GHz, H-Polarization, Using the Waveguide Probe	55
A.11	3D X-Plane Amplitude and Phase Field Probe Plot Taken at 8.2 GHz, H-Polarization, Using the Horn Probe	56
A.12	3D Y-Plane Amplitude and Phase Field Probe Plot Taken at 8.2 GHz, H-Polarization, Using the Horn Probe	57
A.13	X-Plane Amplitude and Phase Field Probe Plot Taken at 12.0 GHz, V-Polarization, Using the Horn Probe	58
A.14	Y-Plane Amplitude and Phase Field Probe Plot Taken at 12.0 GHz, V-Polarization, Using the Horn Probe	59
A.15	X-Plane Amplitude and Phase Field Probe Plot Taken at 12.0 GHz, V-Polarization, Using the Waveguide Probe	60
A.16	Y-Plane Amplitude and Phase Field Probe Plot Taken at 12.0 GHz, V-Polarization, Using the Waveguide Probe	61

LIST OF ILLUSTRATIONS (Cont'd)

FIGURE		PAGE
A.17	3D X-Plane Amplitude and Phase Field Probe Plot Taken at 12.0 GHz, V-Polarization, Using the Horn Probe	62
A.18	3D Y-Plane Amplitude and Phase Field Probe Plot Taken at 12.0 GHz, V-Polarization, Using the Horn Probe	63
A.19	X-Plane Amplitude and Phase Field probe Plot Taken at 12.0 GHz, H-Polarization, Using the Horn Probe	64
A.20	Y-Plane Amplitude and Phase Field Probe Plot Taken at 12.0 GHz, H-Polarization, Using the Horn Probe	65
A.21	X-Plane Amplitude and Phase Field probe Plot Taken at 12.0 GHz, H-Polarization, Using the Waveguide Probe	66
A.22	Y-Plane Amplitude and Phase Field Probe Plot Taken at 12.0 GHz, H-Polarization, Using the Waveguide Probe	67
A.23	3D X-Plane Amplitude and Phase Field Probe Plot Taken at 12.0 GHz, H-Polarization, Using the Horn Probe	68
A.24	3D Y-Plane Amplitude and Phase Field Probe Plot Taken at 12.0 GHz, Polarization, Using the Horn Probe	69
A.25	X-Plane Amplitude and Phase Field Probe Plot Taken at 12.4 GHz, V-Polarization, Using the Horn Probe	70
A.26	Y-Plane Amplitude and Phase Field Probe Plot Taken at 12.4 GHz, V-Polarization, Using the Horn Probe	71
A.27	X-Plane Amplitude and Phase Field Probe Plot Taken at 12.4 GHz, V-Polarization, Using the Waveguide Probe	72
A.28	Y-Plane Amplitude and Phase Field Probe Plot Taken at 12.4 GHz, V-Polarization, Using the Waveguide Probe	73
A.29	3D X-Plane Amplitude and Phase Field Probe Plot Taken at 12.4 GHz, V-Polarization, Using the Horn Probe	74
A.30	3D Y-Plane Amplitude and Phase Field Probe Plot Taken at 12.4 GHz, V-Polarization, Using the Horn Probe	75
A.31	X-Plane Amplitude and Phase Field Probe Plot Taken at 12.4 GHz, H-Polarization, Using the Horn Probe	76
A.32	Y-Plane Amplitude and Phase Field Probe Plot Taken at 12.4 GHz, H-Polarization, Using the Horn Probe	77

LIST OF ILLUSTRATIONS (Cont'd)

FIGURE		PAGE
A.33	X-Plane Amplitude and Phase Field Probe Plot Taken at 12.4 GHz, H-Polarization, Using the Waveguide Probe	78
A.34	Y-Plane Amplitude and Phase Field Probe Plot Taken at 12.4 GHz, H-Polarization, Using the Waveguide Probe	79
A.35	3D X-Plane Amplitude and Phase Field Probe Plot Taken at 12.4 GHz, H-Polarization, Using the Horn Probe	80
A.36	3D Y-Plane Amplitude and Phase Field Probe Plot Taken at 12.4 GHz, H-Polarization Using the Horn Probe	81
A.37	X-Plane Amplitude and Phase Field Probe Plot Taken at 18.0 GHz, V-Polarization, Using the Horn Probe	82
A.38	Y-Plane Amplitude and Phase Field Probe Plot taken at 18.0 GHz, V-Polarization, Using the Horn Probe	83
A.39	X-Plane Amplitude and Phase Field Probe Plot Taken at 18.0 GHz, V-Polarization, Using the Waveguide Probe	84
A.40	Y-Plane Amplitude and Phase Field Probe Plot Taken at 18.0 GHz, V-Polarization, Using the Waveguide Probe	85
A.41	3D X-Plane Amplitude and Phase Field probe Plot Taken at 18.0 GHz, V-Polarization, Using the Horn Probe	86
A.42	3D Y-Plane Amplitude and Phase Field Probe Plot Taken at 18.0 GHz, V-Polarization, Using the Horn Probe	87
A.43	X-Plane Amplitude and Phase Field Probe Plot Taken at 18.0 GHz, H-Polarization, Using the Horn Probe	88
A.44	Y-Plane Amplitude and Phase Field Probe Plot Taken at 18.0 GHz, H-Polarization, Using the Horn Probe	89
A.45	X-Plane Amplitude and Phase Field Probe Plot Taken at 18.0 GHz, H-Polarization, Using the Waveguide Probe	90
A.46	Y-Plane Amplitude and Phase Field Probe Plot Taken at 18.0 GHz, H-Polarization, Using the Waveguide Probe	91
A.47	3D X-Plane Amplitude and Phase Field Probe Plot Taken at 18.0 GHz, H-Polarization, Using the Horn Probe	92
A.48	3D Y-Plane Amplitude and Phase Field Probe Plot Taken at 18.0 GHz, H-Polarization, Using the Horn Probe	93

LIST OF ILLUSTRATIONS (Cont'd)

FIGURE		PAGE
A.49	X-Plane Amplitude and Phase Field Probe Plot Taken at 18.0 GHz, H-Polarization, Using the Horn Probe	94
A.50	Y-Plane Amplitude and Phase Field Probe Plot Taken at 18.0 GHz, V-Polarization, Using the Horn Probe	95
A.51	X-Plane Amplitude and Phase Field Probe Plot Taken at 18.0 GHz, V-Polarization,Using the Waveguide Probe	96
A.52	Y-Plane Amplitude and Phase Field Probe Plot Taken at 18.0 GHz, V-Polarization, Using the Waveguide Probe	97
A.53	3D X-Plane Amplitude and Phase Field Probe Plot Taken at 18.0 GHz, V-Polarization, Using the Horn Probe	98
A.54	3D Y-Plane Amplitude and Phase Field Probe Plot Taken at 18.0 GHz, V-Polarization, Using the Horn Probe	99
A.55	X-Plane Amplitude and Phase Field Probe Plot Taken at 18.0 GHz, H-Polarization, Using the Horn Probe	100
A.56	Y-Plane Amplitude and Phase Field Probe Plot Taken at 18.0 GHz, H-Polarization, Using the Horn Probe	101
A.57	X-Plane Amplitude and Phase Field Probe Plot Taken at 18.0 GHz, H-Polarization, Using the Waveguide Probe	102
A.58	Y-Plane Amplitude and Phase Field Probe Plot Taken at 18.0 GHz, H-Polarization, Using the Waveguide Probe	103
A.59	3D X-Plane Amplitude and Phase Field Probe Plot Taken at 18.0 GHz, H-Polarization, Using the Horn Probe	104
A.60	3D X-Plane Amplitude and Phase Field Probe Plot Taken at 18.0 GHz, H-Polarization, Using the Horn Probe	105
A.61	X-Plane Amplitude and Phase Field Probe Plot Taken at 26.0 GHz, V-polarization, Using the Horn Probe	106
A.62	Y-Plane Amplitude and Phase Field Probe Plot Taken at 26.0 GHz, V-Polarization, Using the Horn Probe	107
A.63	3D X-Plane Amplitude and Phase Field Probe Plot Taken at 26.0 GHz, V-Polarization, Using the Horn Probe	108
A.64	3D Y-Plane Amplitude and Phase Field Probe Plot Taken at 26.0 GHz, V-Polarization, Using the Horn Probe	109

LIST OF ILLUSTRATIONS (Concluded)

FIGURE		PAGE
A.65	X-Plane Amplitude and Phase Field Probe Plot Taken at 26.0 GHz, H-Polarization, Using the Horn Probe	110
A.66	Y-Plane Amplitude and Phase Field Probe Plot Taken at 26.0 GHz, H-Polarization, Using the Horn Probe	111
A.67	3D X-Plane Amplitude and Phase Field Probe Plot Taken at 26.0 GHz, H-Polarization, Using the Horn Probe	112
A.68	3D Y-Plane Amplitude and Phase Field Probe Plot Taken at 26.0 GHz, H-Polarization, Using the Horn Probe	113

SECTION I

INTRODUCTION

There exists a clear and present need to develop indoor facilities for measuring the radiation and scattering properties of antennas and other aerospace components of interest. In the past, these measurements were performed on large outdoor measurement ranges. The distance between the transmitting and receiving antenna (for the antenna pattern range) or target (for the backscatter range) is normally dictated by the "far field" criteria. For a typical antenna or radar cross section (RCS) range, this requirement is commonly specified as:

$$R \geq \frac{2 D_1 D_2}{\lambda} \qquad (1)$$

where R is the minimum range, D_1 is the maximum transverse dimension of the transmit antenna (aperture), D_2 is the maximum transverse dimension of the receive antenna (target), and is the operating wavelength. For instance, if $D_1 = D_2 = 1.5$ meters, frequency = 15 GHz ($\lambda = 0.02$m), then

$$R \geq 225\text{m (738.2 ft.)} \qquad (2)$$

From Equation 2, it is evident why outdoor antenna facilities require larger distances between the transmit and receive antennas, in order to meet the planewave criteria of +/- 0.5 dB amplitude taper and +/-22.5 degrees of phase taper over the receive antenna (target). Figure 1 illustrates this concept.

An indoor compact RCS range has been developed by the AFWAL Avionics Laboratory. At present, this indoor compact measurement range has met the far field criteria from 8.2 - 26.0 GHz. In the future, this spectrum is expected to reach from 3.95 - 96.0 GHz.

This report presents actual near field probe data for the AFWAL Compact Measurement Range which undoubtedly demonstrate the planarity of the incident field.

This document is organized in the following manner. Section II presents the compact range configuration and examines how the aperture field is measured. Section III examines the test matrix used in measuring the wavefront's planarity and explains corrective measures for non-planarity. Finally, Section IV contains

conclusions and describes future planned far field alignment testing. An Appendix is supplied with complete test matrix data from 8.2 - 26.0 GHz.

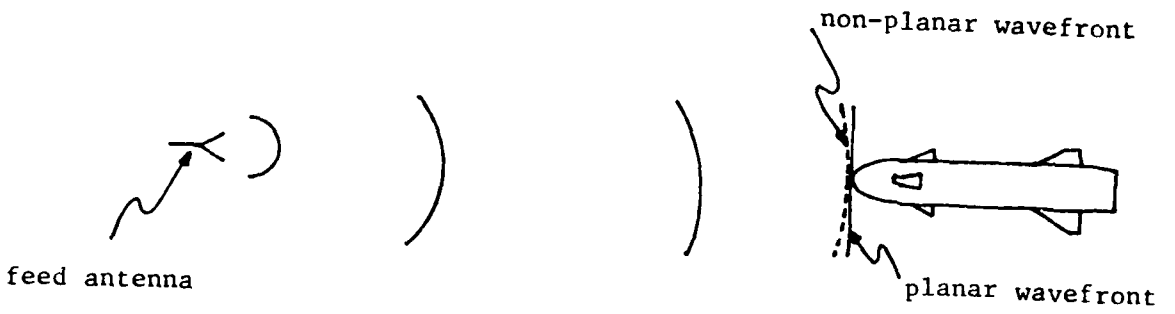


Figure 1. Planewave Approximation to Diverging Spherical Wavefront (Far Field)

SECTION II

MEETING THE FAR FIELD CRITERIA: HARDWARE AND METHODS

It is well known that illuminating a parabolic reflector from its focus with a spherical wavefront creates a planar wavefront in the aperture region. Mathematically this concept is quite simple. In reality, it is somewhat difficult to position an antenna feed precisely at the focus of a paraboloid reflector antenna. In any case, one should actually measure the aperture field of the reflector to verify that the feed is correctly aligned at the focal point. This section describes the measurement setup, hardware, and techniques used at the Avionics Laboratory to verify that the feed antenna for the compact range is properly positioned.

A schematic diagram and top view of the compact measurement range is shown in Figures 2 and 3 respectively. The two most essential items in the creation of a planar wavefront are: 1) a large parabolic reflector with dimensions roughly 20 percent larger than the desired measurement area, and 2) feed antennas with low backlobes which do not strongly illuminate the edges of the reflector, which prevents diffracted rays from contaminating the desired "quiet zone" or plane wave region.

The reflector used by the Avionics Laboratory was once part of a larger reflector used as a radio telescope (Figure 4). The reflector was shipped to its present location and aligned by the National Bureau of Standards in 1980 (Reference 1). When first obtained, the reflector had serrated edges on all sides (Figure 5). In order to reduce bottom edge diffraction which perturbed the "quiet zone" plane wave test region, the bottom edge was equipped with a metal extension (Figure 6). (This will be discussed in Section III.) The reflector's surface tolerance is 30 microns RMS, which should allow testing up to or exceeding 100 GHz.

In selecting a feed antenna, the horn type was chosen because of its size and simplicity. A pair of horn antennas were selected for three measurement bands: 8.2 - 12.4 GHz (X-band), 12.4 - 18.0 GHz (Ku-band), and 18.0 - 26.0 GHz (K-band). Each measurement band requires its own feed antenna, which has been conveniently designed to fit on a portable cart. On each cart is a five axis optical positioner (Figures 7 and 8) with either one horn (X-band) or two horn antennas (Ku and K-bands). The optical positioners allow fine movement of the antennas in the three orthogonal

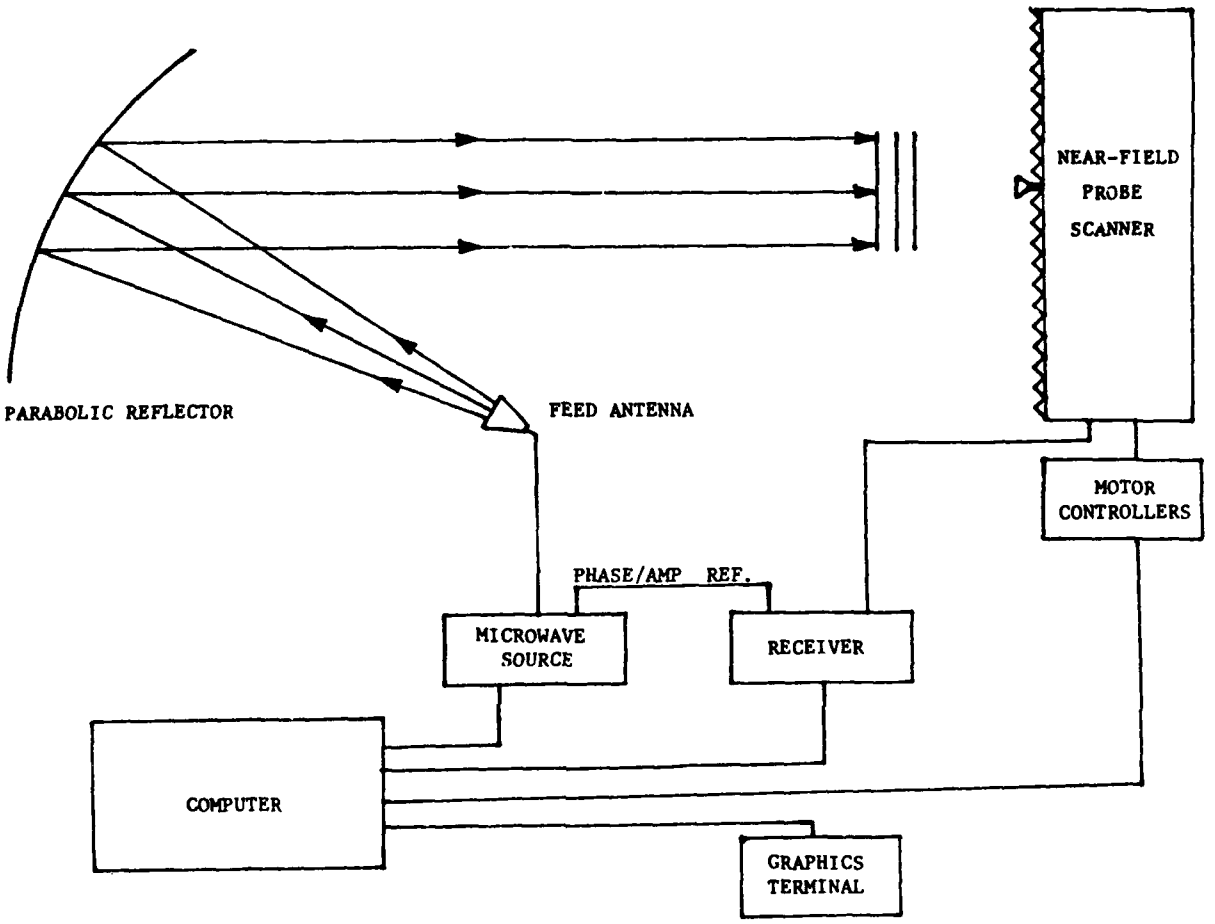


Figure 2. Schematic Diagram of the Compact Radar Cross Section Measurement Range



Figure 3. Photograph of the Compact Radar Cross Section Measurement Range

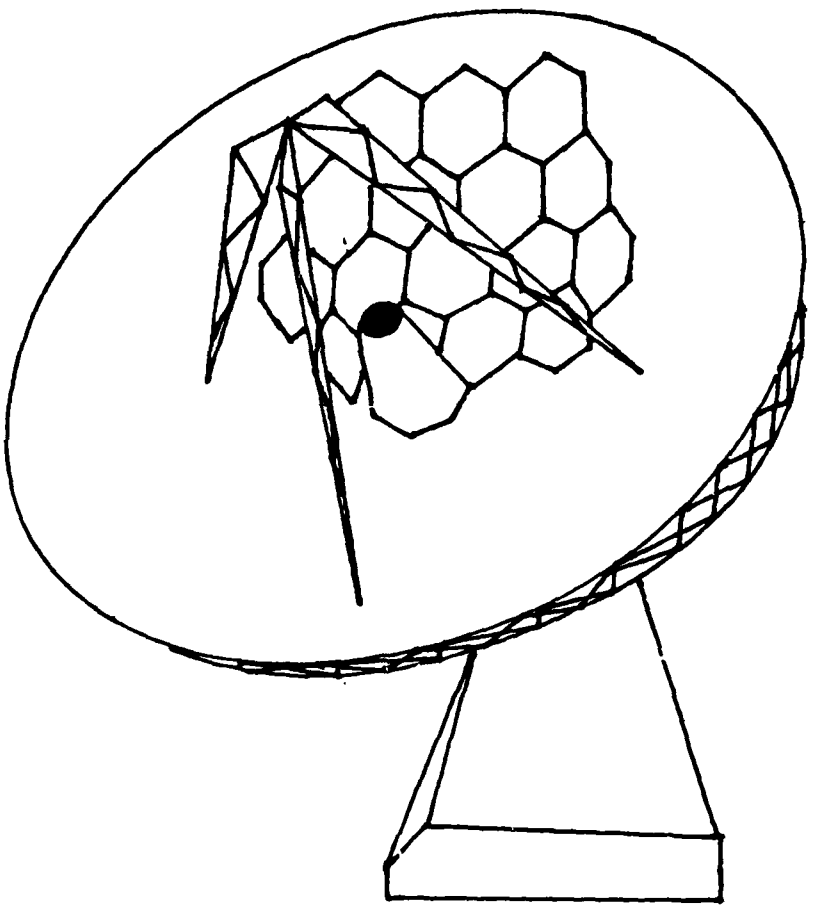


Figure 4. Section of Paraboloid Shown in Original Radio Telescope

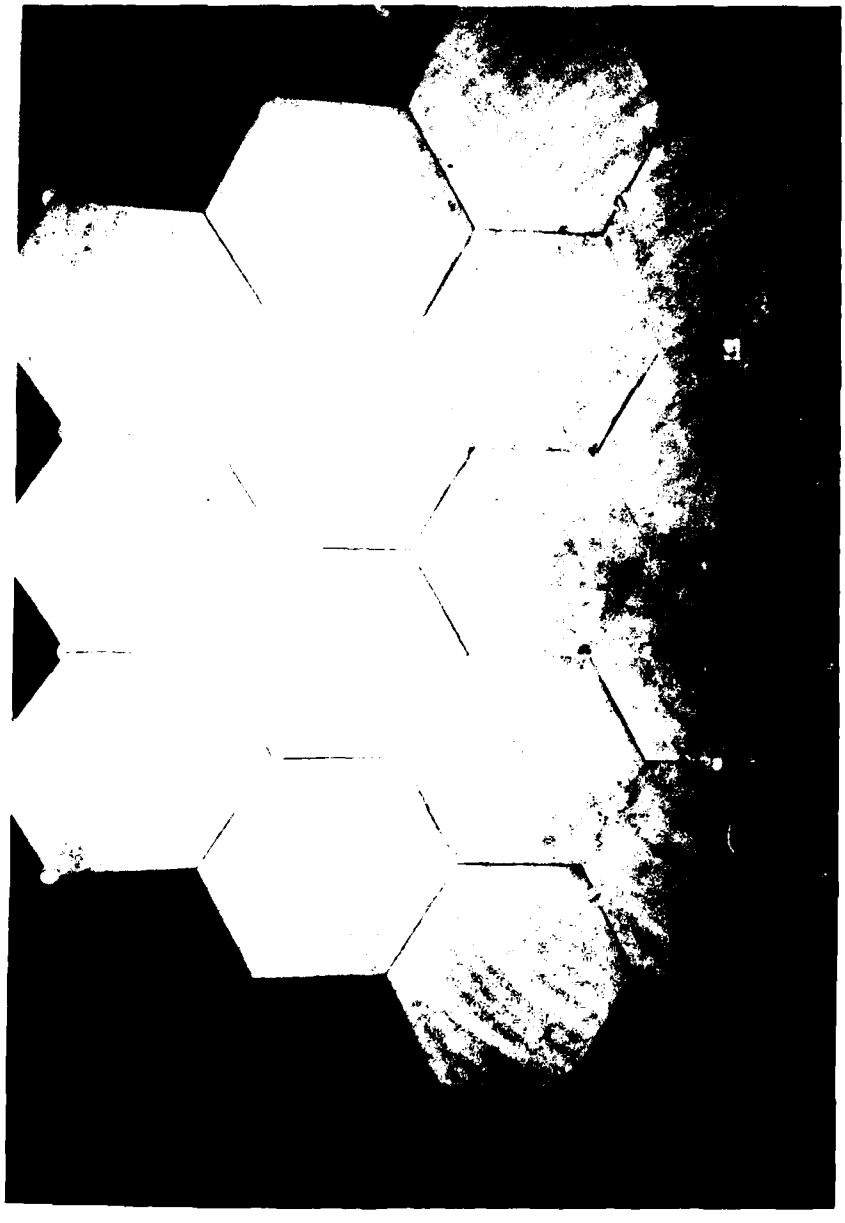


Figure 5. Compact Range Reflector Prior to Installation of Lower Edge Treatment

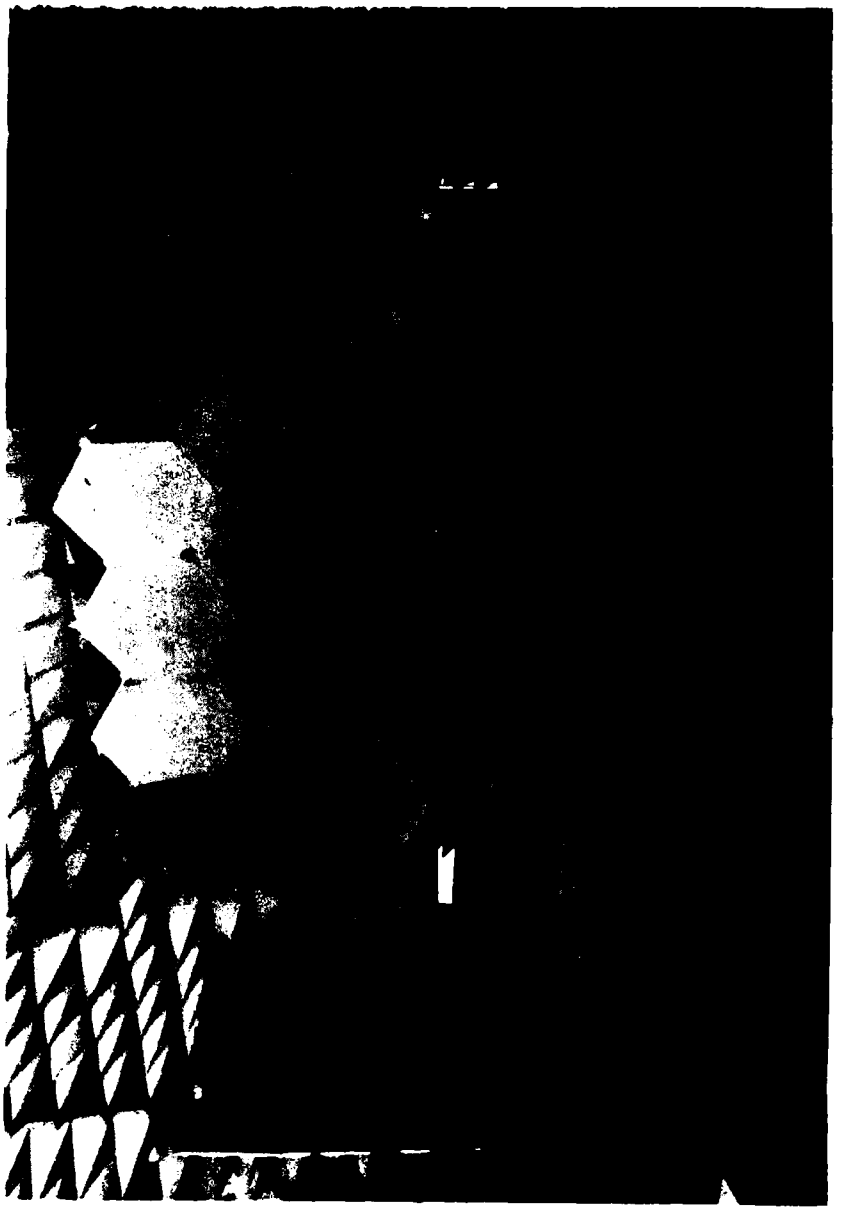


Figure 6. Compact Range Reflector After Installation of Lower Edge Treatment



Figure 7. X-Band (8.2 - 12.4 GHz) Feed Antenna Positioner



Figure 8. Ku Band (12.4 - 18.0 GHz) Band Dual Feed Antenna Positioner

coordinate axes plus elevation and azimuth directions. Experience has shown that antenna radiation and backscatter type measurements can be improved by isolating the transmit and receive feed antennas. One way to do this is to use a separate transmit and receive antenna at the reflector's focus. In X-band, however, it was decided to try a single horn feed system. The differences between single and dual horn systems will be discussed in a future report.

One of the two antennas located at the reflector's focus (designated a transmit horn whose focal position is yet to be verified) illuminates the reflector with a spherical wavefront. During AFWAL's measurements, a Watkins Johnson 1204A Synthesized Frequency Source (Figure 9) was used. The reflected wavefront travels to a two axis field probe scanner located about 25 feet from the base of the reflector. This scanner (Figure 10) was built by Martin Marietta in the mid-1970s, and houses a field probe (usually a horn antenna or open-ended waveguide, Figure 11) whose position is controlled by a two-axis positioning system. Each axis is controlled by separate "stepping motors" (Superior Electric, Figure 12) which can repeatedly position the scanner probe within fractions of an inch. These motors are controlled by a Hewlett Packard 1000 Series Computer (Figure 13), and move the probe assembly in two orthogonal directions, designated the x and y planes (Figure 14). As the probe "scans" the reflected field, the receiver (Scientific Atlanta 1750, Figure 15) samples the field in amplitude and phase, with respect to a constant reference signal coupled directly from the microwave source. After the reflected field has been discretely sampled, the amplitude and phase are plotted on a Hewlett Packard 2623A graphics terminal (Figure 15 center). From these plots the user may identify improper positioning of the feed antennas and take corrective action.

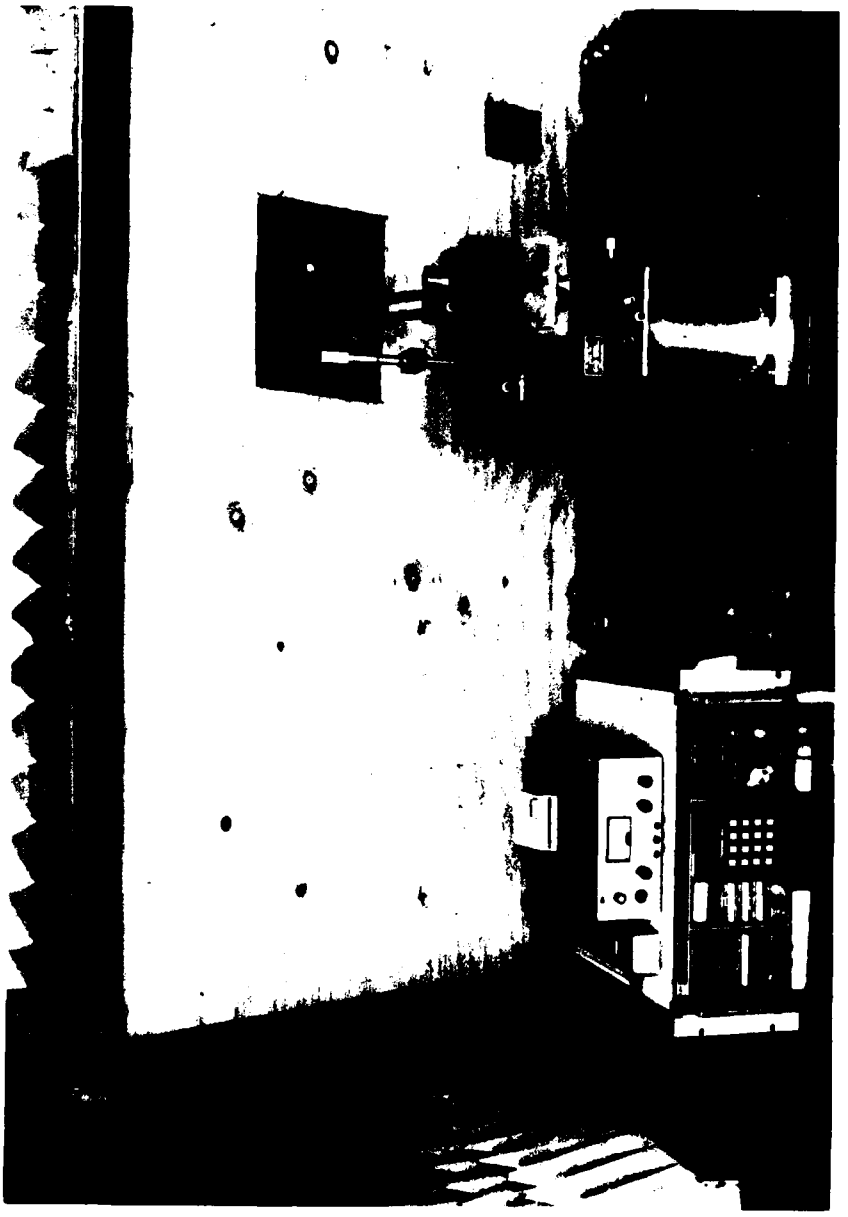


Figure 9. Microwave Synthesizer Used During Experiments (Lower Left)

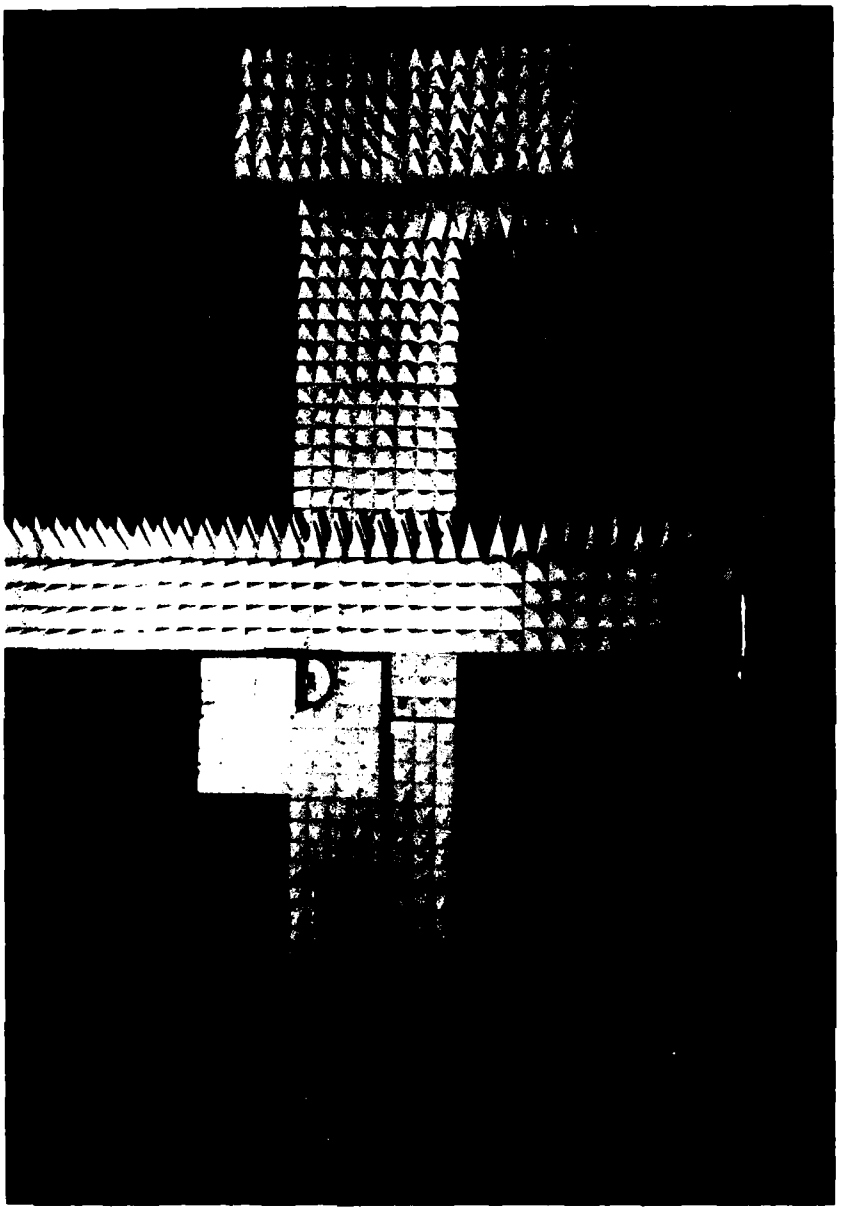


Figure 10. Near Field Two Axis Probe Scanner

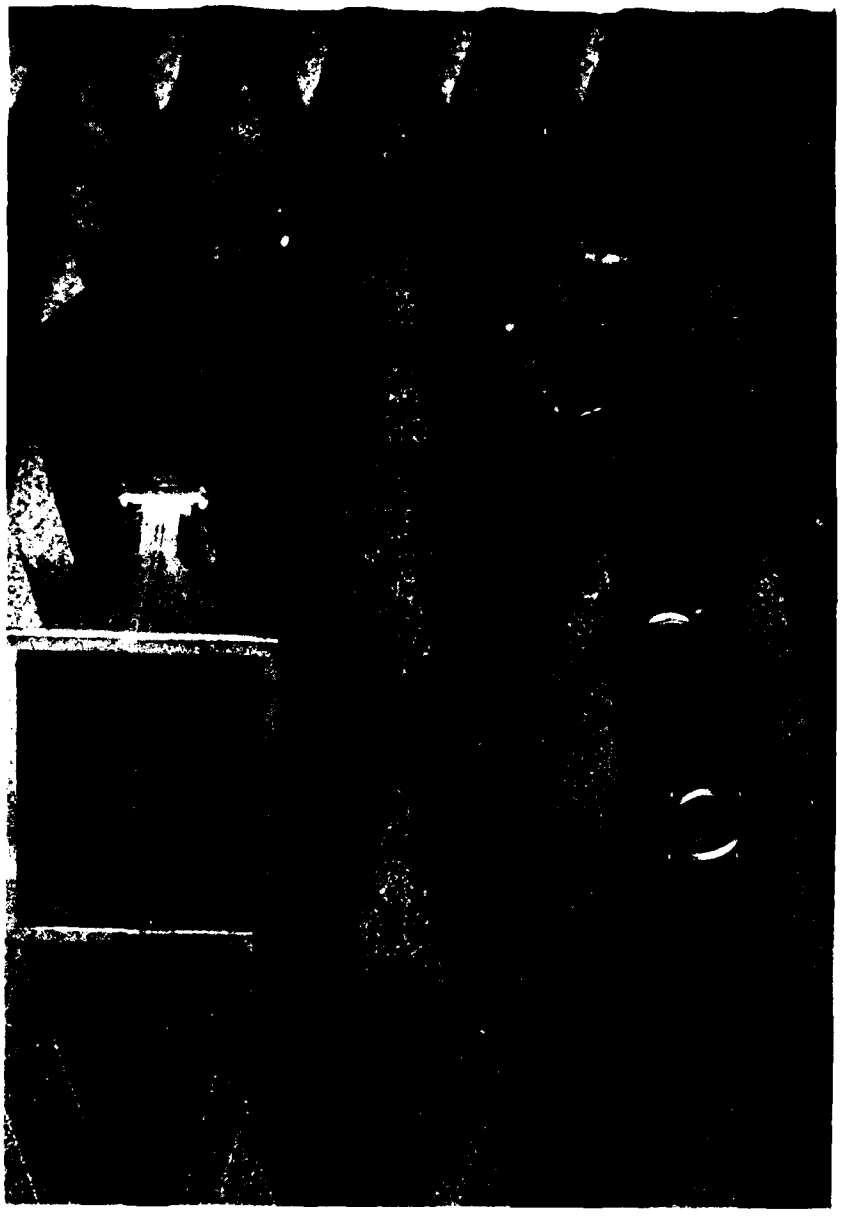


Figure 11. Field Probes Used During Experiments
(Horn Probe - Left) (Waveguide - Right)

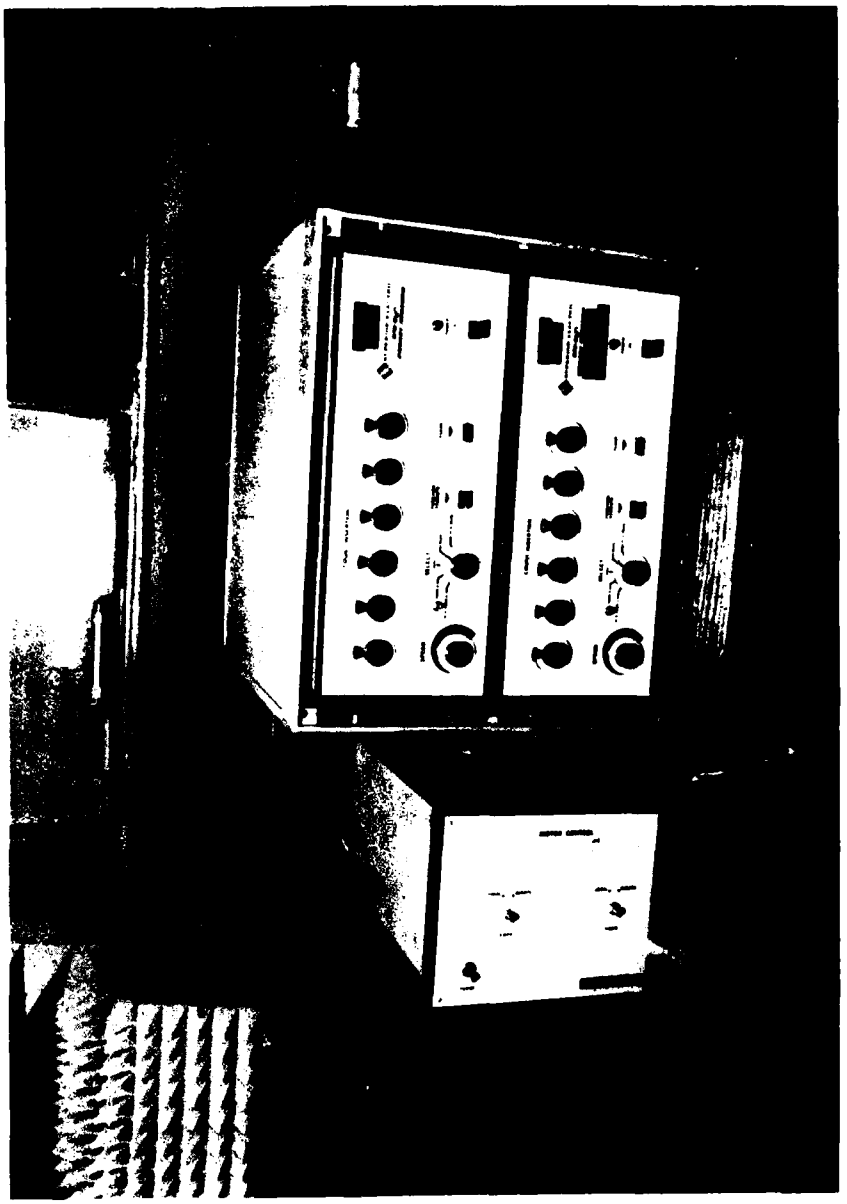


Figure 12. Computer Controlled Motor Positioners



Figure 13. Mainframe Computer Used to Control Motor Positioners and Store Field Probe Amplitude and Phase Information

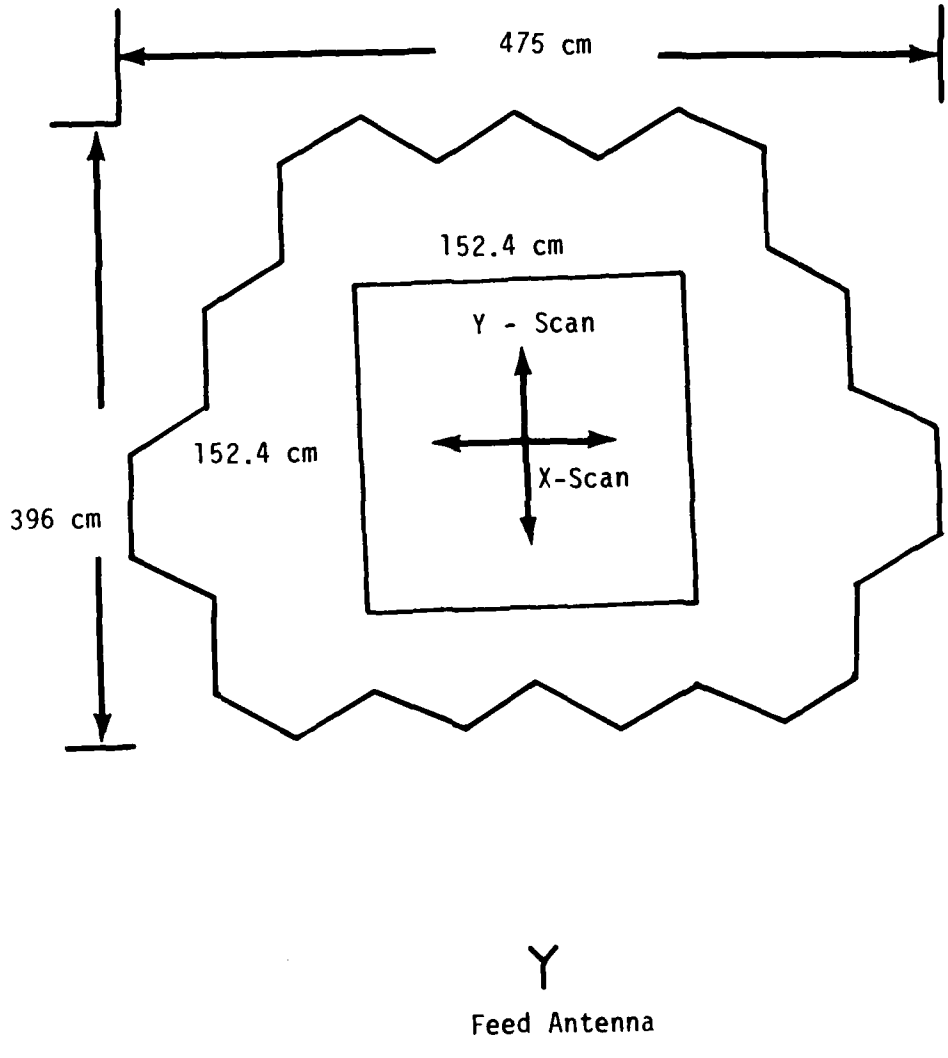


Figure 14. Principle Plane Measurements as Seen by the Field Probe

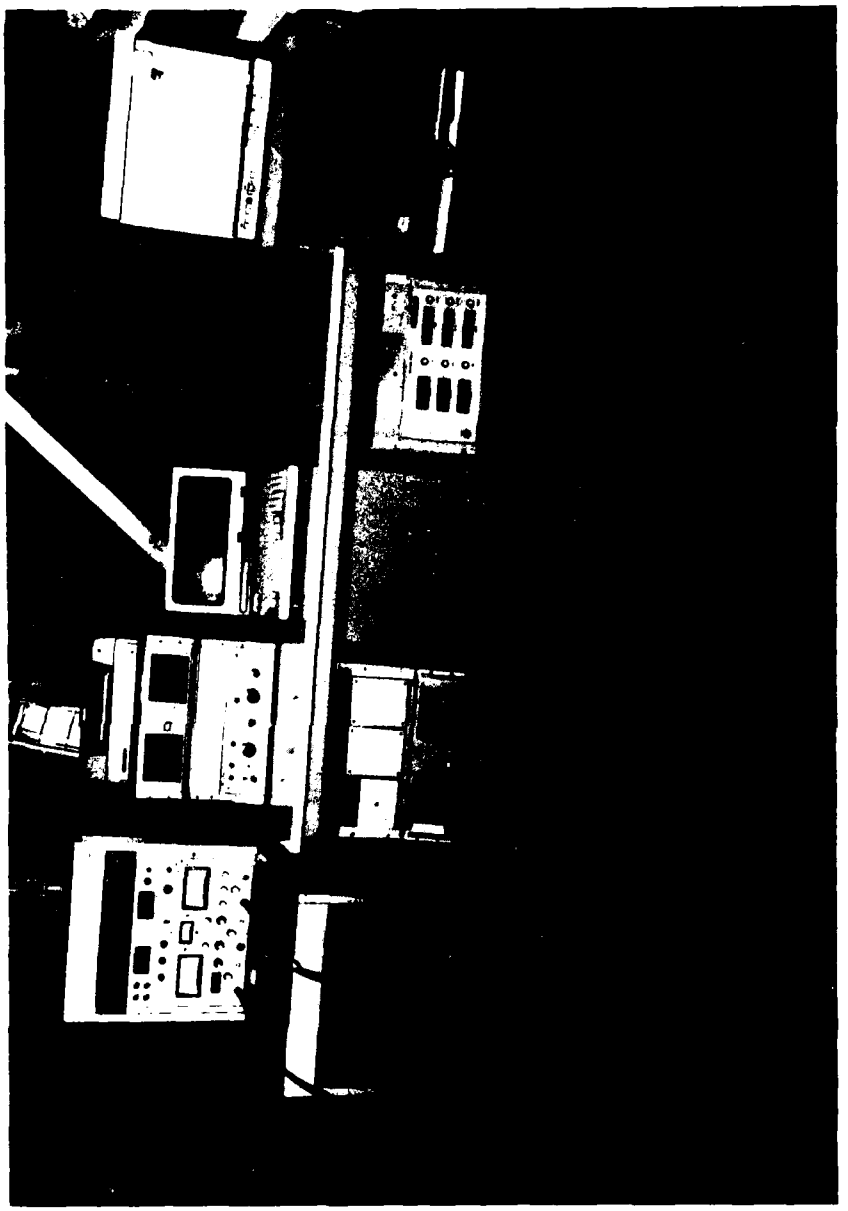


Figure 15. Microwave Receiver Used During Experiments

SECTION III

THE TEST MATRIX

So far, we have shown that one can create a large measurement zone which simulates an incident plane wave by using the compact range technique, without requiring much real estate. As mentioned earlier, aligning a compact range requires the precise positioning of feed antennas at the focus of a parabolic reflector. In this report, the planarity of the aperture field is actually measured to verify the alignment of the primary feed antennas. This is done by using a near field measurement scanner probe to sample as much of the aperture field as possible, in both amplitude and phase. Unfortunately, one cannot fully characterize the alignment of the feed antennas by simply looking at the aperture field amplitude and phase at one polarization, one frequency, and in one principal plane. We need to perform an entire series of tests to fully check the alignment versus polarization and frequency. Table 1 illustrates the test matrix which will be used to validate the broadband alignment of the compact range feed antennas.

The test matrix applied to the compact measurement range has 24 tests for each of the three measurement bands and is arranged as shown in Table 1.

TABLE 1

FIELD PROBE TEST MATRIX

Band Upper Frequency:

Vertical Polarization Tests:	Horizontal Polarization Tests:
X - Plane (horn probe)	X - Plane (horn probe)
X - Plane (waveguide probe)	X - Plane (waveguide probe)
X - Plane (horn probe 3D)	X - Plane (horn probe 3D)
Y - Plane (horn probe)	Y - Plane (horn probe)
Y - Plane (waveguide probe)	Y - Plane (waveguide probe)
Y - Plane (horn probe 3D)	Y - Plane (horn probe 3D)

Band Lower Frequency:

Vertical Polarization Tests:	Horizontal Polarization Tests:
X - Plane (horn probe)	X - Plane (horn probe)
X - Plane (waveguide probe)	X - Plane (waveguide probe)
X - Plane (horn probe 3D)	X - Plane (horn probe 3D)
Y - Plane (horn probe)	Y - Plane (horn probe)
Y - Plane (waveguide probe)	Y - Plane (waveguide probe)
Y - Plane (horn probe 3D)	Y - Plane (horn probe 3D)

One can see that this is quite an exhaustive set of tests. Fortunately, the test are computer automated, making the test matrix quite manageable. This section will describe each of the above tests and their impact on the feed antenna alignment process.

An initial guess in locating the reflector's focus is to position the feed one focal length from the reflector, in this case 412.32 cm (13.53 ft). A fixture set in concrete is located at the approximate focal point which provides a stable mount for the three antenna carts (Figure 9, right). The reader should keep in mind that positioning the feed antennas one focal length from the reflector only gives a coarse estimate of the feed antenna position. The final alignment position requires careful field probe measurements to help correct alignment errors.

Although there are 24 matrix measurements, only two dominate the alignment process; the x and y principal plane scans. By sampling these two principal planes, the user can figure out any linear translational errors in the feed antenna position. The additional measurements help charcterize the test wavefront and give useful information concerning the operation of the measurement facility.

Since the wavelength at x band is larger than the other two measurement regions, and less susceptible to phase errors (caused by minor position changes with respect to the reflector's focus), it was the initial measurement band chosen for testing our feed antenna alignment process.

After selecting the X-band antenna for initial alignment, its associated antenna cart is positioned onto the fixed steel base support structure. The test matrix begins with vertical polarization field probes, with samples taken in both the x and y principle plane at the upper band frequency of 12.0 GHz. Initial field probes were performed to accurately position the horn antenna for vertical polarization. (Recall that for horn antennas, the phase center for H-polarization is different than for V-polarization. Therefore, it is necessary to align the horn feeds at both polarizations, making note of the feed positioner micrometer settings for each polarization.)

During principle plane scans, the scanner probe fixture is guided across the measurement zone in the x and y planes. During the scans, the amplitude and phase

of the aperture field is sampled at equal spacial intervals. Examples of principal plane near field probe plots are shown in Figures 16 and 17. Notice that these field probes far exceed the necessary far field criteria; that is to say the amplitude and phase variations are limited to +/- 0.5 dB and +/- 22.5 degrees respectively. Keep in mind, however, that it is necessary to verify the far field criteria over the entire measurement zone. Clearly, principle plane scans are just the beginning.

As stated earlier, the original reflector did not have the bottom edge extension. With the "untreated edge", significant edge diffractions from the bottom edge contaminated the measurement zone, as shown by the principal plane field probe scan of Figure 18 (top). To verify this assertion, the entire aperture was probed, the results of which are shown in Figure 18 (bottom). Obviously, the feed antennas strongly illuminate the bottom edge, causing the strong interference between the principle reflected wave and the edge diffracted wave. A simple analysis showed that this edge diffraction could be eliminated by extending the electrical surface of the reflector all the way down to the microwave absorber located on the floor (Figure 6). It turned out that it was not necessary to precisely match the extension and reflector surface. As long as edge transition was smooth, the bottom edge could be aligned to reflect energy into the microwave absorber located along the floor. This edge treatment significantly reduced the massive amplitude and phase variations, as verified by the field probe of Figure 25. The edge extension concept was so successful that it was immediately implemented by compact measurement ranges at NASA/Langley and The Ohio State University (Reference 2).

Although the bottom edge treatment reduces the amplitude variations in the measurement region, we still must assure that the feed antennas are properly aligned. The first step in aligning the feed antennas after performing a principal plane scan is to closely examine the amplitude and phase plots. For example, is the amplitude distribution across the reflector's aperture symmetric or nonsymmetric? Does the phase profile appear to be flat, slanted, or curved? For instance, a nonsymmetrical amplitude distribution requires feed antenna adjustment in the azimuth (x-scan) or elevation (y-scan) directions, as shown in Figure 19. A slanted phase profile (Figure 20) indicates that the feed antenna is correctly located in the reflector's focal plane but is still linearly offset from the focal point. This requires a translation of the feed antenna parallel to the reflector, vertically for a y-scan and horizontally for an x-scan. When a curved phase distribution is

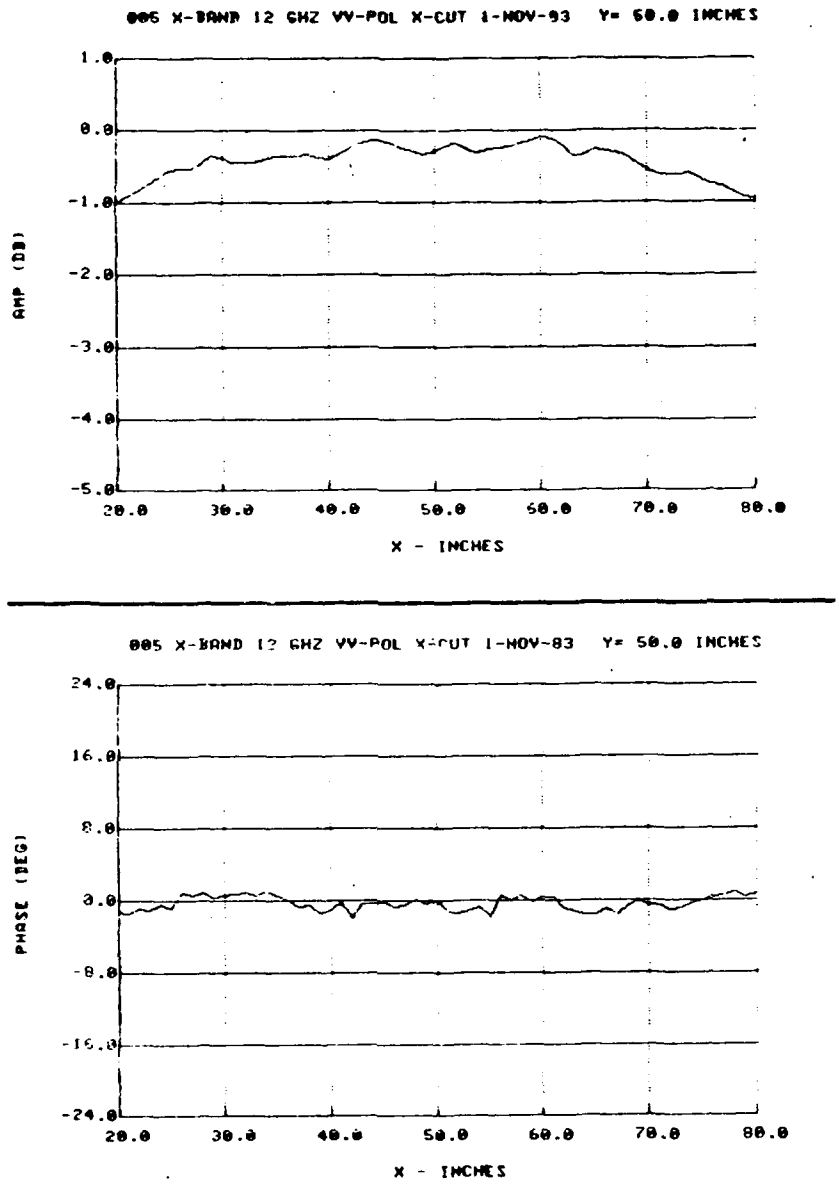


Figure 16. X-Plane Amplitude and Phase Field Probe Plot Taken at 12.0 GHz, V-Polarization, Using the Horn Probe

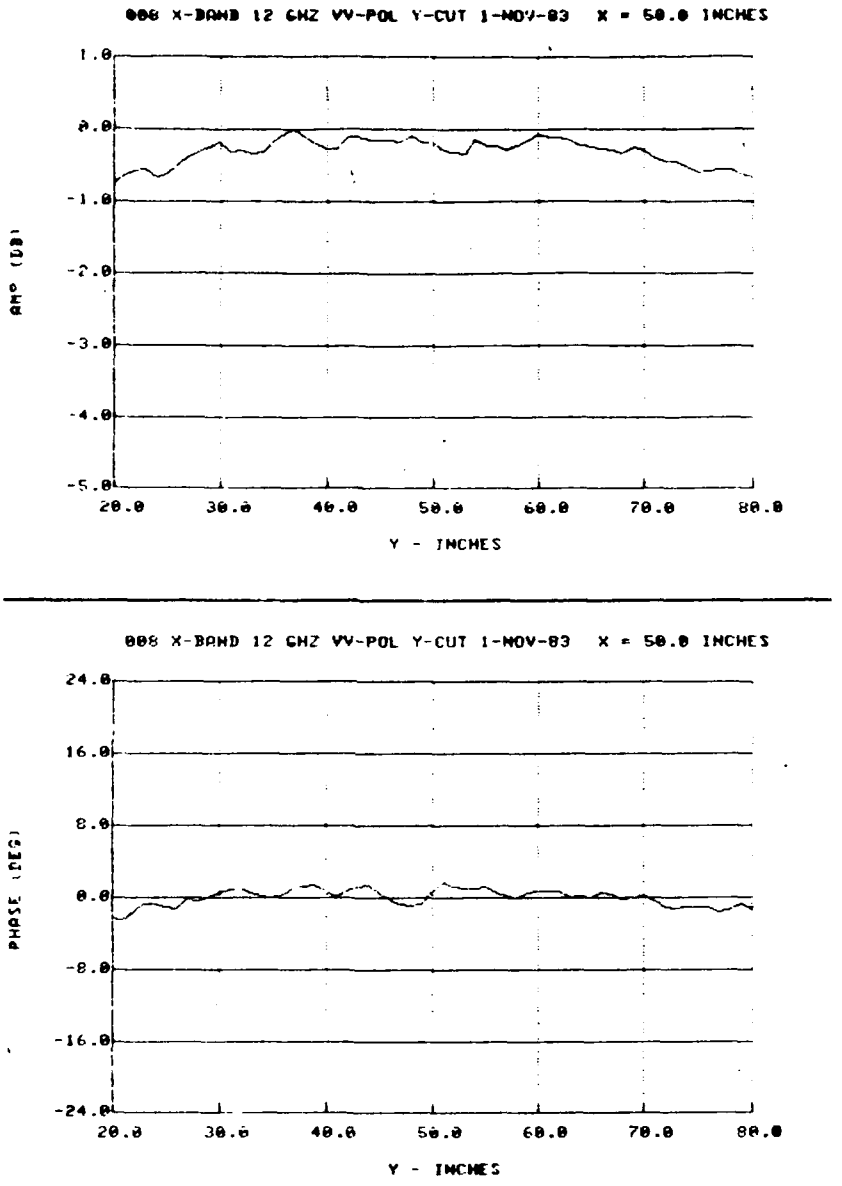


Figure 17. Y-Plane Amplitude and Phase Field Probe Plot Taken at 12.0 GHz, V-Polarization, Using the Horn Probe

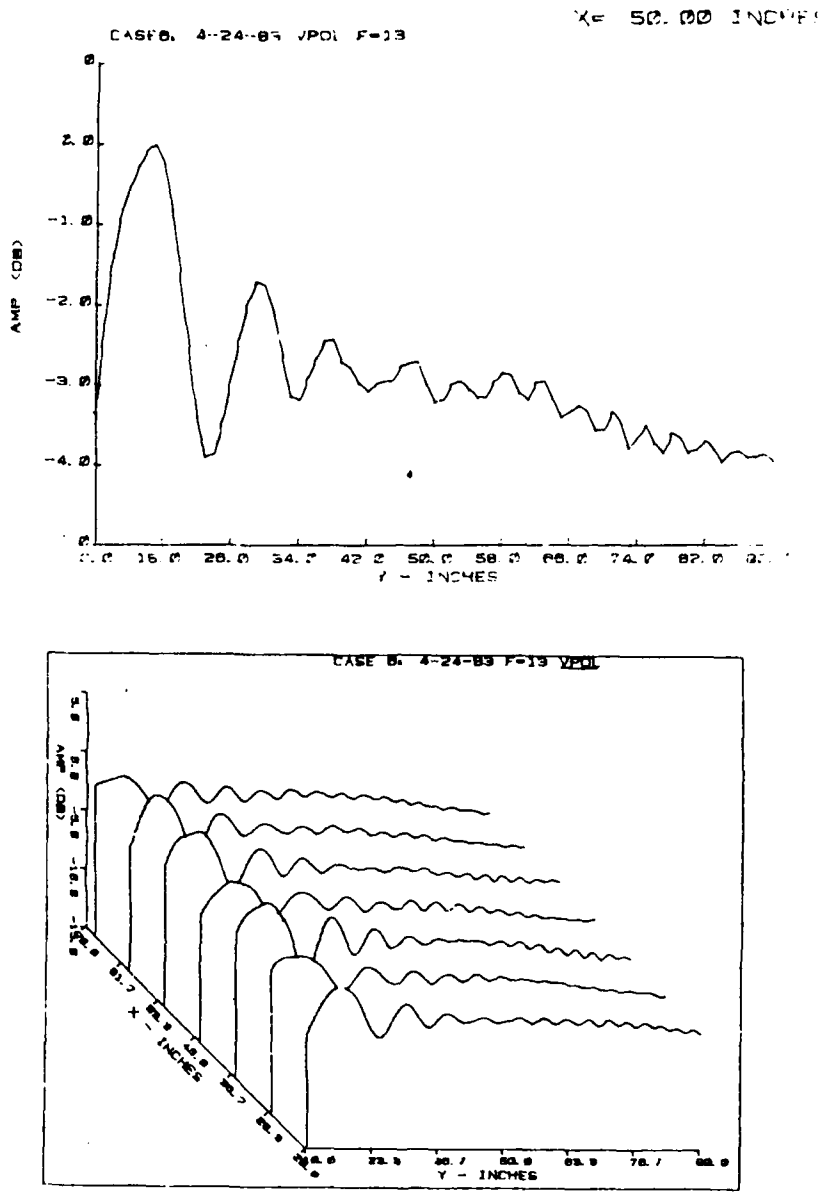
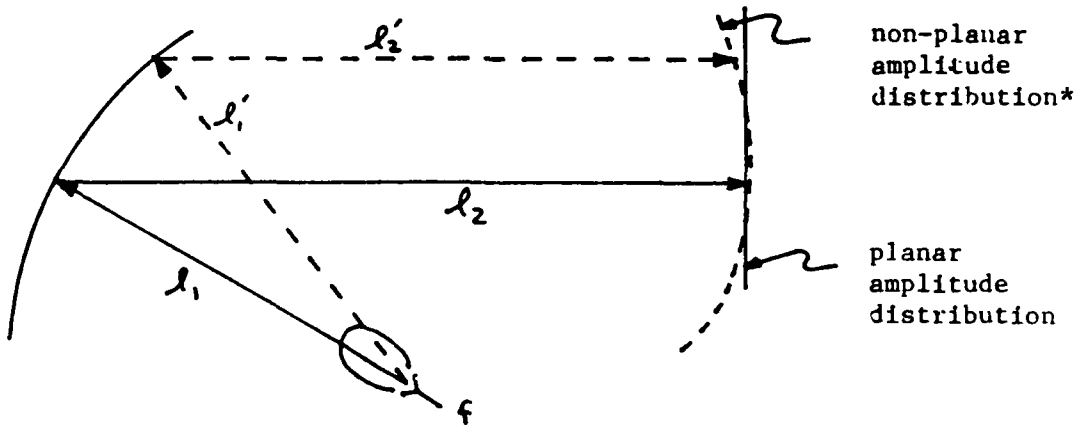


Figure 18. (Top) Y-Plane Amplitude Field Probe Plot, 13 GHz, V-Polarization (Bottom) Full "Quiet Zone" Y-Plane Field Probe Plot, 13 GHz, V-Polarization (Untreated Bottom Edge)



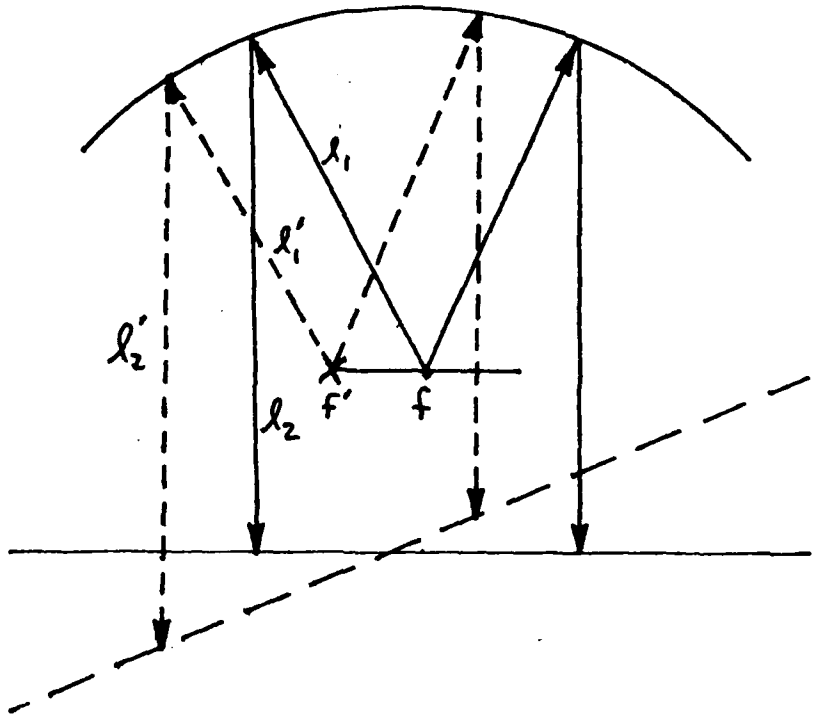
$$L_1 + L_2 = L_1' + L_2' \qquad f = \text{focus}$$

* The Non-planar amplitude distribution is a result of 2 factors:

1) The feed horn pattern is tapered in the direction of the reflector's edges.

2) Increased spatial attenuation from the horn to the edges of the relector.

Figure 19. Unsymmetrical Amplitude Distribution Due to Incorrect Feed Antenna Positioning (Azimuth or Elevation)



$L_1 + L_2 = L_1' + L_2'$

f = True Focus

f' = Offset Feed Antenna Position

Figure 20. Slanted Phase Profile Due to Incorrect Feed Antenna Positioning

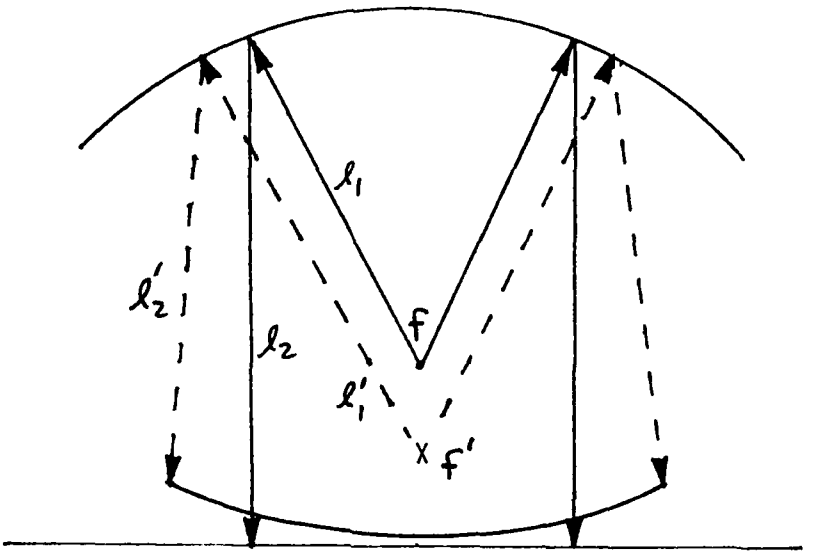
encountered, the feed antenna is not in the reflector's focal plane requiring adjustment normal to the reflector, as shown in Figure 21.

Aligning the feed antenna is an iterative process. Field probes must be performed, the feed antenna positions adjusted, and measurements repeated. At first the process was very slow; with time and experience, however, it was possible to accurately interpret the field probe results.

Once the plane wave criteria is met in the reflector's principle planes, we proceed to the waveguide probe tests. Typical radiation patterns for the selected horn antenna probe and waveguide probe are shown in Figure 22. Note that the horn antenna has a sharp main lobe, while the waveguide probe has a broad main lobe. Using the waveguide probe allows the users to more accurately evaluate the total field across the measurement zone (reflected wavefront plus interference terms). The principal plane scans made with the waveguide probe help reveal perturbations in the aperture field rather than aid in the antenna alignment process. A sample waveguide field probe plot is shown in Figures 23 and 24.

The next measurement to be performed is referred to as a "three dimension" scan. In reality, this measurement consists of a rastor scan over the full (quiet) zone region. Although the probe is only scanned in two dimensions, the plots project the contour of the wavefront in the aperture of the reflector in three dimensions, as demonstrated by Figures 25 and 26. In general, the three dimension scans are only performed to verify the plane wave criteria across the aperture; they are too time consuming to be used for aligning the feed antennas.

After performing the vertical polarization measurements, the horn probe and feed antennas are set up for horizontal polarization. It is not unreasonable to expect slightly different feed antenna position settings when switching from one polarization to the other. This is caused by a shift in the mechanical and electrical phase center of the feed antennas with changing polarization. Since the position of the feed antennas change slightly with polarization, the same measurement process is used to align the antenna in both polarizations, as shown in the test matrix.



$$L_1 + L_2 = L_1' + L_2'$$

f = True Focus

f' = Offset Feed Antenna Position

Figure 21. Curved Phase Profile Due to Incorrect Feed Antenna Positioning

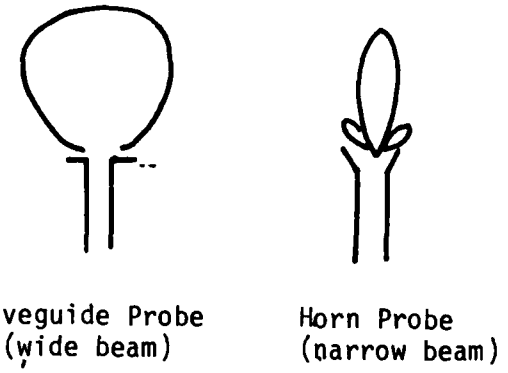


Figure 22. Radiation Patterns for the Selected Horn Probe (Right) and Waveguide Probe (Left)

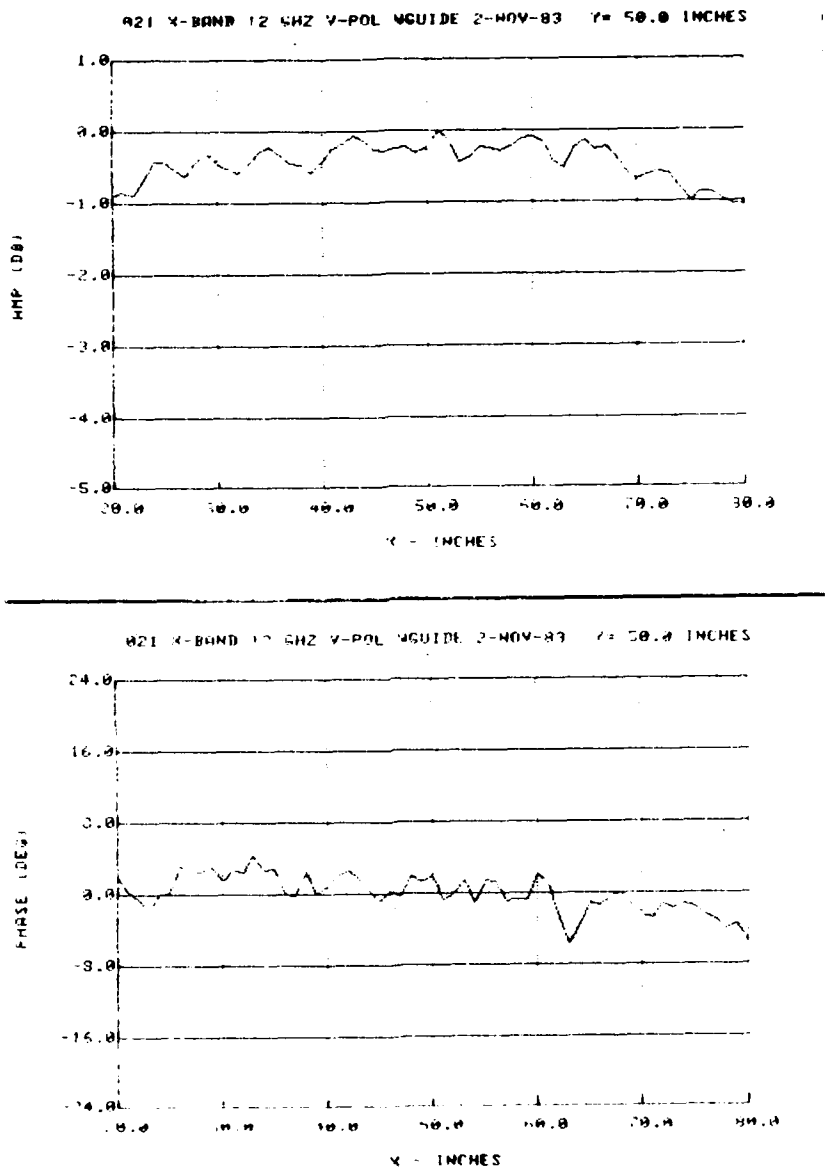


Figure 23. X-Plane Amplitude and Phase Field Probe Plot Taken at 12.0 GHz, V-Polarization, Using the Waveguide Probe

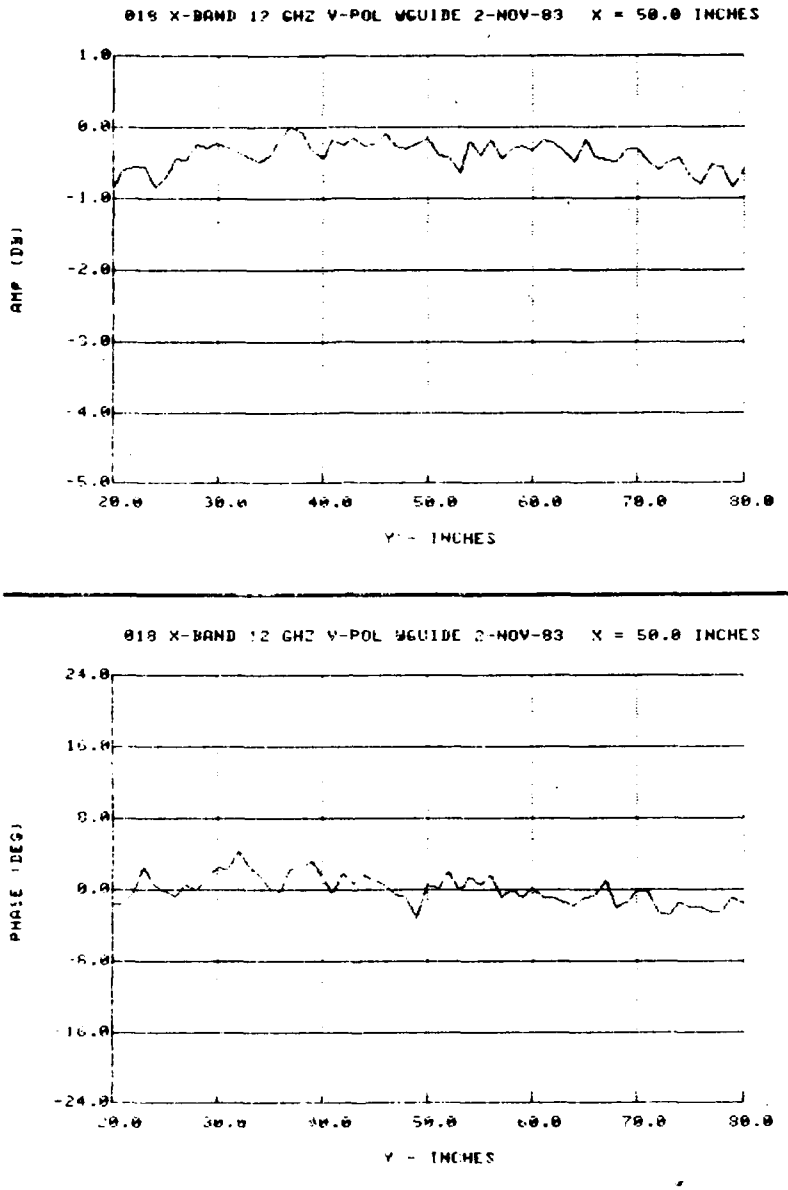


Figure 24. Y-Plane Amplitude and Phase Field Probe Plot taken at 12.0 GHz, V-Polarization, Using the Waveguide Probe

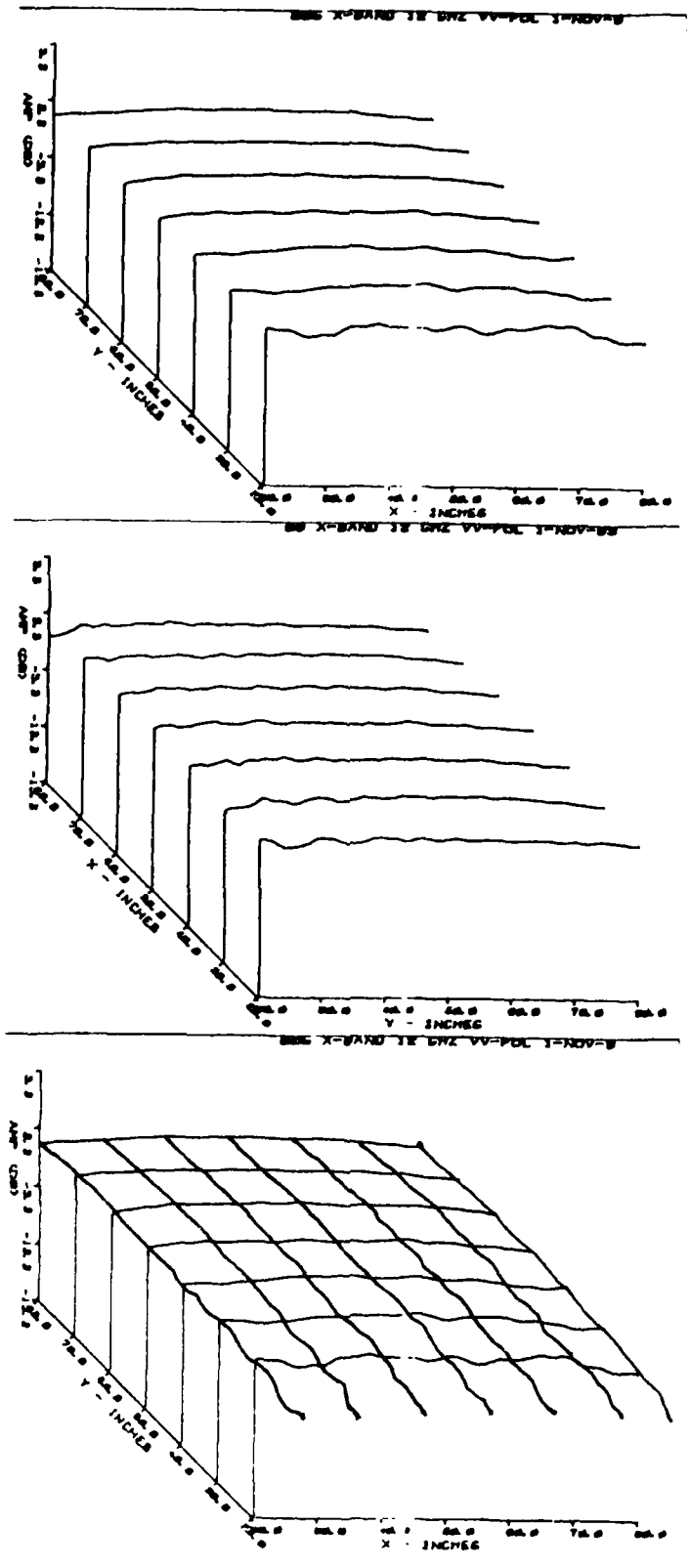


Figure 25. 3D Amplitude Field Probe Plot Taken at 12.0 GHz, V-Polarization, Using the Horn Probe (X - Y Layover at Bottom)

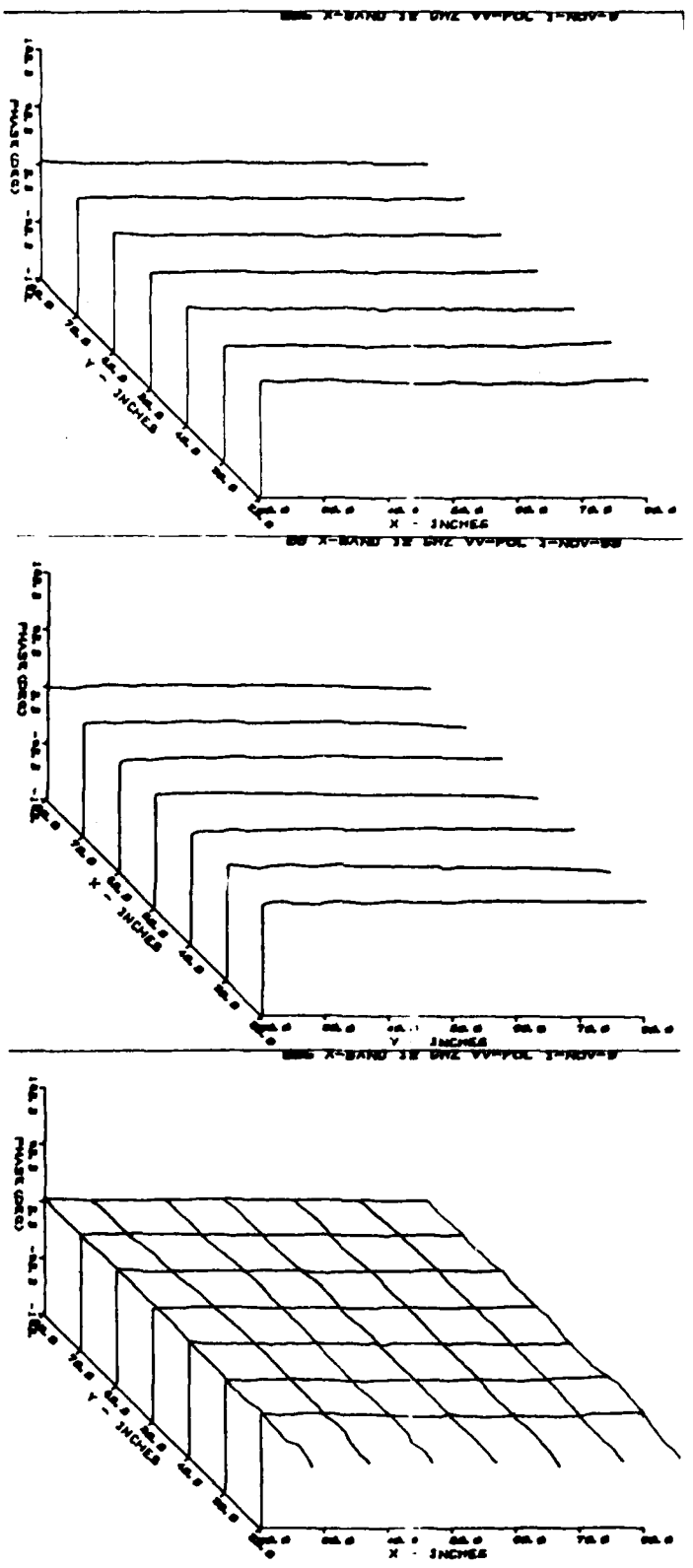


Figure 26. 3D Phase Field probe Plot Taken at 12.0 GHz, V-Polarization, Using the Horn Probe (X - Y Layover at Bottom)

The feed antenna alignment is performed at the higher, more sensitive end of the measurement band. Experience has shown that once the antenna is aligned at the highest frequency in band, the lowest frequency of the band is automatically aligned (Figures 27 and 28). Despite this, however, it was decided to perform a complete set of field probes at the lower frequency limit of the band. Again, these tests are used to verify wavefront planarity, and not for alignment purposes.

After completing the alignment tests at X-band, the same tests were repeated at Ku and K-bands. All test data for the three measurement bands is located in the Appendix.

Throughout the measurement process, a few measurement problems were encountered. For instance, the phase measurements were often contaminated when the coaxial cables which connect the probe to the measurement receiver bent during the scanning process. Remember that a physical change in electrical length translates into an undesired additive phase shift. Figure 29 demonstrates how cable flexing translates into measured "spikes" in the phase field probe plots. Many different coaxial configuration were tried until this problem was minimized. Another problem often encountered was the loss of phase lock in the receiver. This irritating problem was caused by instabilities in AFWAL's 15 year old Scientific Atlanta 1750 microwave receiver. Since the measurements were performed, a new Scientific Atlanta 1783 receiver has been procured which should permanently solve this problem in the future.

Although it was conclusively demonstrated that the edge diffractions from the lower edge of the reflector was eliminated by the lower edge "skirt" treatment, clearly the entire diffraction problem has not been eliminated. Although the top and side edges are not as strongly illuminated, they also contribute edge diffracted interference terms in the quiet zone region. To eliminate this problem, The Ohio State University and NASA/Langley Research Center conclusively demonstrated that attaching elliptically curved edge treatments to the rim of the reflector effectively reduces this undesired edge diffraction. The curved edge modification is shown in Figure 30. The reduction in the edge diffracted interference is clearly demonstrated in Figures 31 and 32 respectively. Figure 31 shows a field probe amplitude profile as one scans across an untreated edge, and compares the measured diffraction with predicted edge diffractions. Figure 32 shows the same amplitude

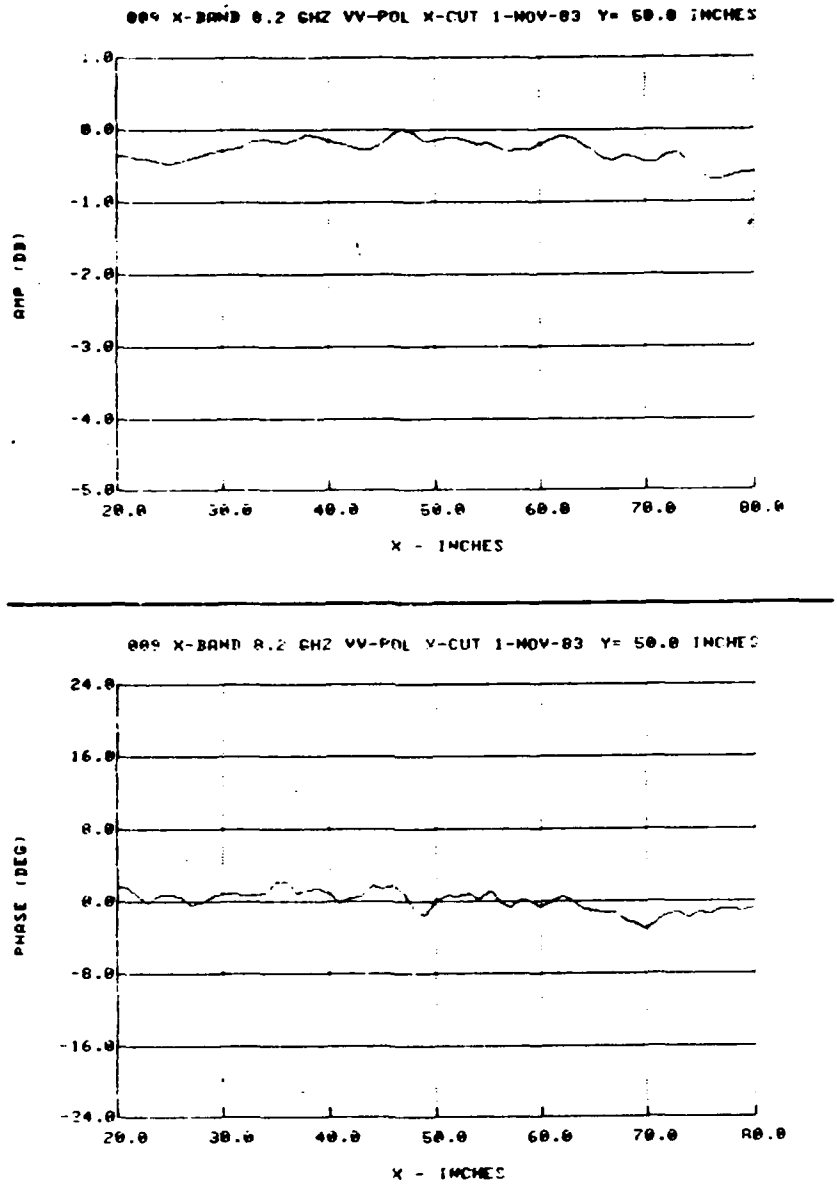


Figure 27. X-Plane Amplitude and Phase Field Probe Plot Taken at 8.2 GHz, V-Polarization, Using the Horn Probe

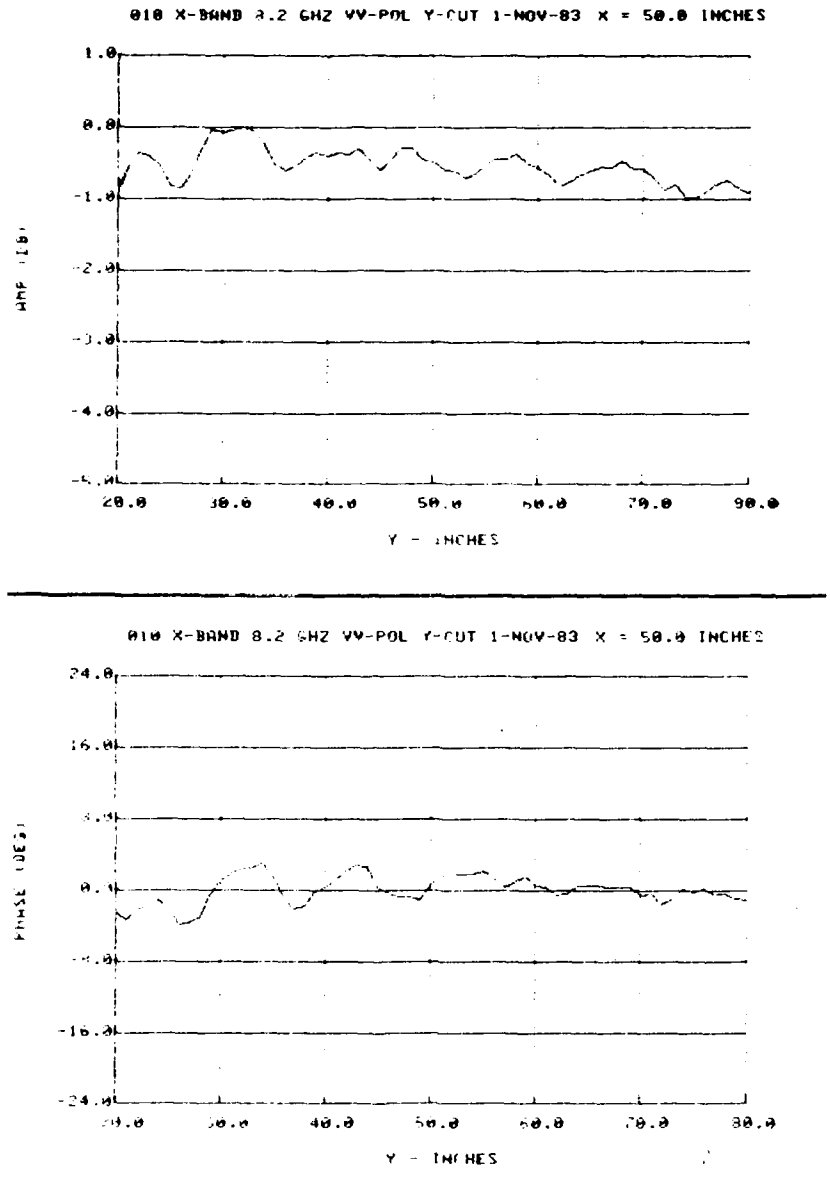


Figure 28. Y-Plane Amplitude and Phase Field Probe Plot Taken at 8.2 GHz, V-Polarization, Using the Horn Probe

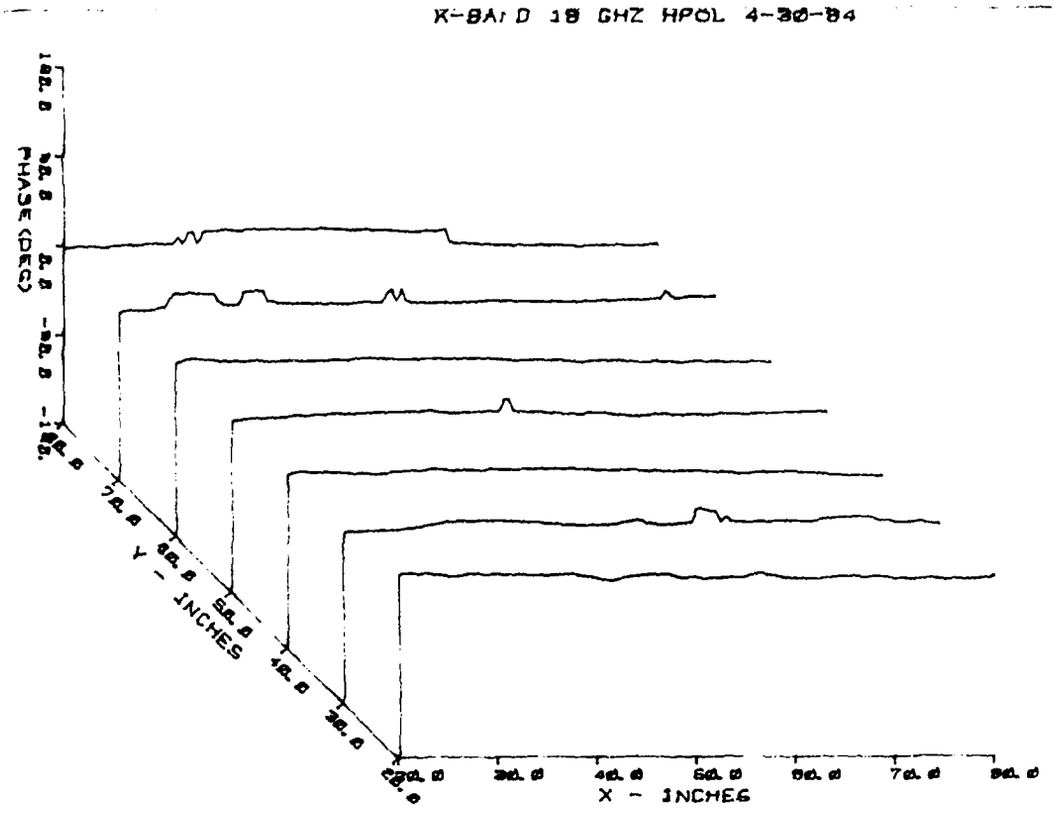


Figure 29. 3D X-Plane Phase Field Probe Plot Taken at 18.0 GHz, H-Polarization, Using the Horn Probe (Note Phase Discontinuities)

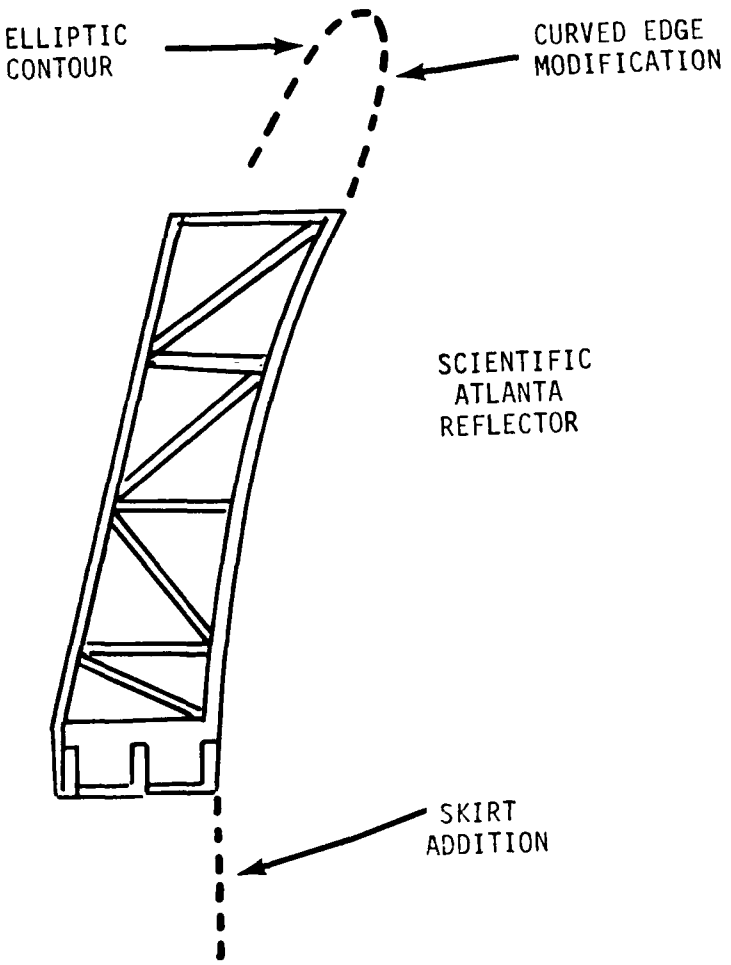


Figure 30. Side View of Elliptical Curved Edge Treatments for the OSU and NASA Compact Range Reflector Antenna

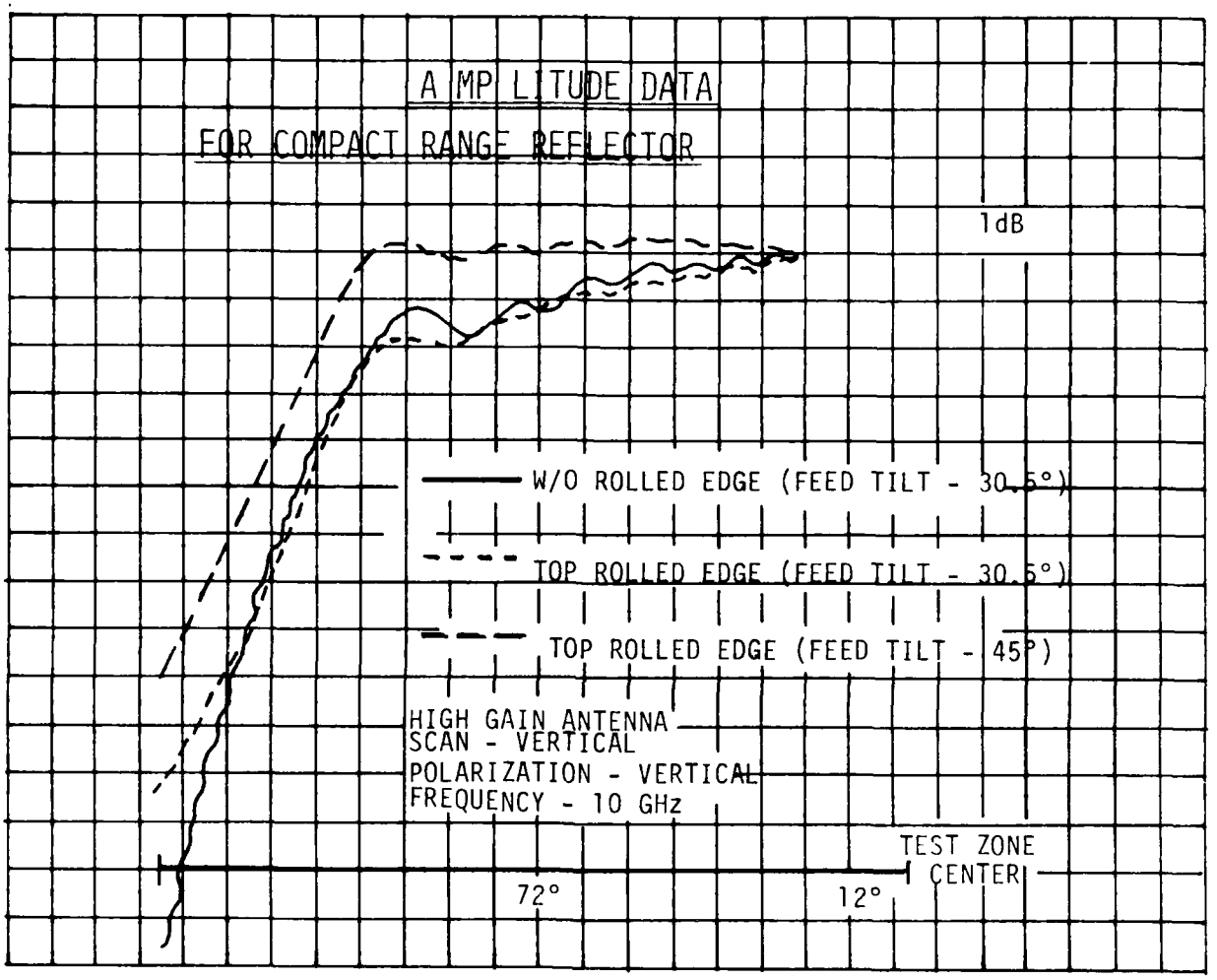


Figure 31. Amplitude Field Probe Taken Across an Exposed Reflector Rim (Measurements are Compared to Moment Method Calculations at 10. GHz)

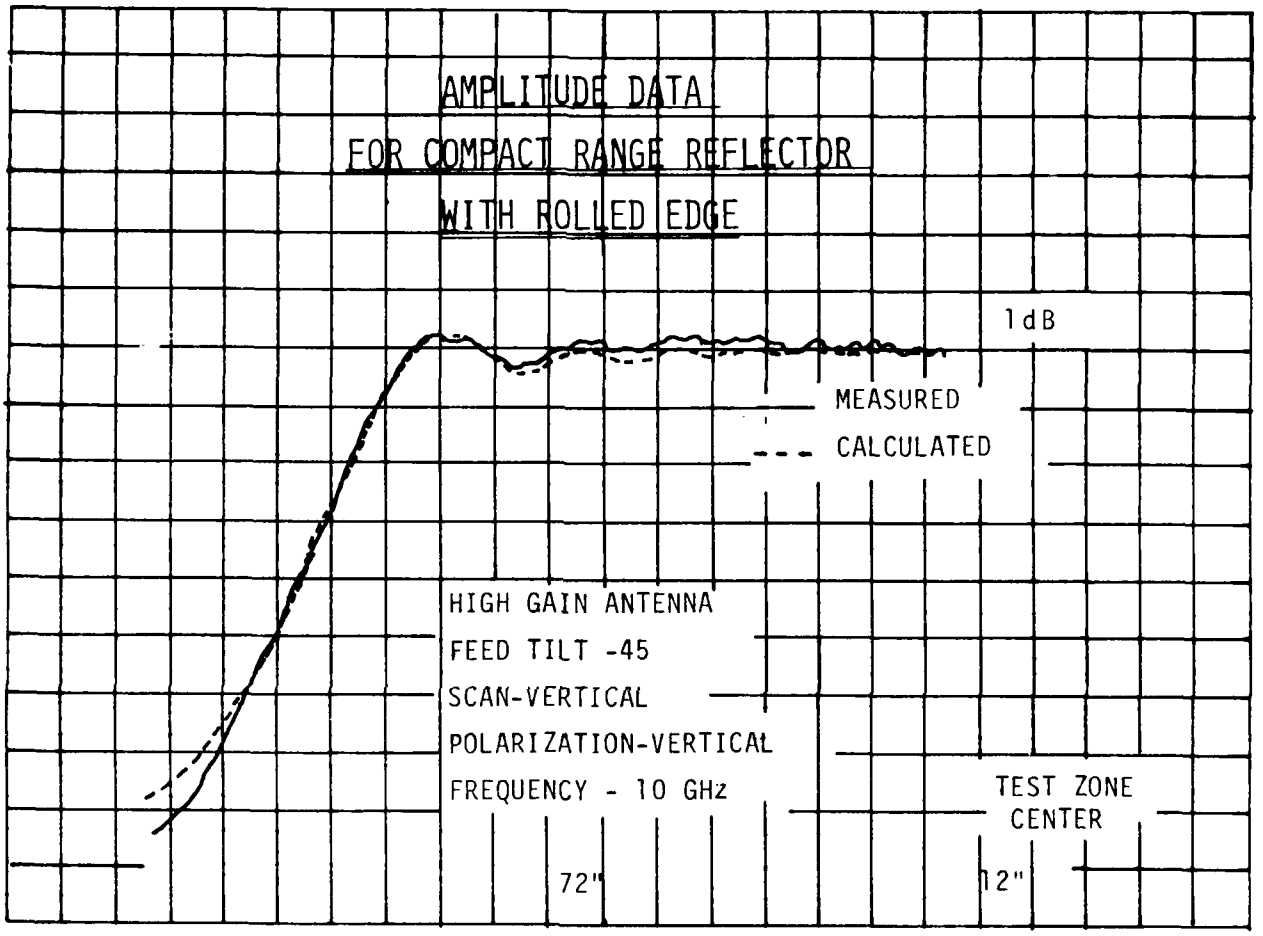


Figure 32. Amplitude Field Probe Taken Across a Modified Curved Edge Treatment (Measurements Compared to Moment Method Calculations at 10. GHz)

profile after the installation of the curved edge modification. Clearly, curved edge treatments will eventually be required around the entire circumference of the AFWAL reflector. For the present time, the feed antennas used will not strongly illuminate the exposed edges. Although this reduces somewhat the effective "target or test zone" region, it is a compromise AFWAL must live with until the curved modifications can be fabricated.

With the entire reflector rim treated, OSU and NASA have conclusively demonstrated the ability of the compact range to make accurate indoor RCS measurements on physically large targets. Once the AFWAL range incorporates these improvements, it should be one of the three finest indoor RCS measurement ranges in the entire country, and a real asset to the Air Force Avionics Laboratory.

SECTION IV

CONCLUSIONS

The objective of this investigation was to present an alternative method of creating and verifying a space limited far field environment for radiation and scattering measurements. This was accomplished and successfully demonstrated through the use of a compact range measurement facility. We found that a compact range accurately produces a very large plane wave measurement area, on the order of 5' by 5'. To verify the planarity of the quiet zone, a microwave probe was used to sample the aperture field amplitude and phase with respect to a known reference. The amplitude and phase distribution across the quiet zone (5 ft. x 5 ft.) has far exceeded the far field criteria of +/-0.5 dB taper and +/-22.5 degrees taper respectively from 8.2 - 26.0 GHz.

In a future report, the installation of the modified edge treatments will be discussed. In addition, actual RCS measurements will be presented on a number of "standard" targets. These targes will be compared to both theoretical values as well as RCS measurements performed on our normal "far field" range, when appropriate.

REFERENCES

1. Robert B. Leighton, "A 10 Meter Telescope for Millimeter and Sub-Millimeter Astronomy" Final Technical Report for National Science Foundation Grant AST 73-04908, May 1978.

2. W. D. Burnside, M. C. Gilreath, B. M. Kent," Rolled Edge Modification of a Compact Range Reflector", Symposium Notes, Antenna Measurement Techniques Association, October 1-2, 1984, San Diego, California.

APPENDIX

Complete Set of Field Probe Measurements as Specified by Table 1.

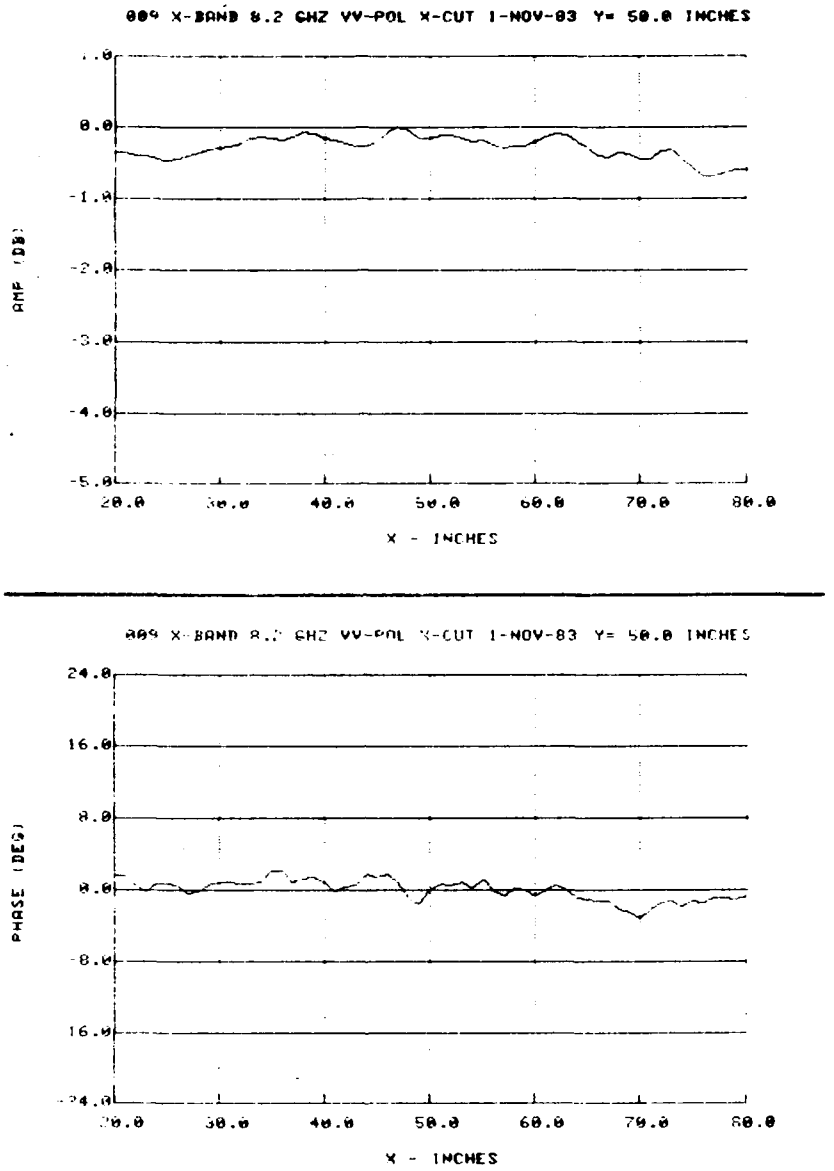


Figure A.1. X-Plane Amplitude and Phase Field Probe Plot Taken at 8.2 GHz, V-Polarization, Using the Horn Probe

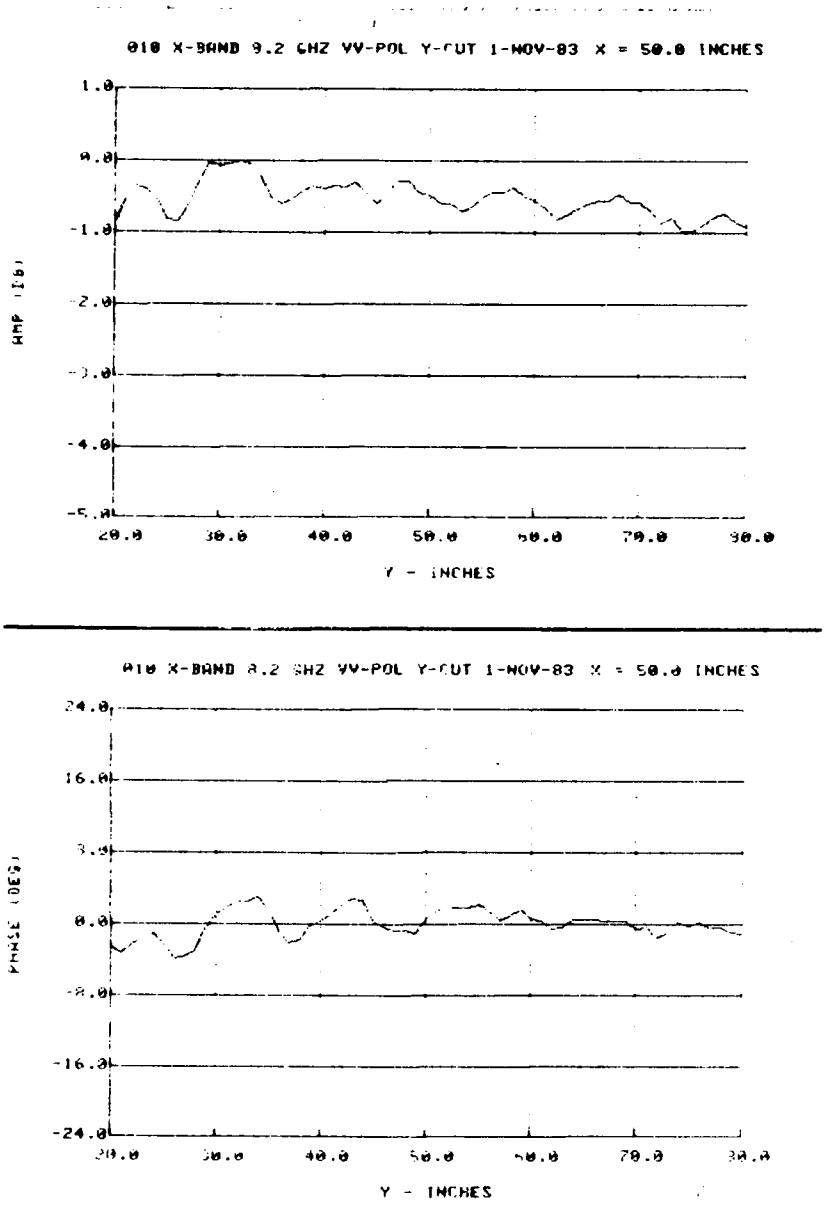


Figure A.2. Y-Plane Amplitude and Phase Field Probe Plot Taken at 8.2 GHz, V-Polarization, Using the Horn Probe

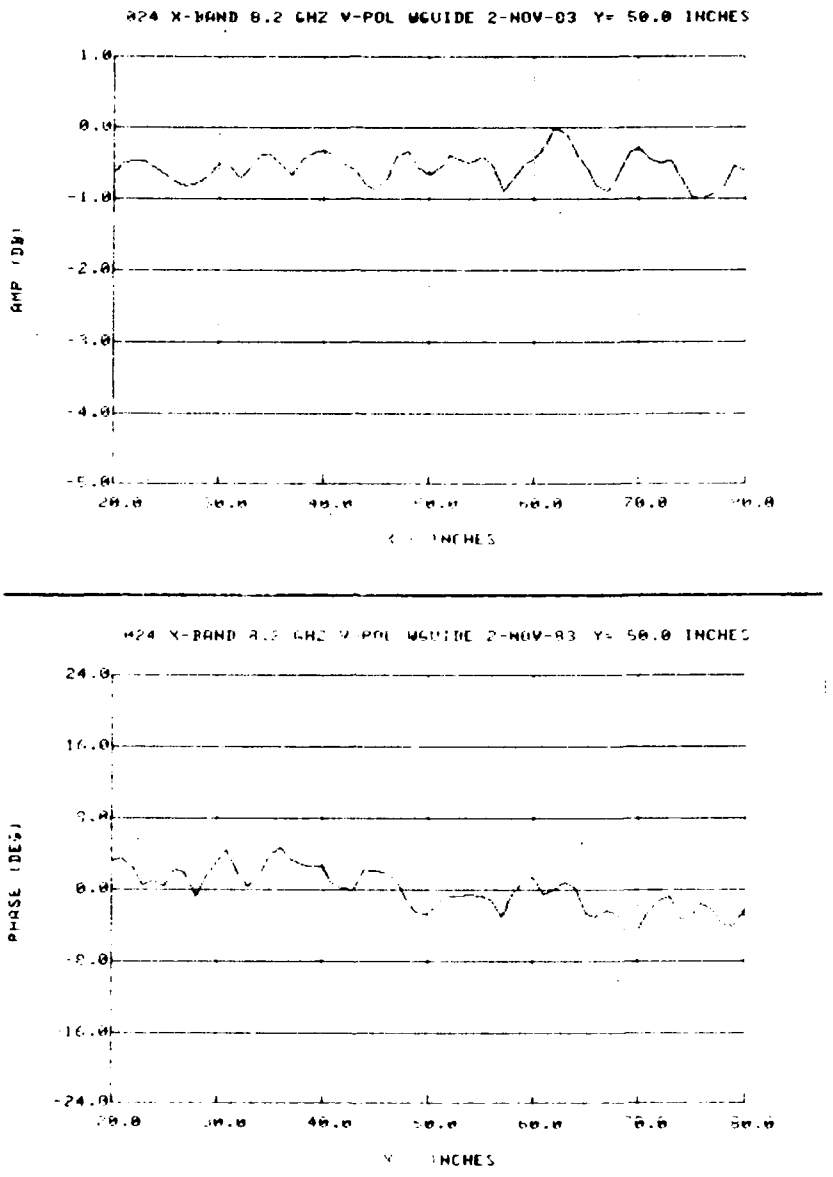


Figure A.3. X-Plane Amplitude and Phase Field Probe Plot Taken at 8.2 GHz, V-Polarization, Using the Waveguide Probe

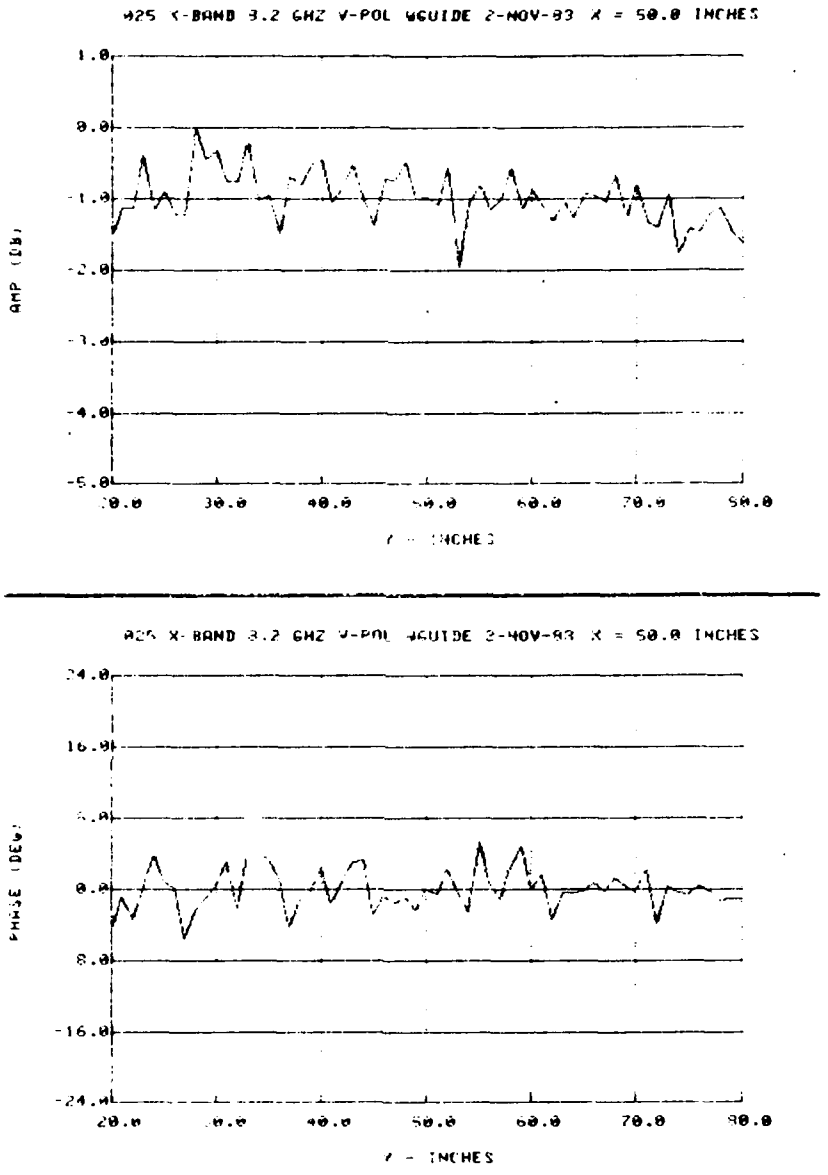


Figure A.4. Y-Plane Amplitude and Phase Field Probe Plot Taken at 8.2 GHz, V-Polarization, Using the Waveguide Probe

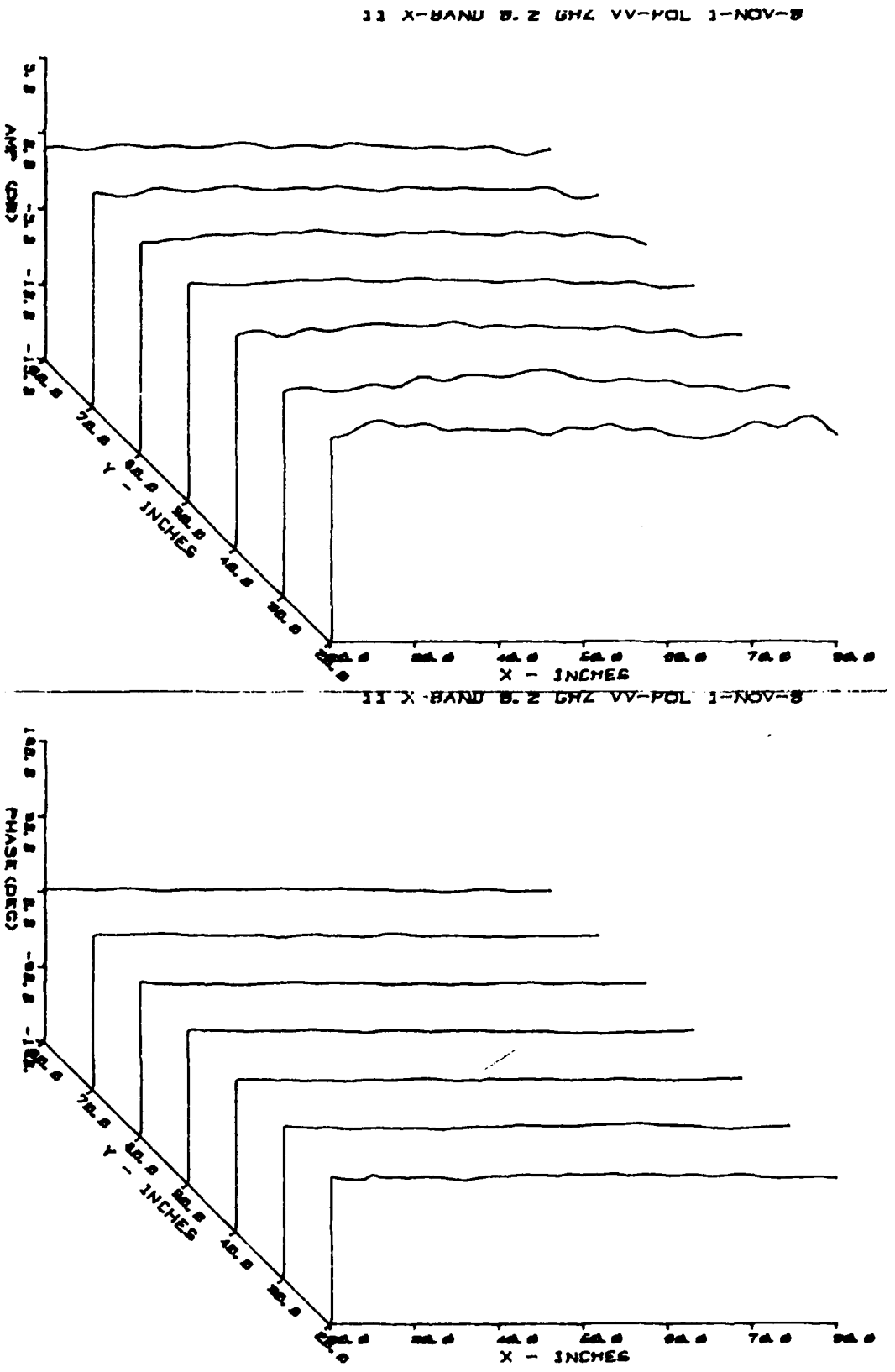


Figure A.5. 3D X-Plane Amplitude and Phase Field Probe Plot Taken at 8.2 GHz, V-Polarization, Using the Horn Probe

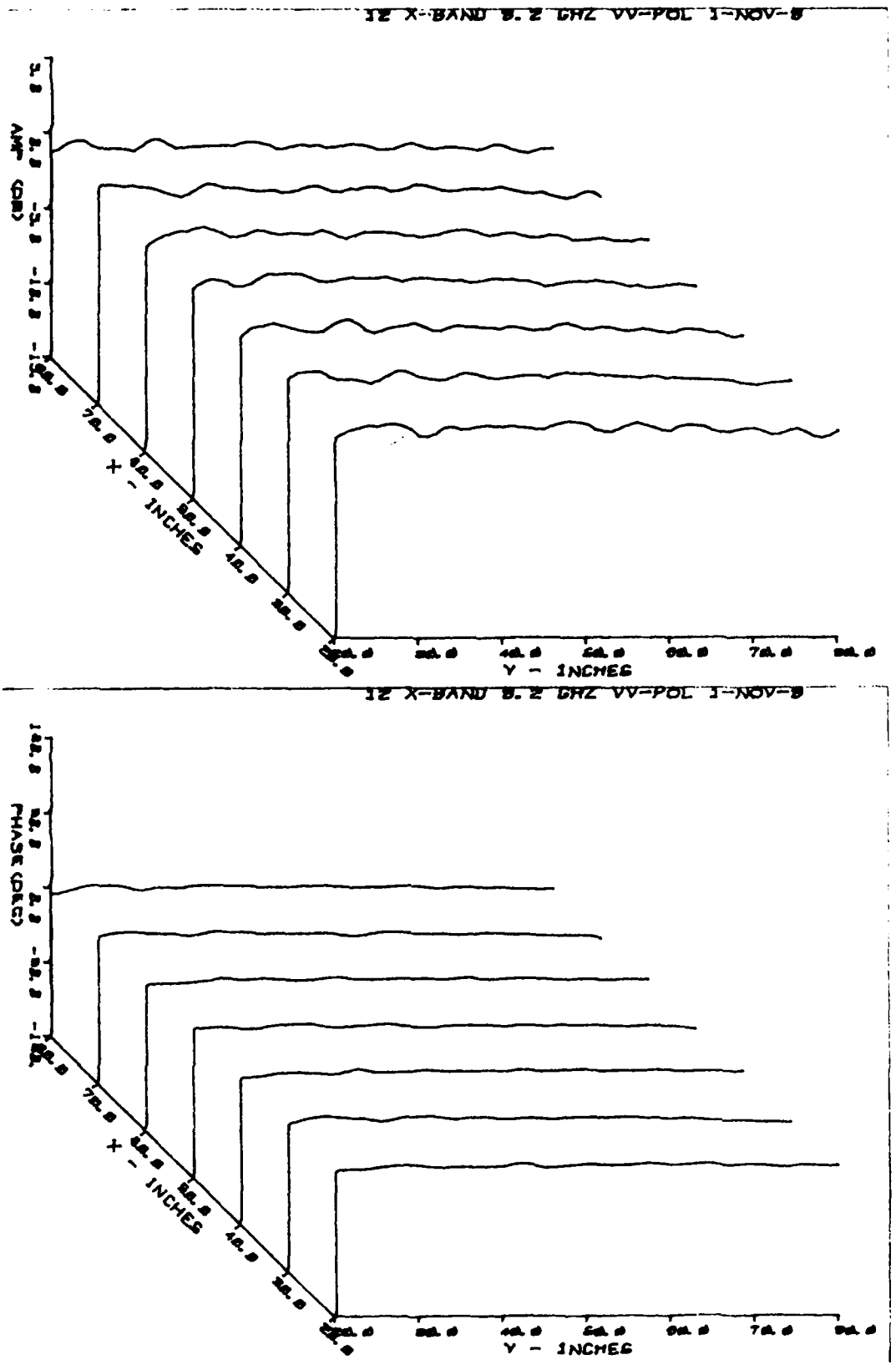


Figure A.6. 3D Y-Plane Amplitude and Phase Field Probe Plot Taken at 8.2 GHz, V-Polarization, Using the Horn Probe

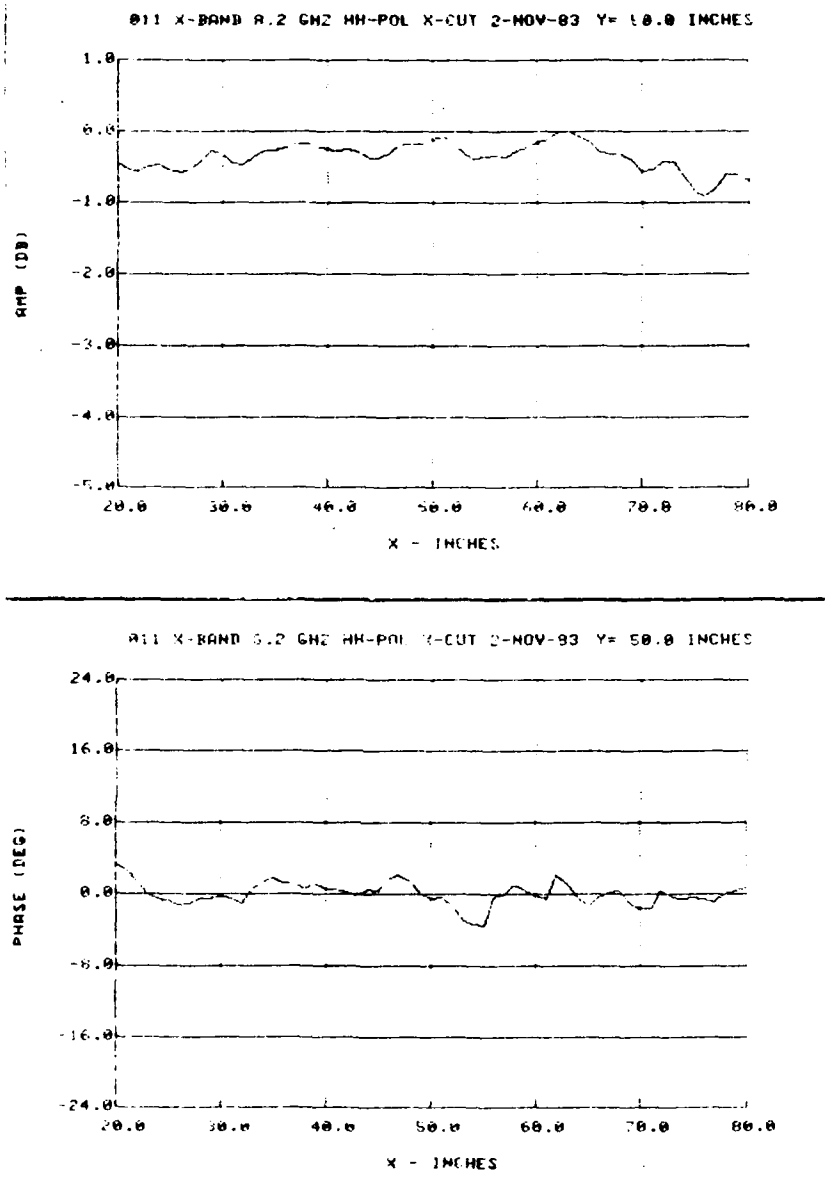


Figure A.7. X-Plane Amplitude and Phase Field Probe Plot Taken at 8.2 GHz, H-Polarization, Using the Horn Probe

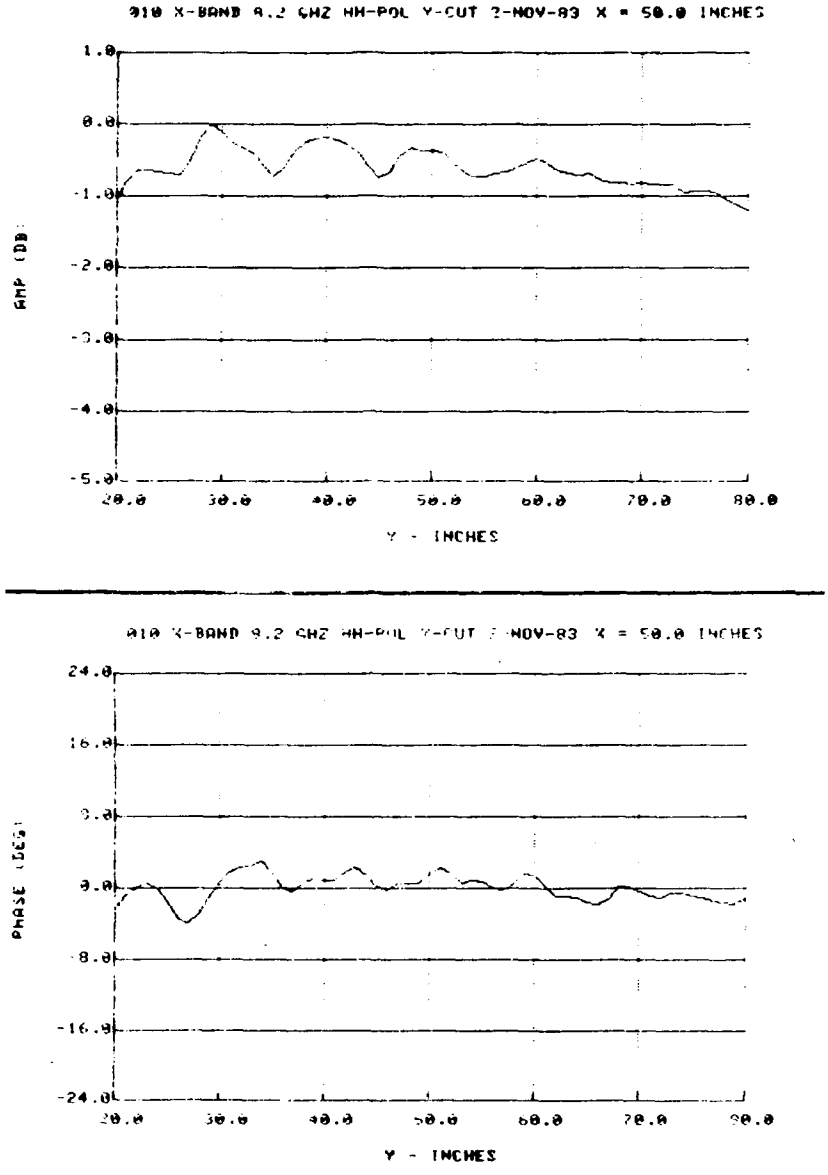


Figure A.8. Y-Plane Amplitude and Phase Field Probe Plot Taken at 8.2 GHz, H-Polarization, Using the Horn Probe

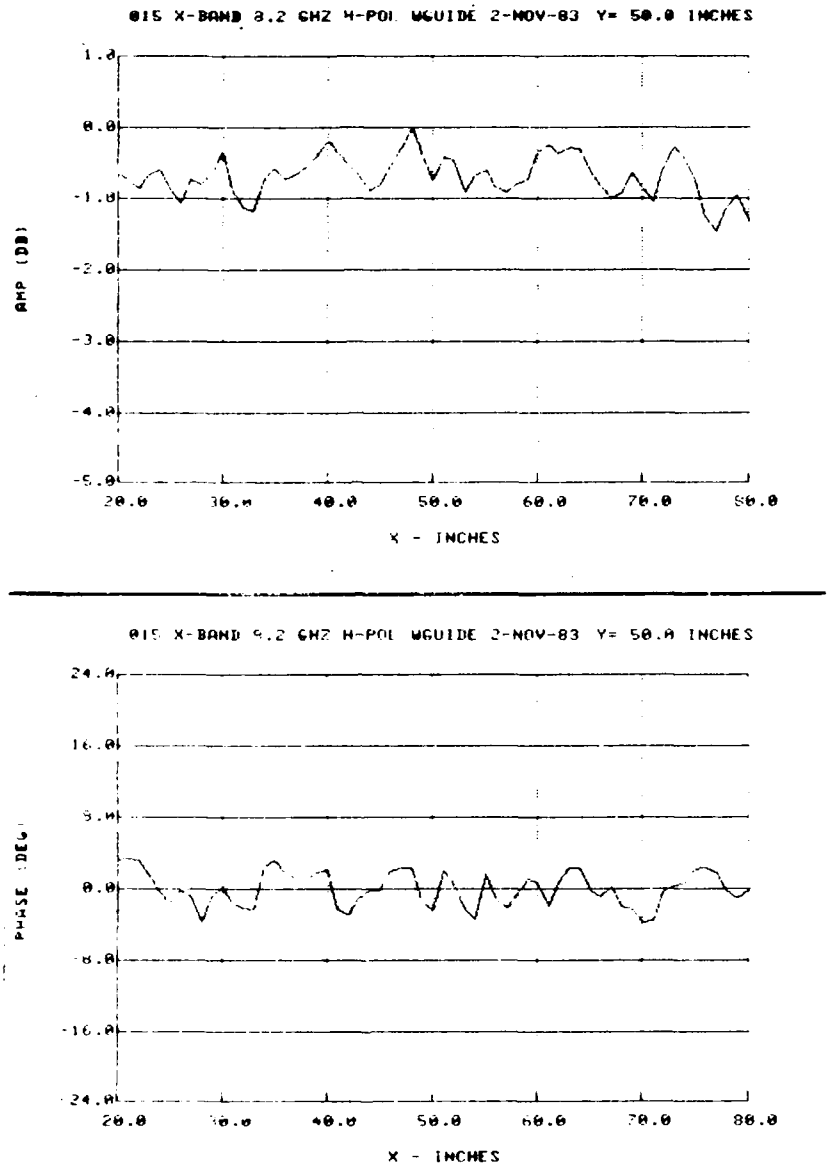


Figure A.9. X-Plane Amplitude and Phase Field Probe Plot Taken at 8.2 GHz, H-Polarization, Using the Waveguide Probe

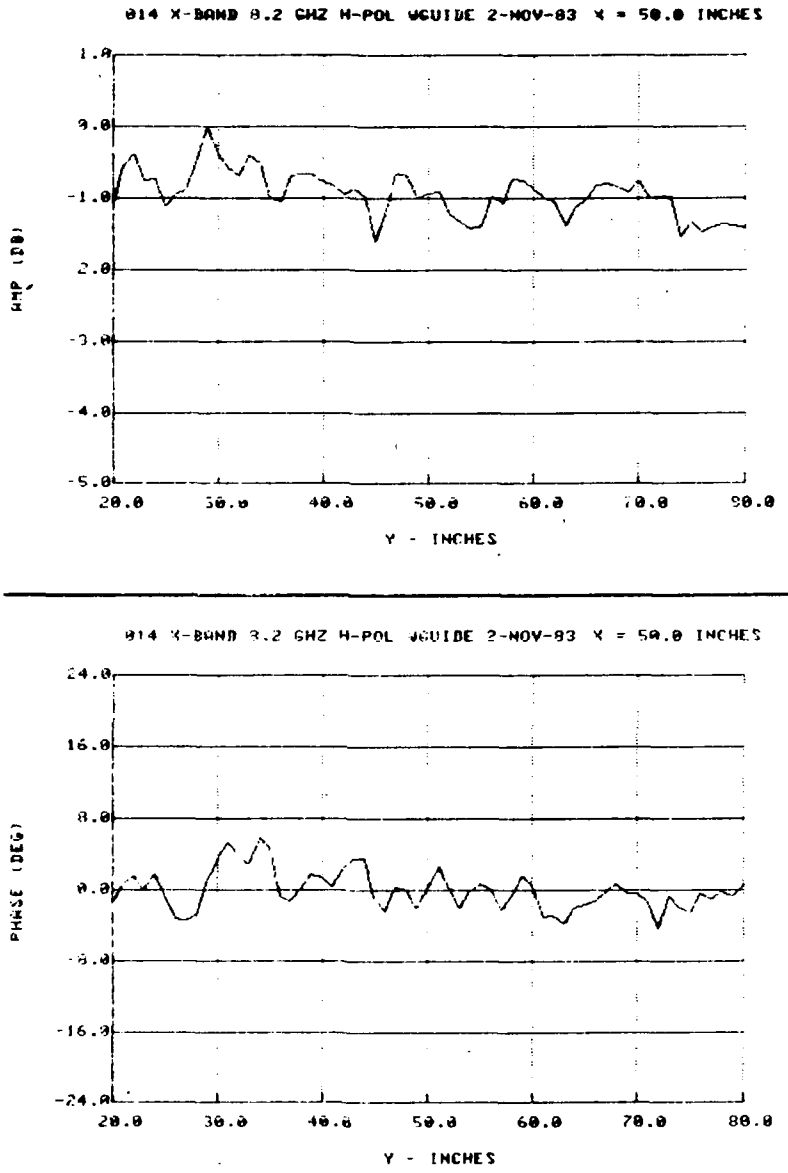


Figure A.10. Y-Plane Amplitude and Phase Field Probe Plot Taken at 8.2 GHz, H-Polarization, Using the Waveguide Probe

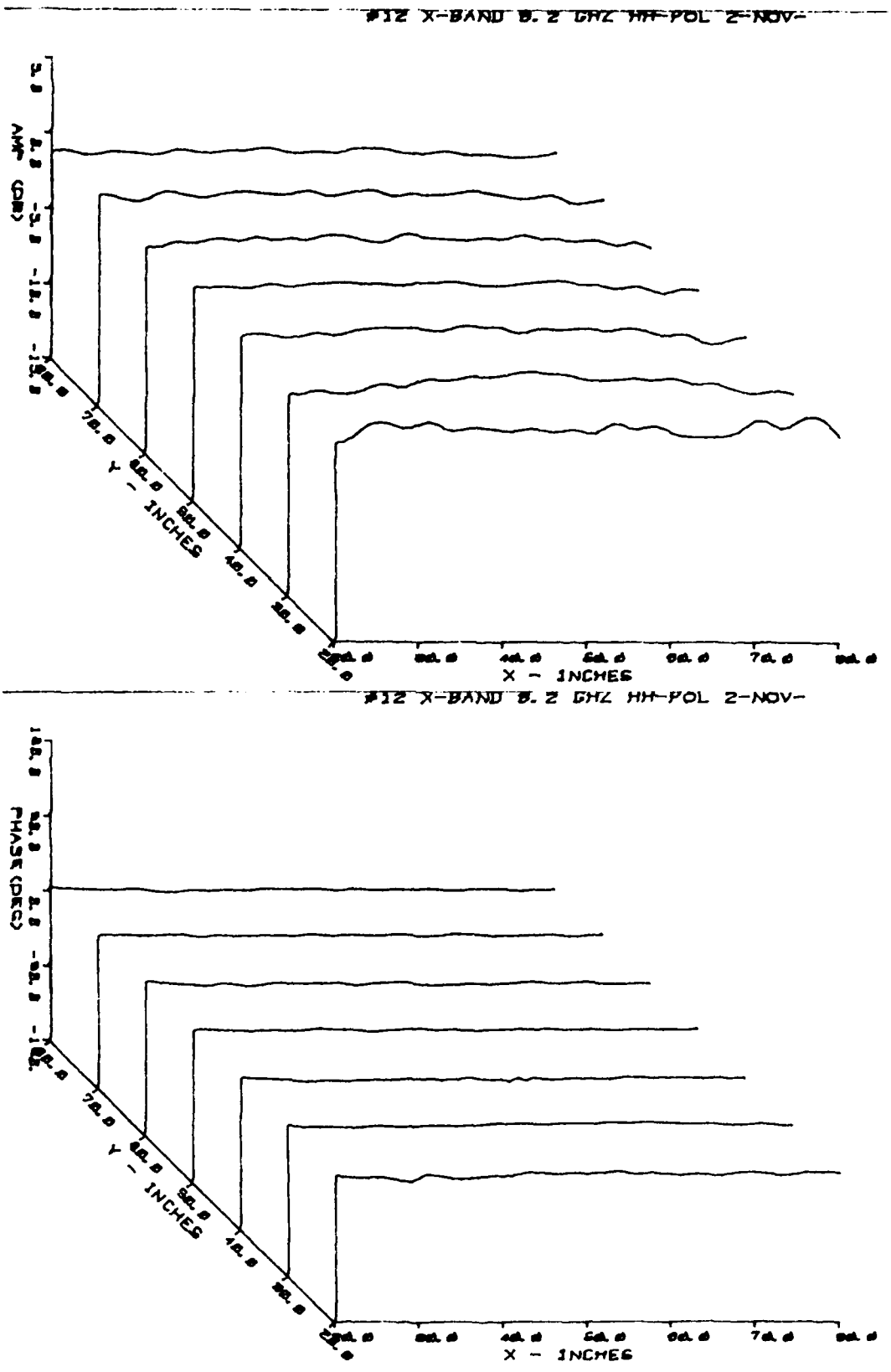


Figure A.11. 3D X-Plane Amplitude and Phase Field Probe Plot Taken at 8.2 GHz, H-Polarization, Using the Horn Probe

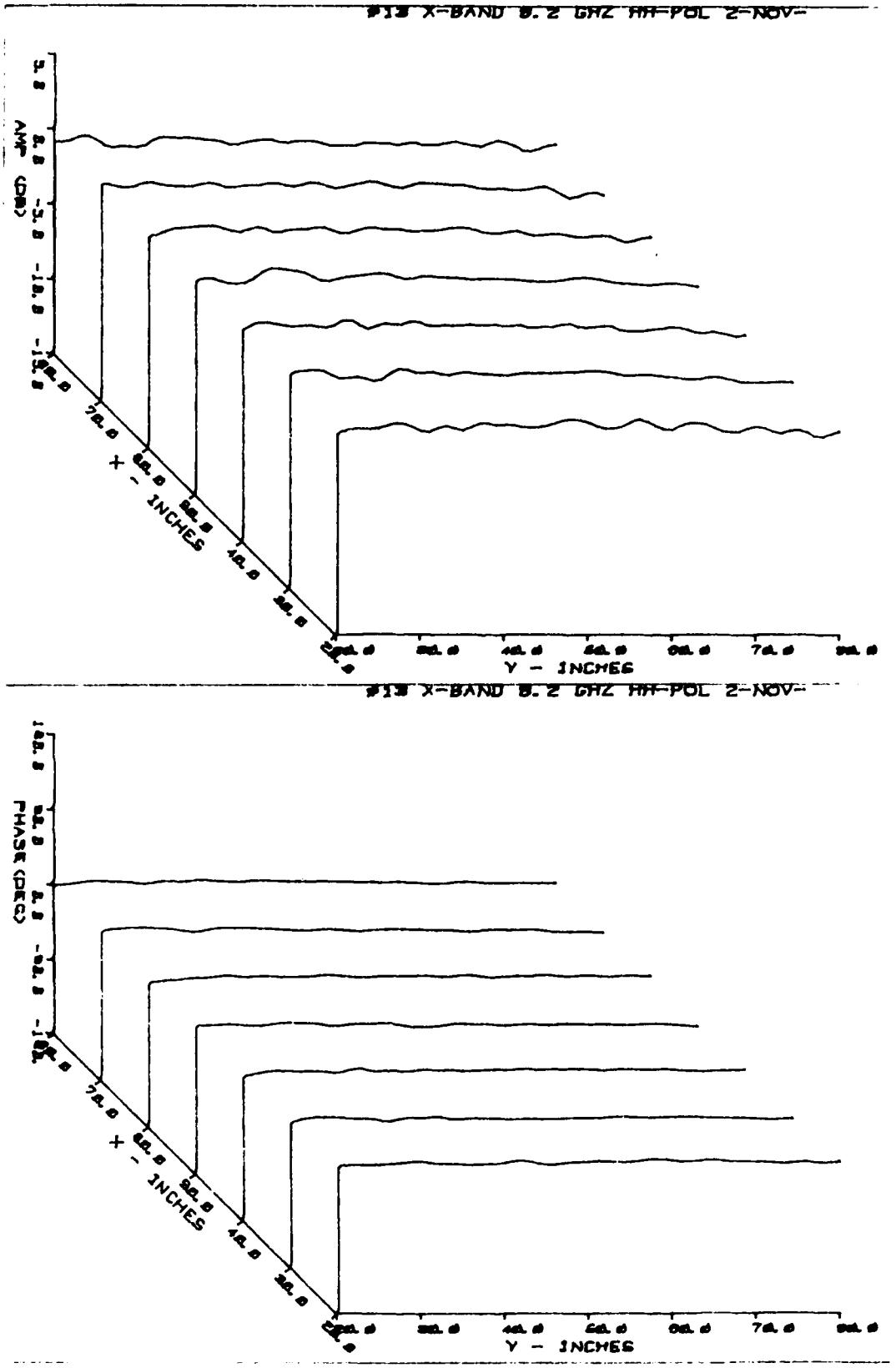


Figure A.12. 3D Y-Plane Amplitude and Phase Field Probe Plot Taken at 8.2 GHz, H-Polarization, Using the Horn Probe

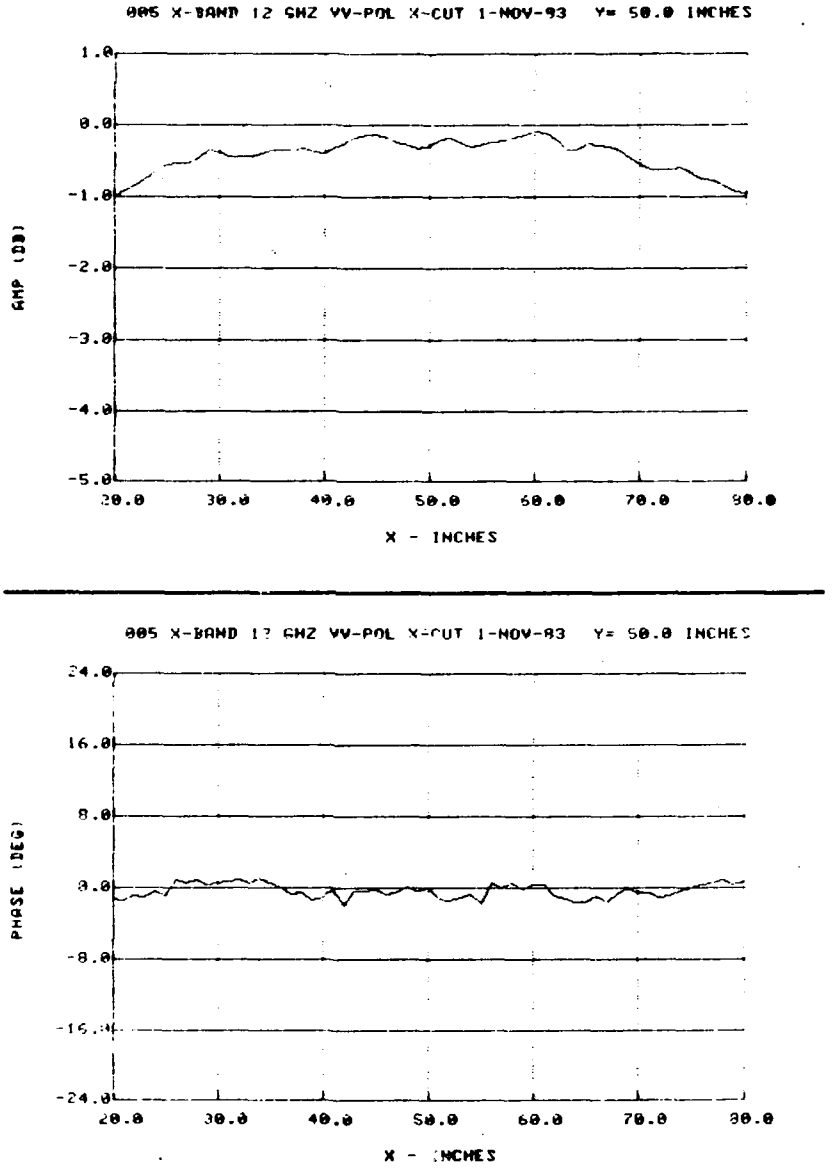


Figure A.13. X-Plane Amplitude and Phase Field Probe Plot Taken at 12.0 GHz, V-Polarization, Using the Horn Probe

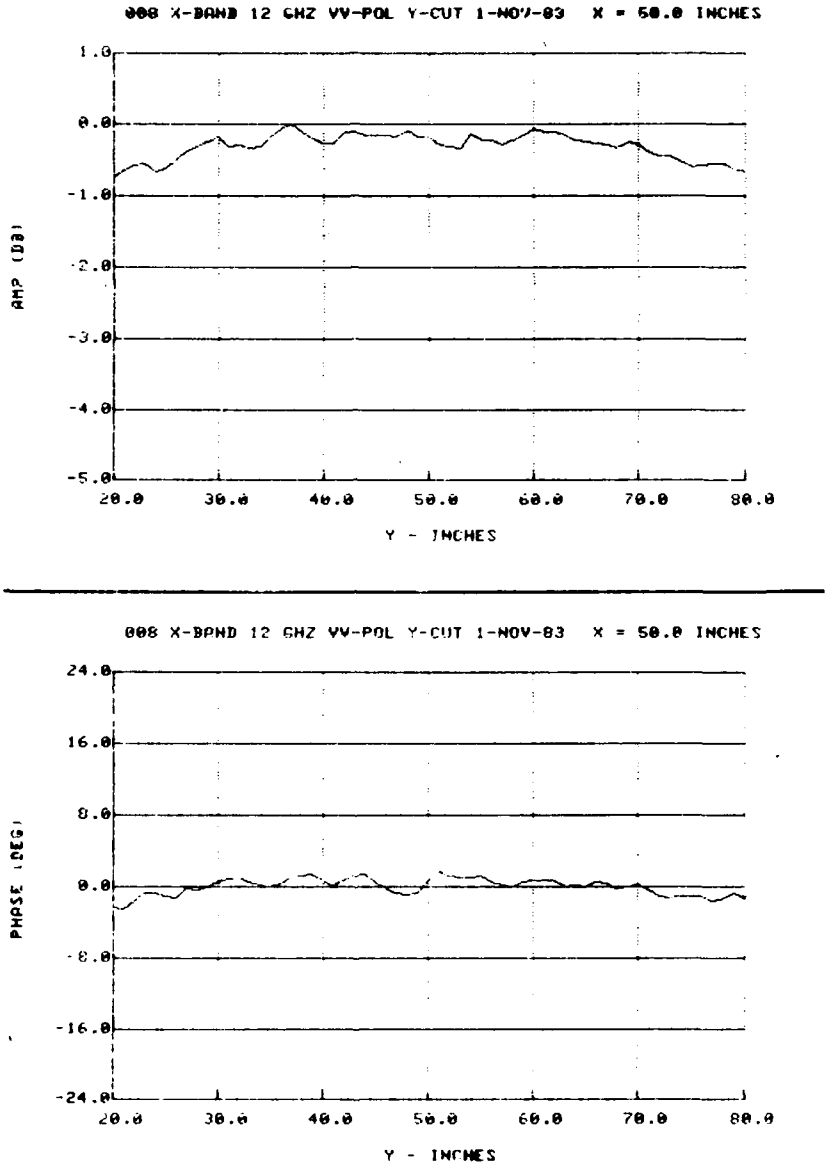


Figure A.14. Y-Plane Amplitude and Phase Field Probe Plot Taken at 12.0 GHz, V-Polarization, Using the Horn Probe

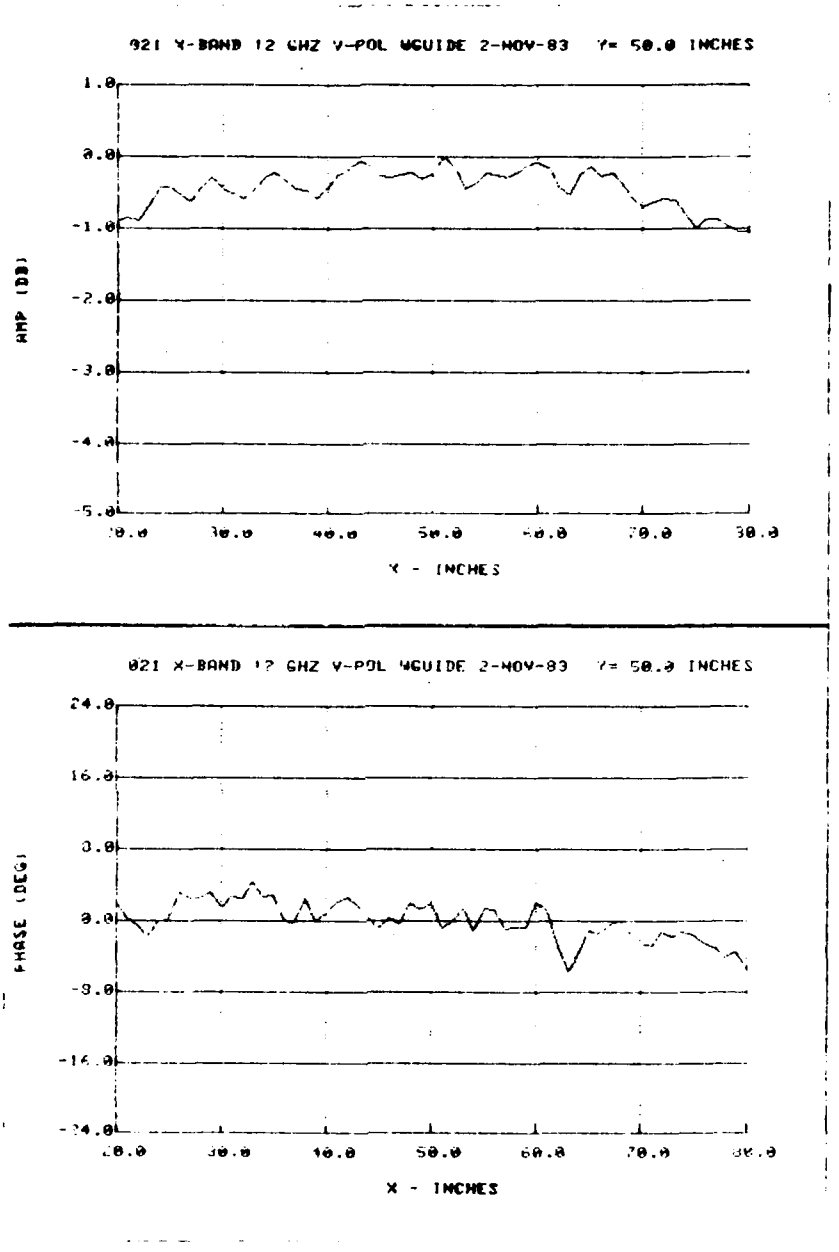


Figure A.15. X-Plane Amplitude and Phase Field Probe Plot Taken at 12.0 GHz, V-Polarization, Using the Waveguide probe

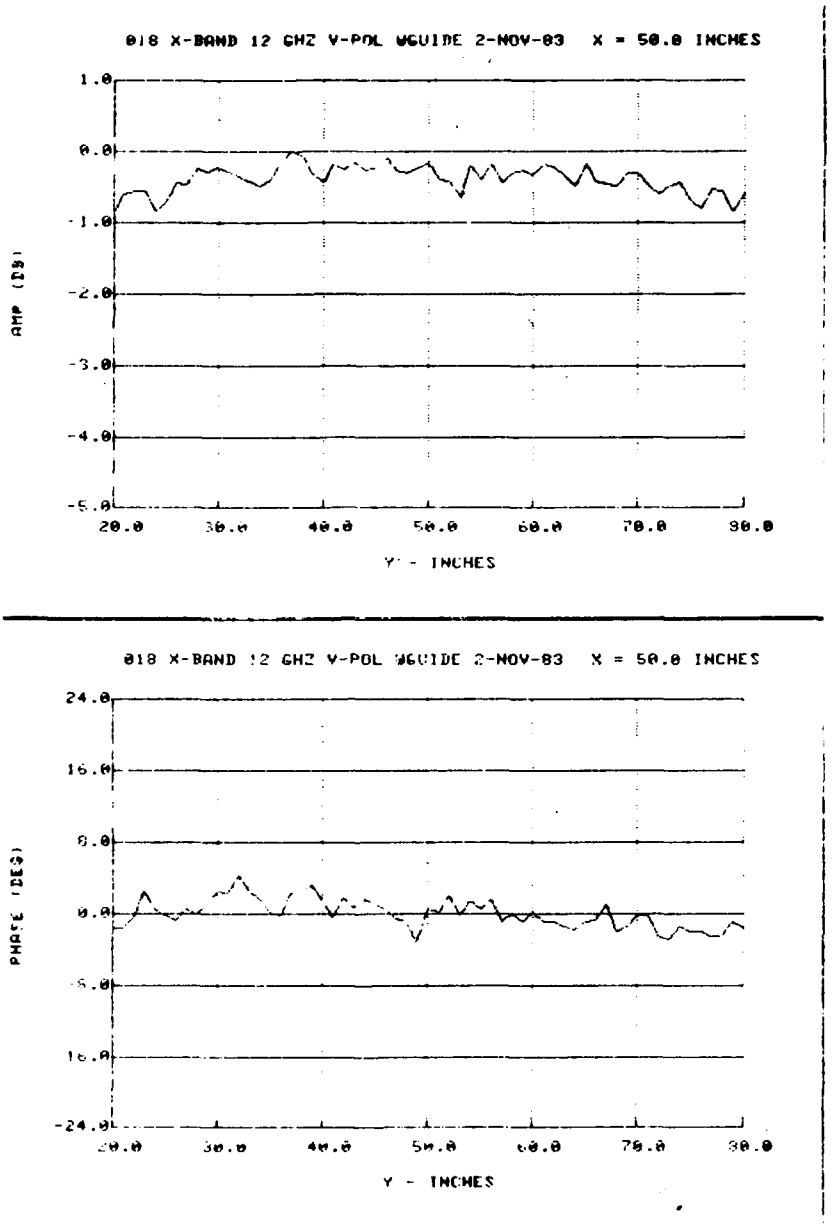


Figure A.16. Y-Plane Amplitude and Phase Field Probe Plot Taken at 12.0 GHz, V-Polarization, Using the Waveguide Probe

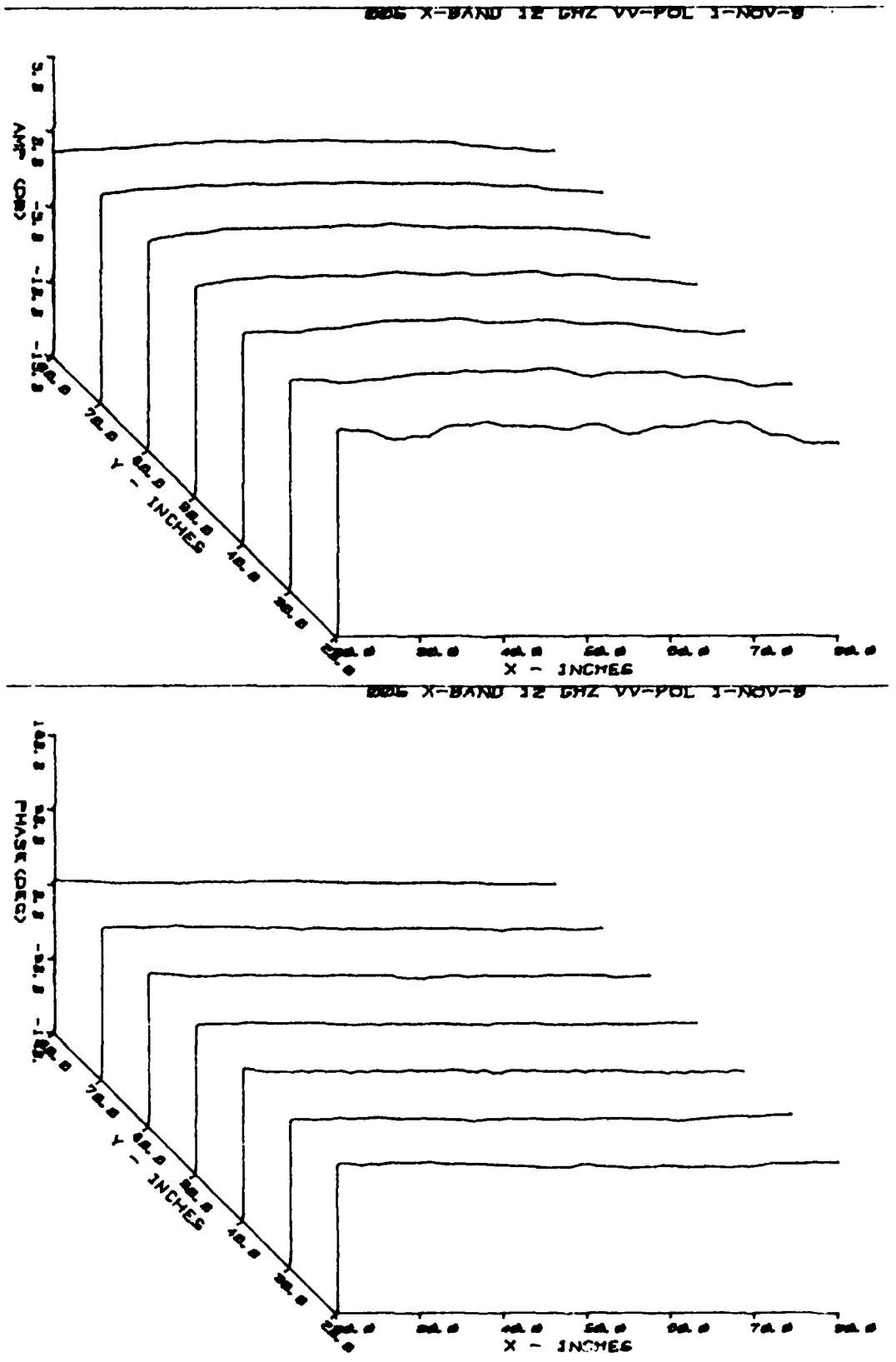


Figure A.17. 3D Y-Plane Amplitude and Phase Field Probe Plot Taken at 12.0 GHz, V-Polarization, Using the Horn Probe

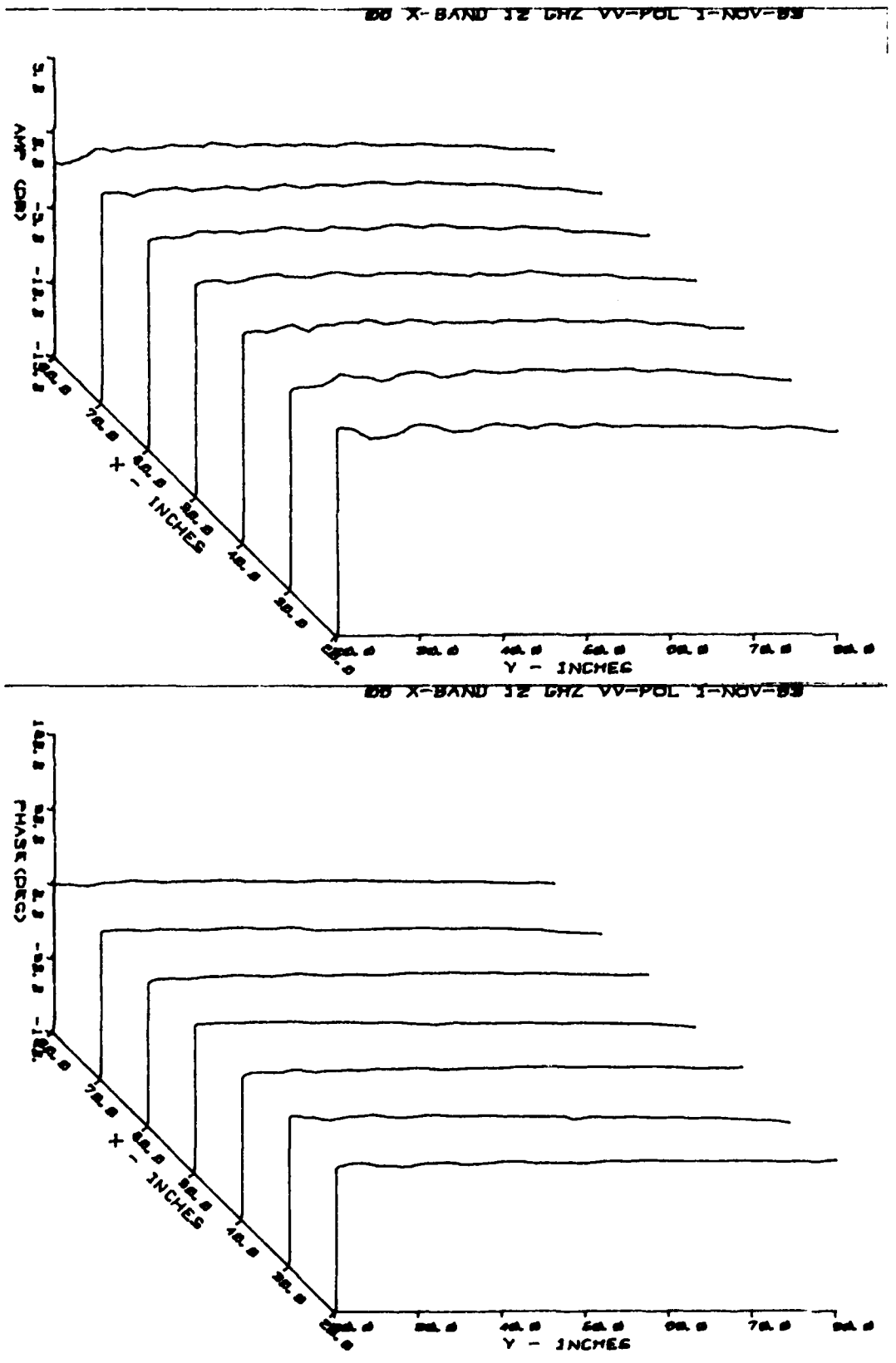


Figure A.18. 3D Y-Plane Amplitude and Phase Field Probe Plot Taken at 12.0 GHz, V-Polarization, Using the Horn Probe

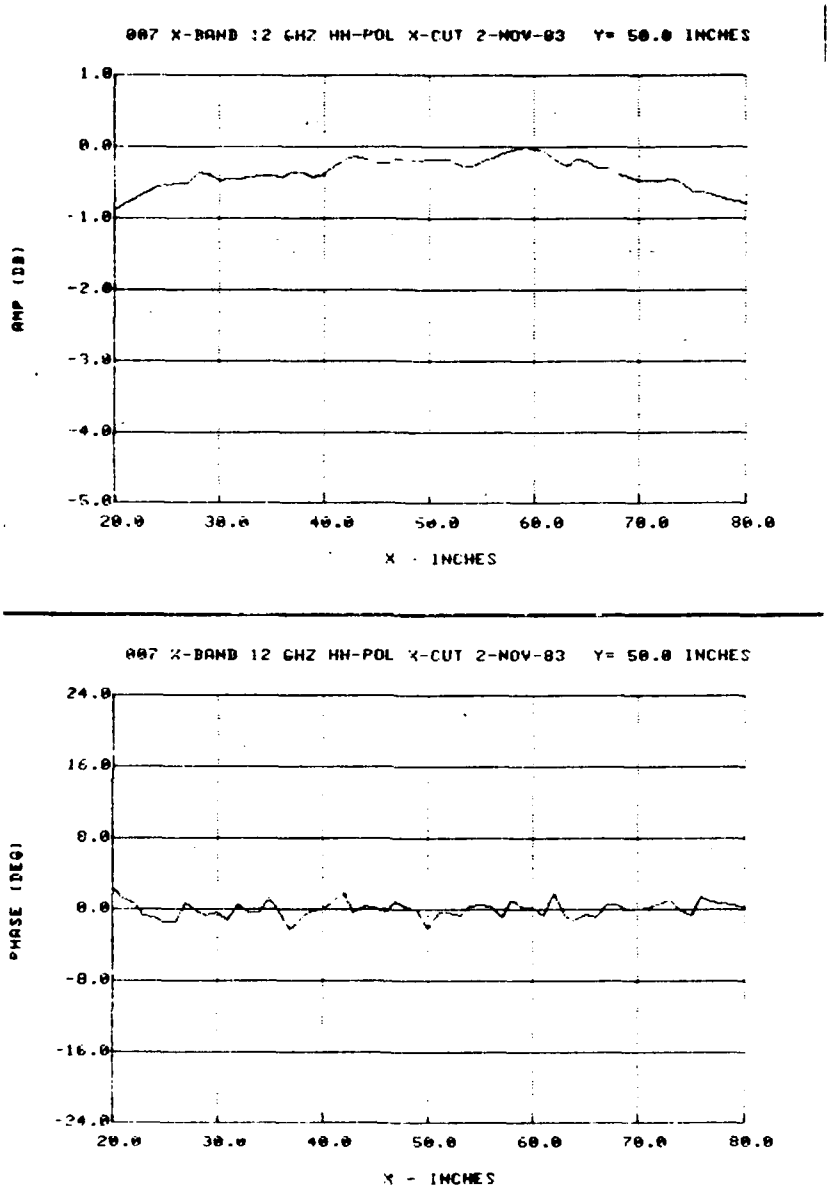


Figure A.19. X-Plane Amplitude and Phase Field Probe Plot Taken at 12.0 GHz, H-Polarization, Using the Horn Probe

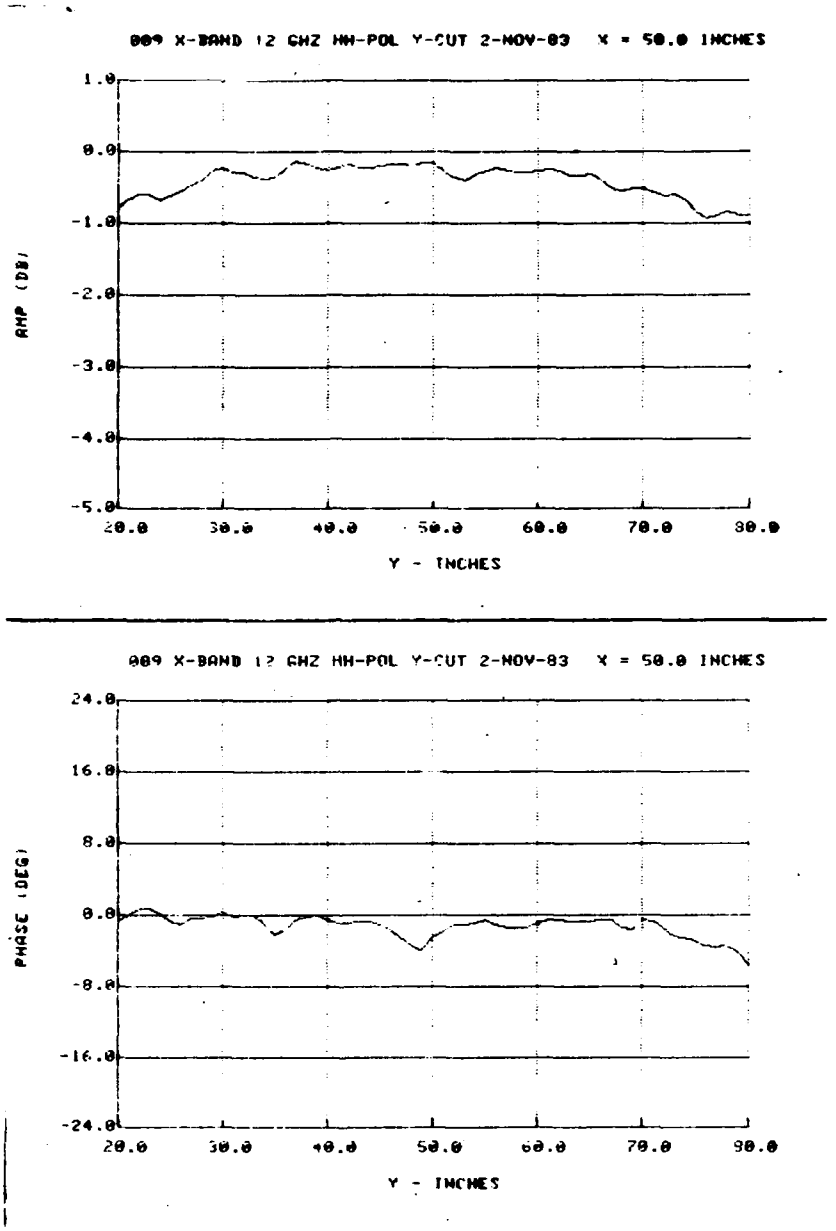


Figure A.20. Y-Plane Amplitude and Phase Field Probe Plot Taken at 12.0 GHz, H-Polarization, Using the Horn Probe

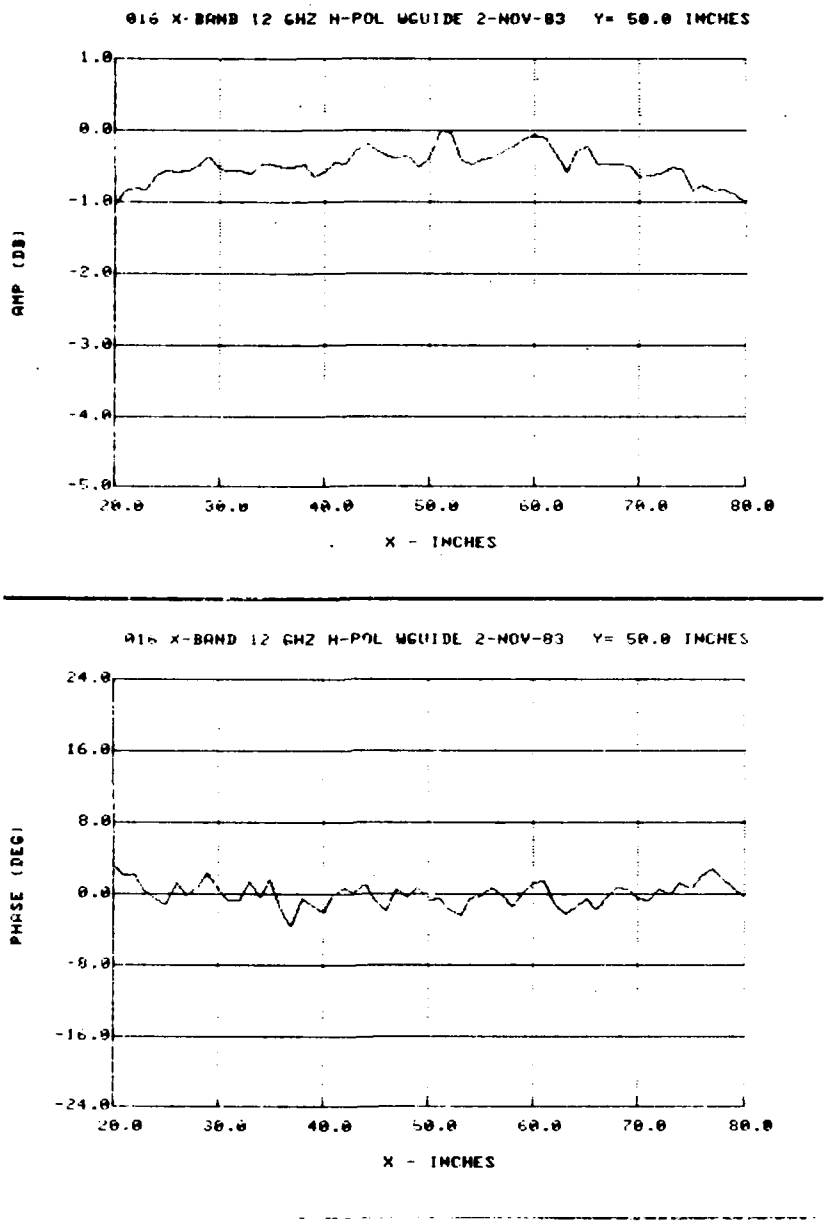


Figure A.21. X-Plane Amplitude and Phase Field Probe Plot Taken at 12.0 GHz, H-Polarization, Using the Waveguide Probe

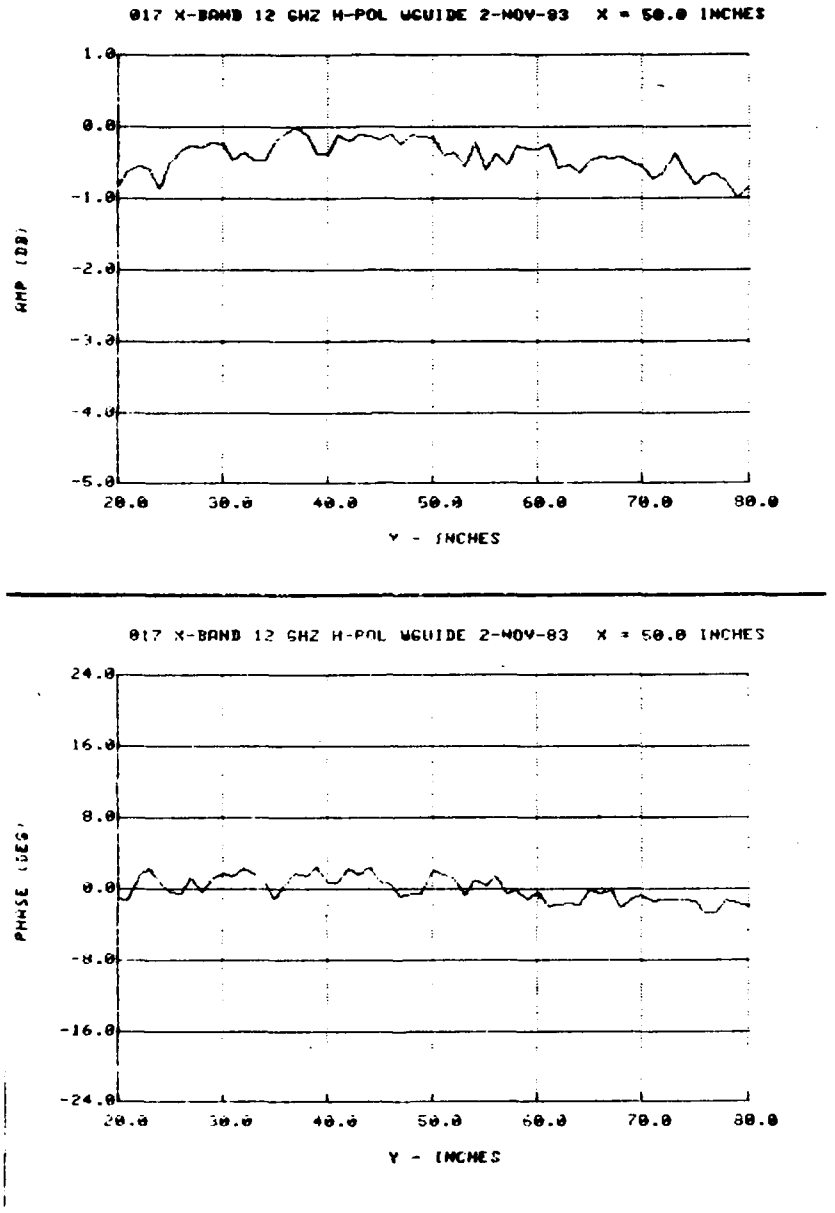


Figure A.22. Y-Plane Amplitude and Phase Field Probe Plot Taken at 12.0 GHz, H-Polarization, Using the Waveguide Probe

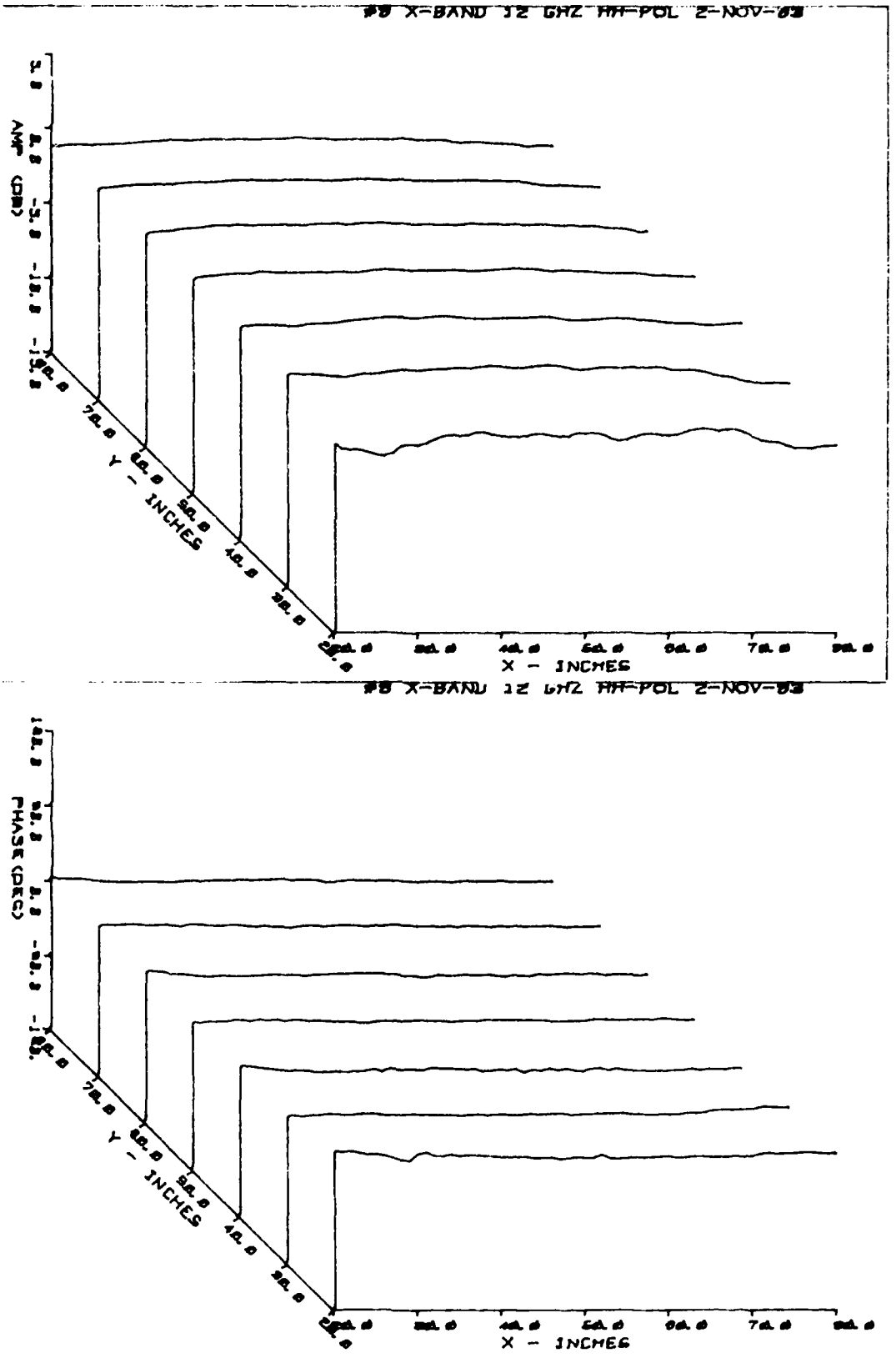


Figure A.23. 3D X-Plane Amplitude and Phase Field Probe Plot Taken at 12.0 GHz, H-Polarization, Using the Horn Probe

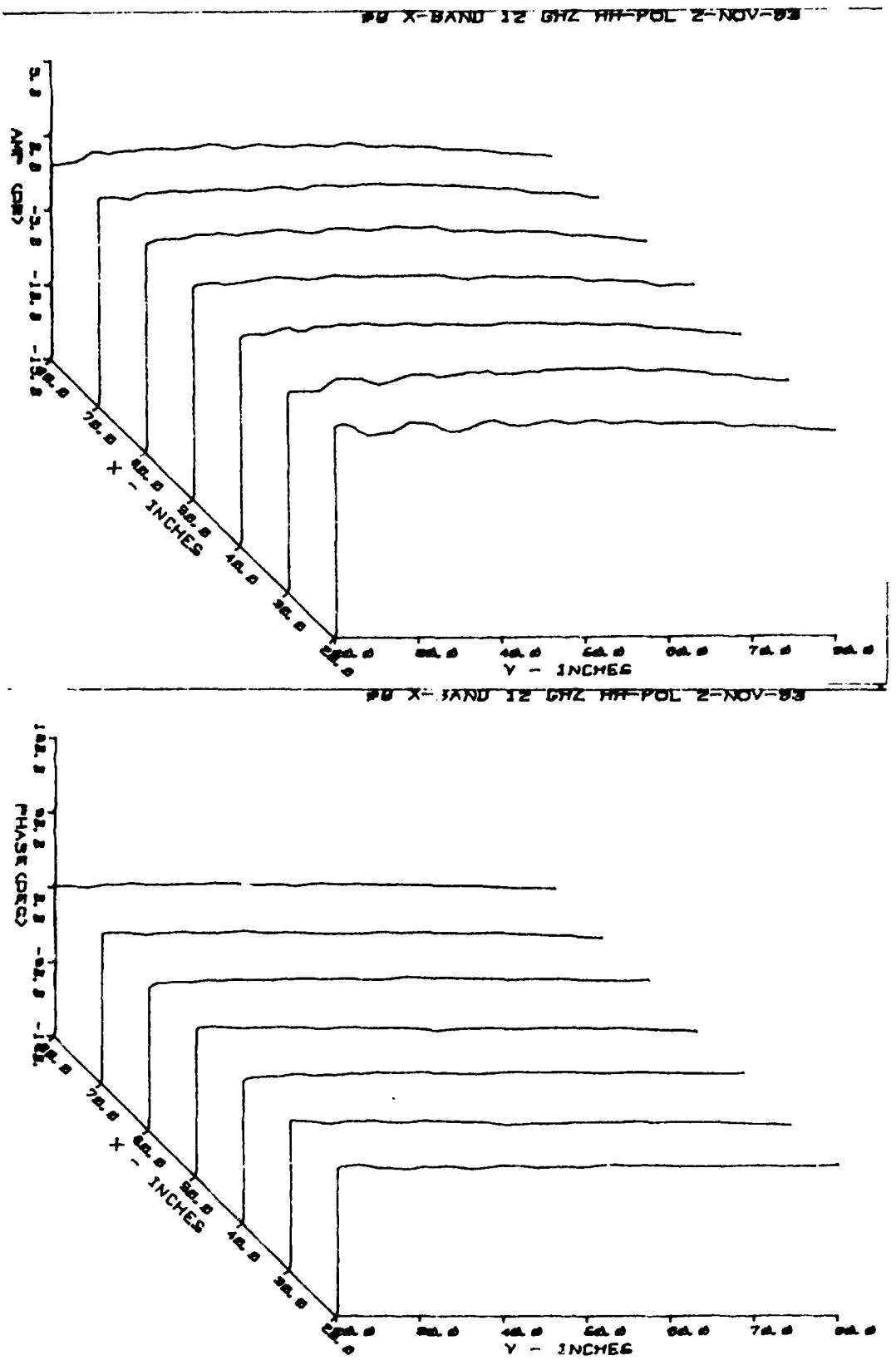


Figure A.24. 3D Y-Plane Amplitude and Phase Field Probe Plot Taken at 12.0 GHz, H-Polarization, Using the Horn Probe

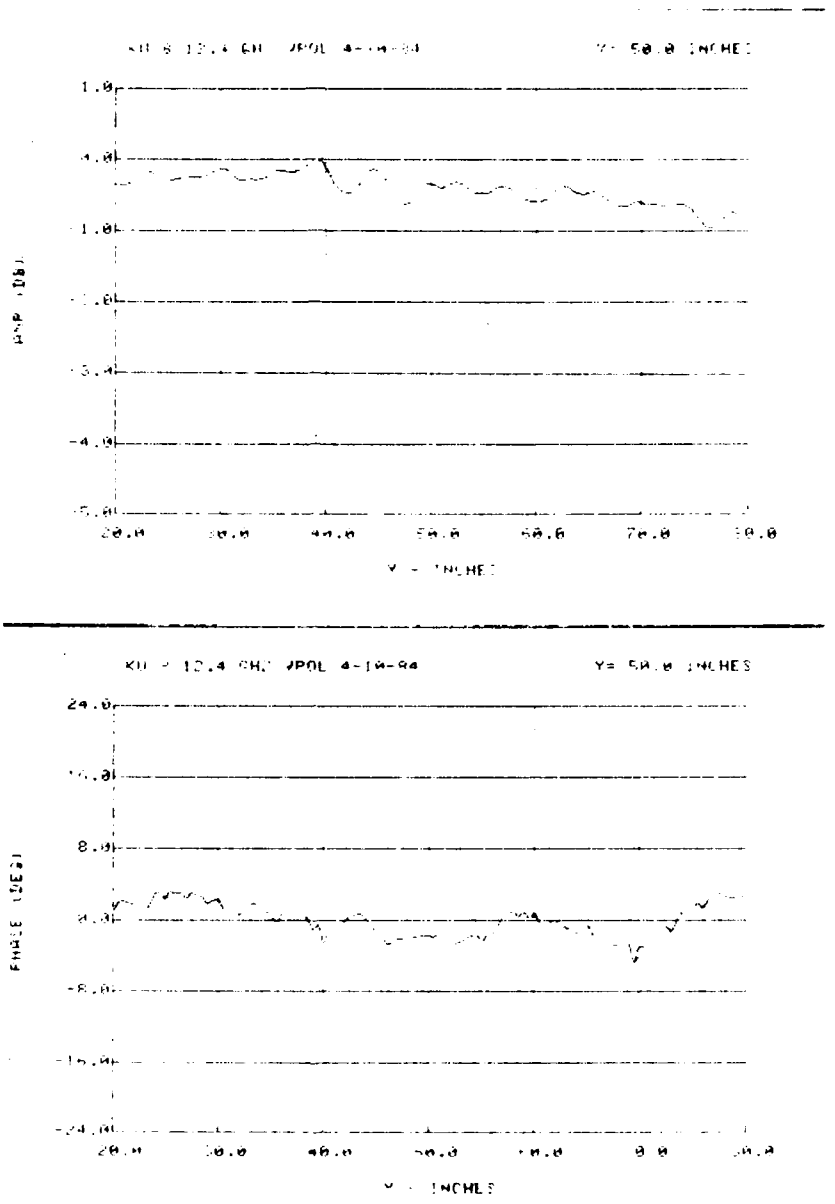


Figure A.25. X-Plane Amplitude and Phase Field Probe Plot Taken at 12.4 GHz, V-Polarization, Using the Horn Probe

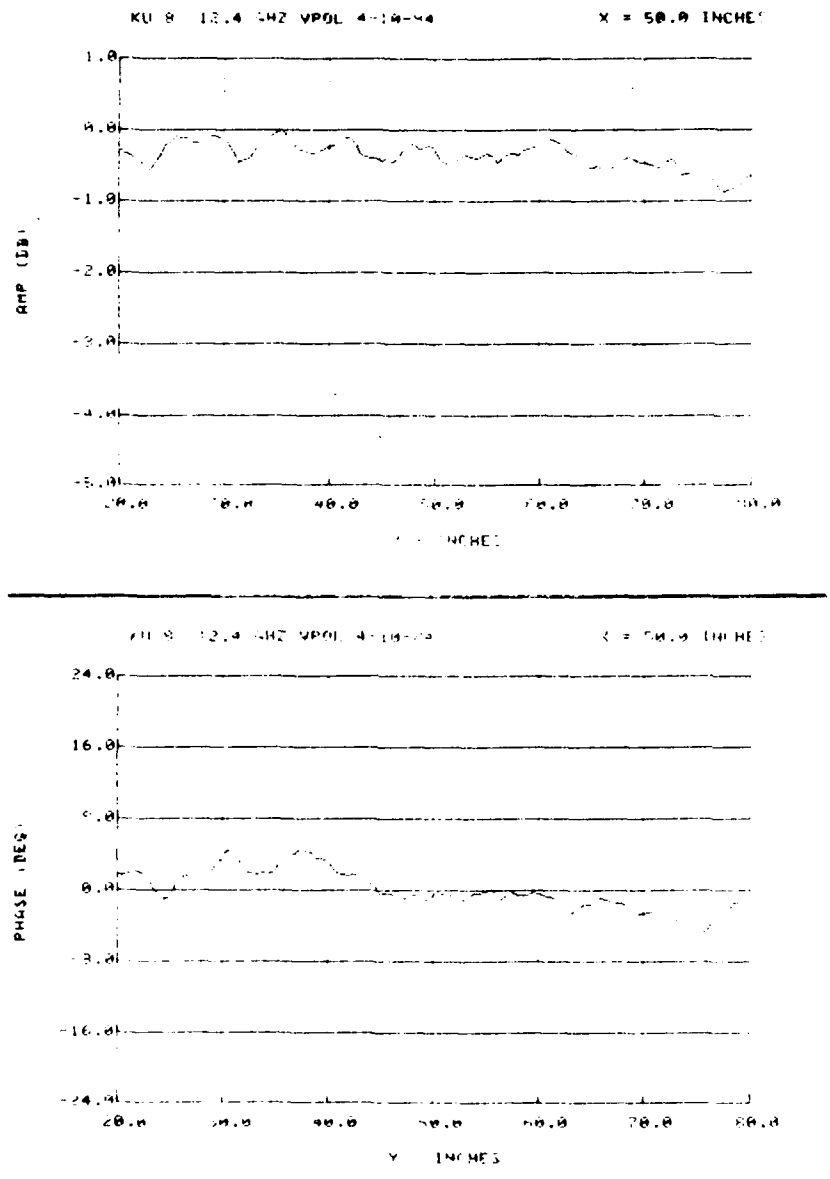


Figure A.26. Y-Plane Amplitude and Phase Field Probe Plot Taken at 12.4 GHz, V-Polarization, Using the Horn Probe

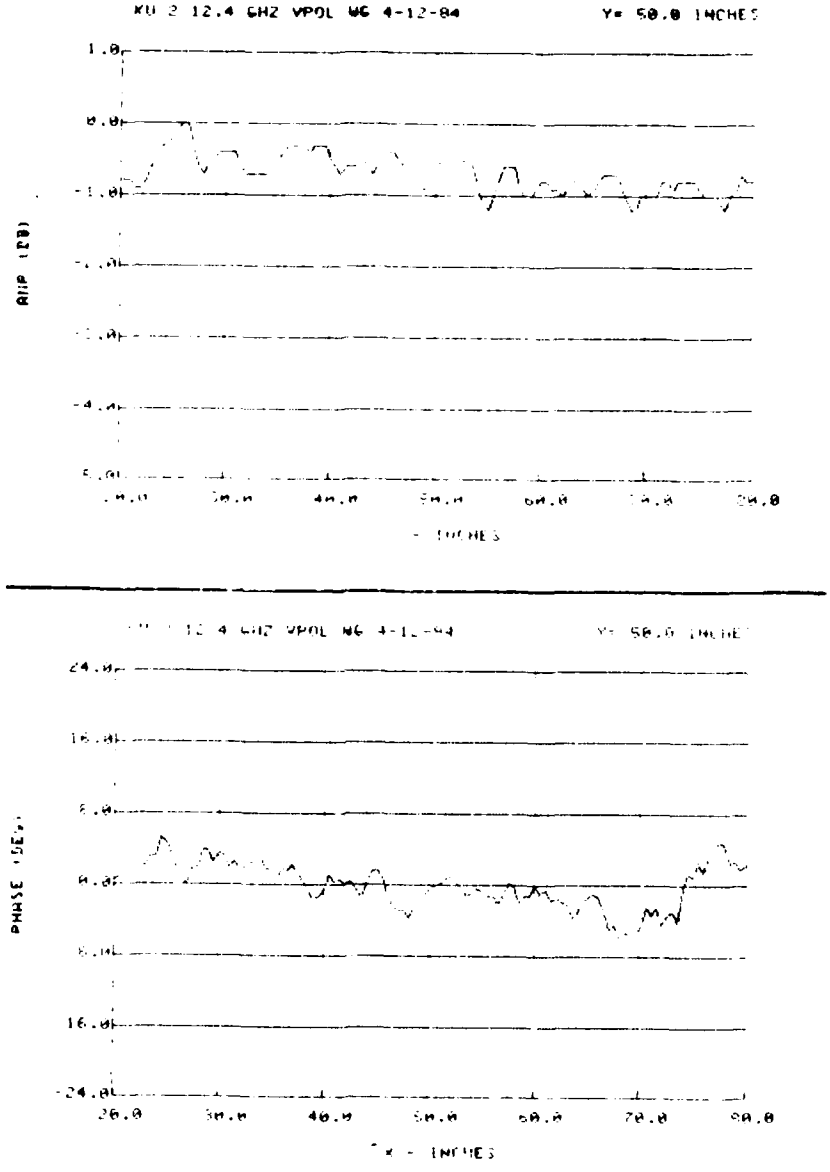


Figure A.27. X-Plane Amplitude and Phase Field Probe Plot Taken at 12.4 GHz, V-Polarization, Using the Waveguide Probe

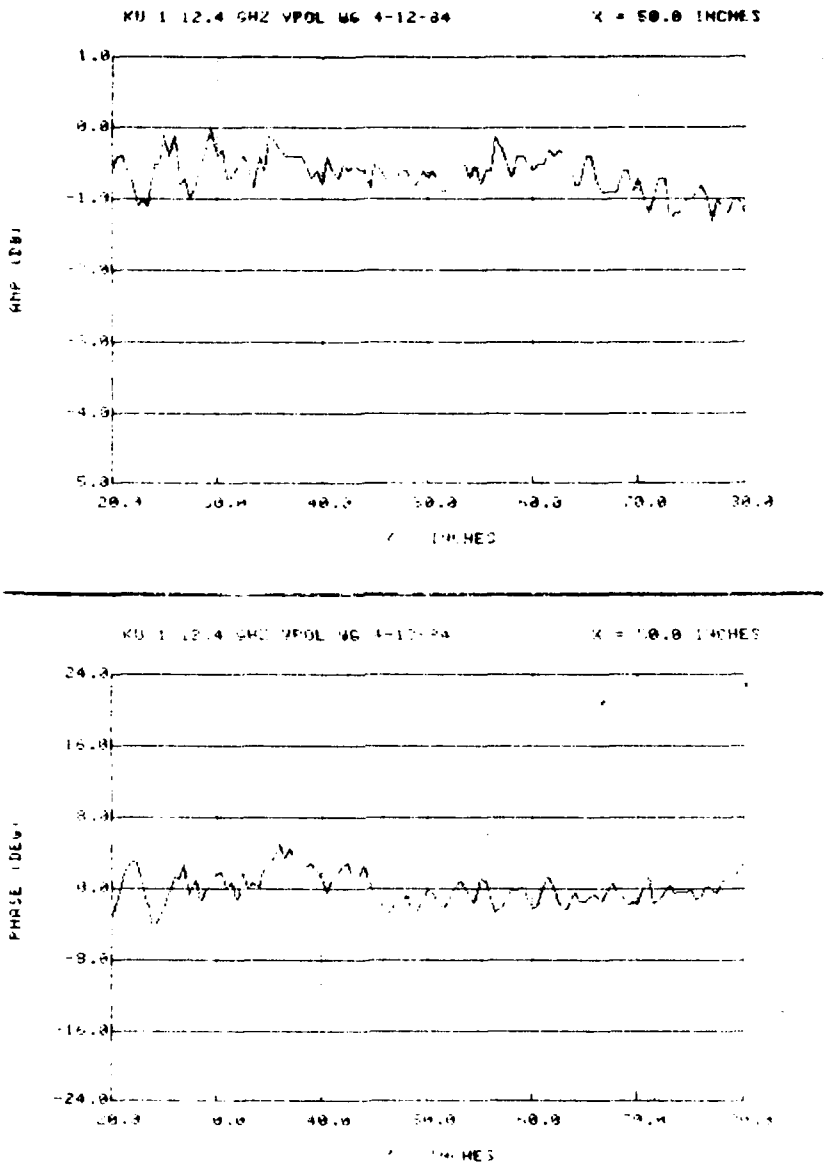


Figure A.28. Y-Plane Amplitude and Phase Field Probe Plot Taken at 12.4 GHz, V-Polarization, Using the Waveguide Probe

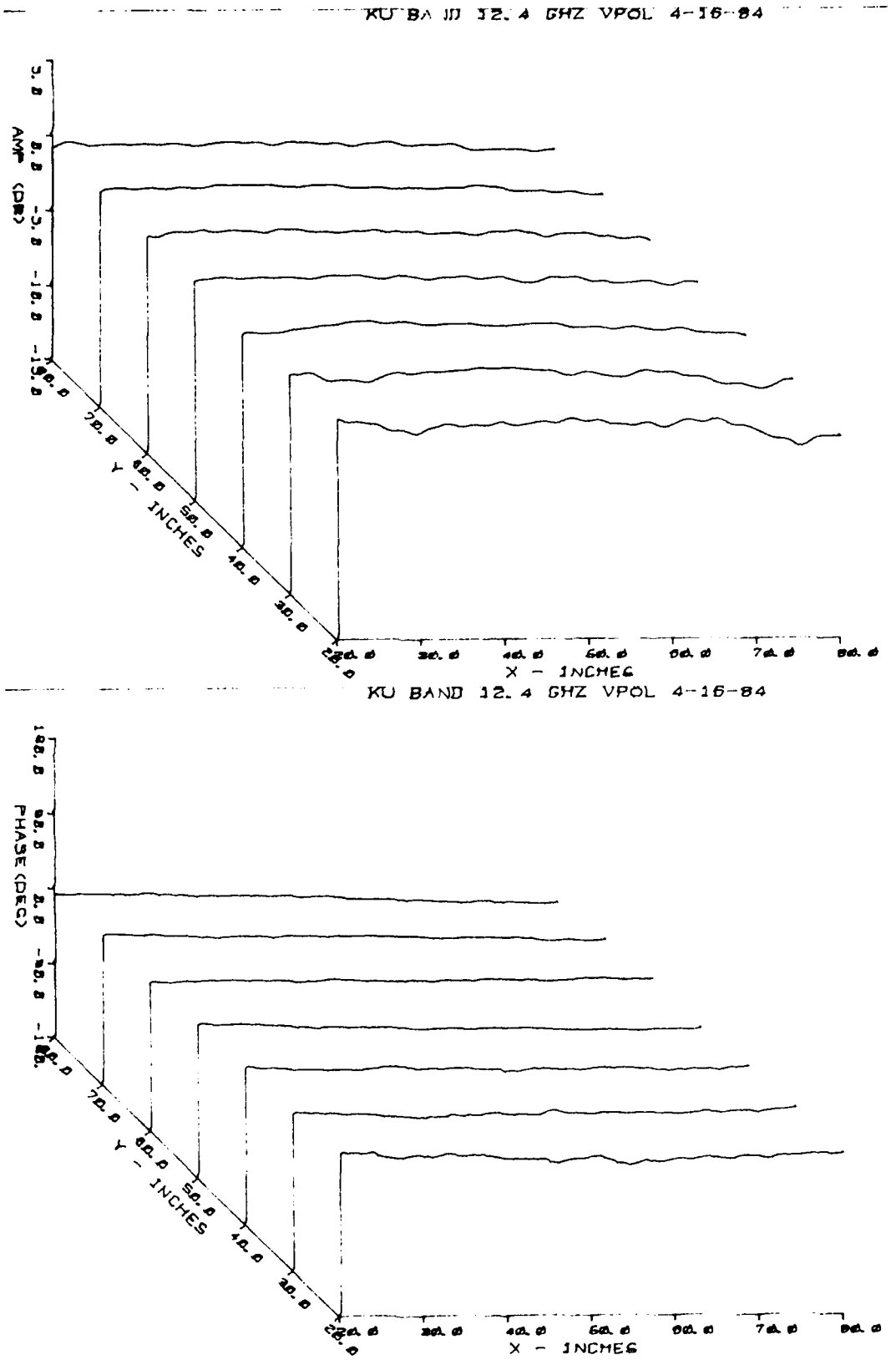


Figure A.29. 3D X-Plane Amplitude and Phase Field Probe Plot Taken at 12.4 GHz, V-Polarization, Using the Horn Probe

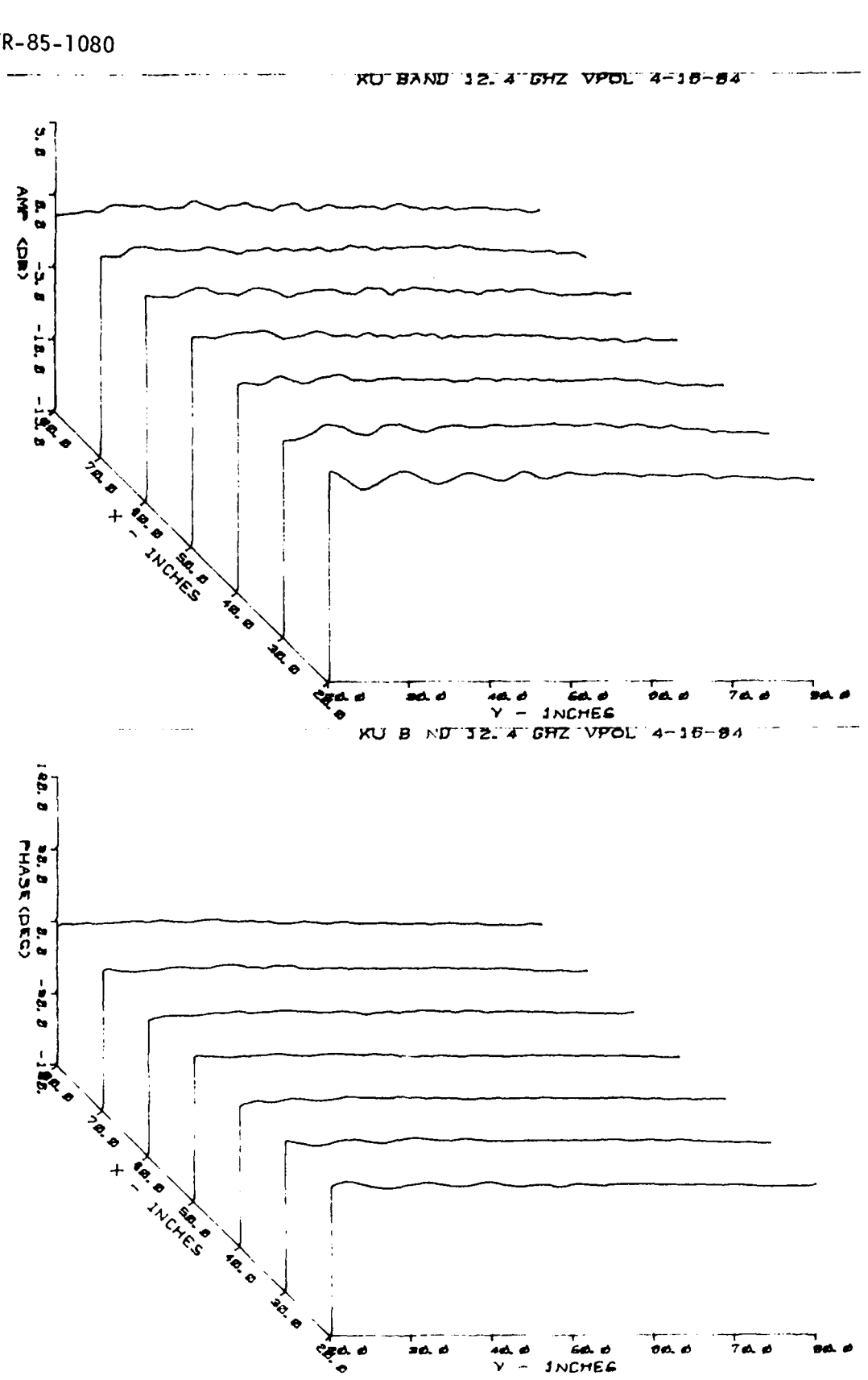


Figure A.30. 3D Y-Plane Amplitude and Phase Field Probe Plot Taken at 12.4 GHz, V-Polarization, Using the Horn Probe

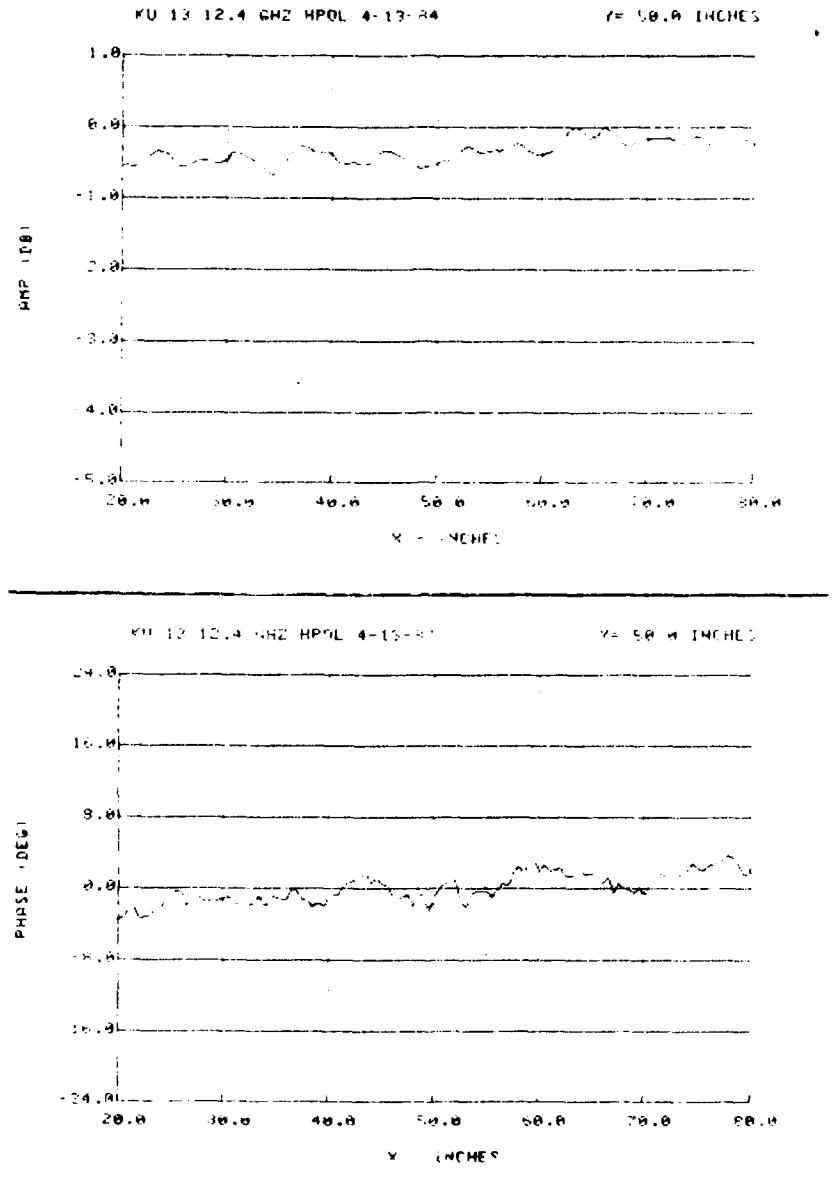


Figure A.31. X-Plane Amplitude and Phase Field Probe Plot Taken at 12.4 GHz, H-Polarization, Using the Horn Probe

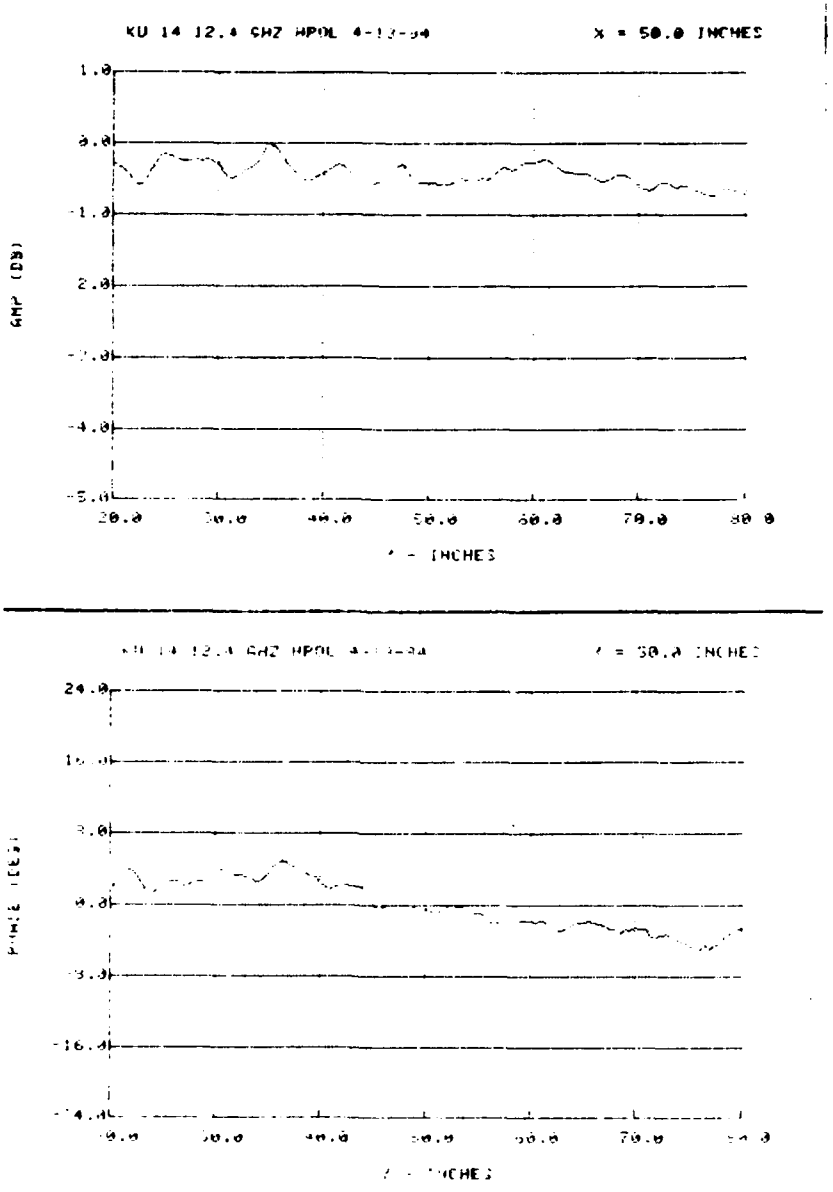


Figure A.32. Y-Plane Amplitude and Phase Field Probe Plot Taken at 12.4 GHz, H-Polarization, Using the Horn Probe

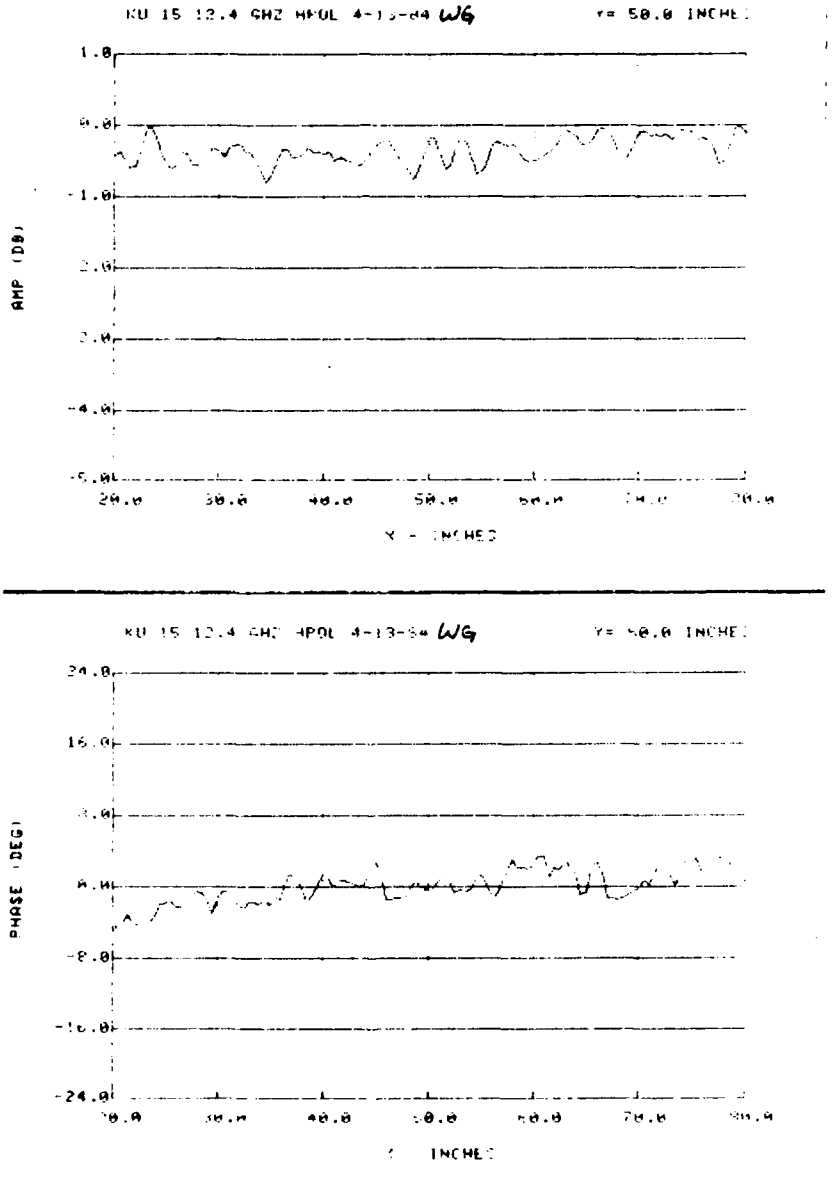


Figure A.33. X-Plane Amplitude and Phase Field Probe Plot Taken at 12.4 GHz, H-Polarization, Using the Waveguide Probe

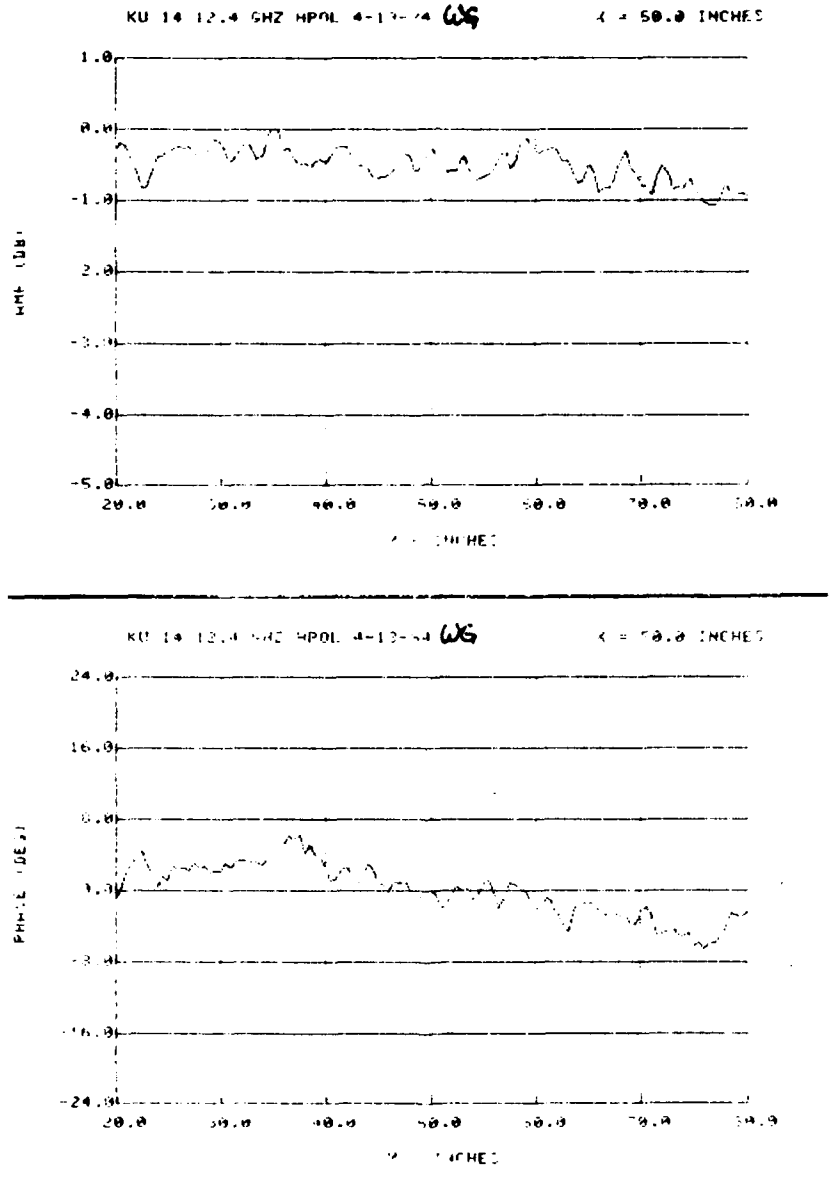


Figure A. 34. Y-Plane Amplitude and Phase Field Probe Plot Taken at 12.4 GHz, H-Polarization, Using the Waveguide Probe

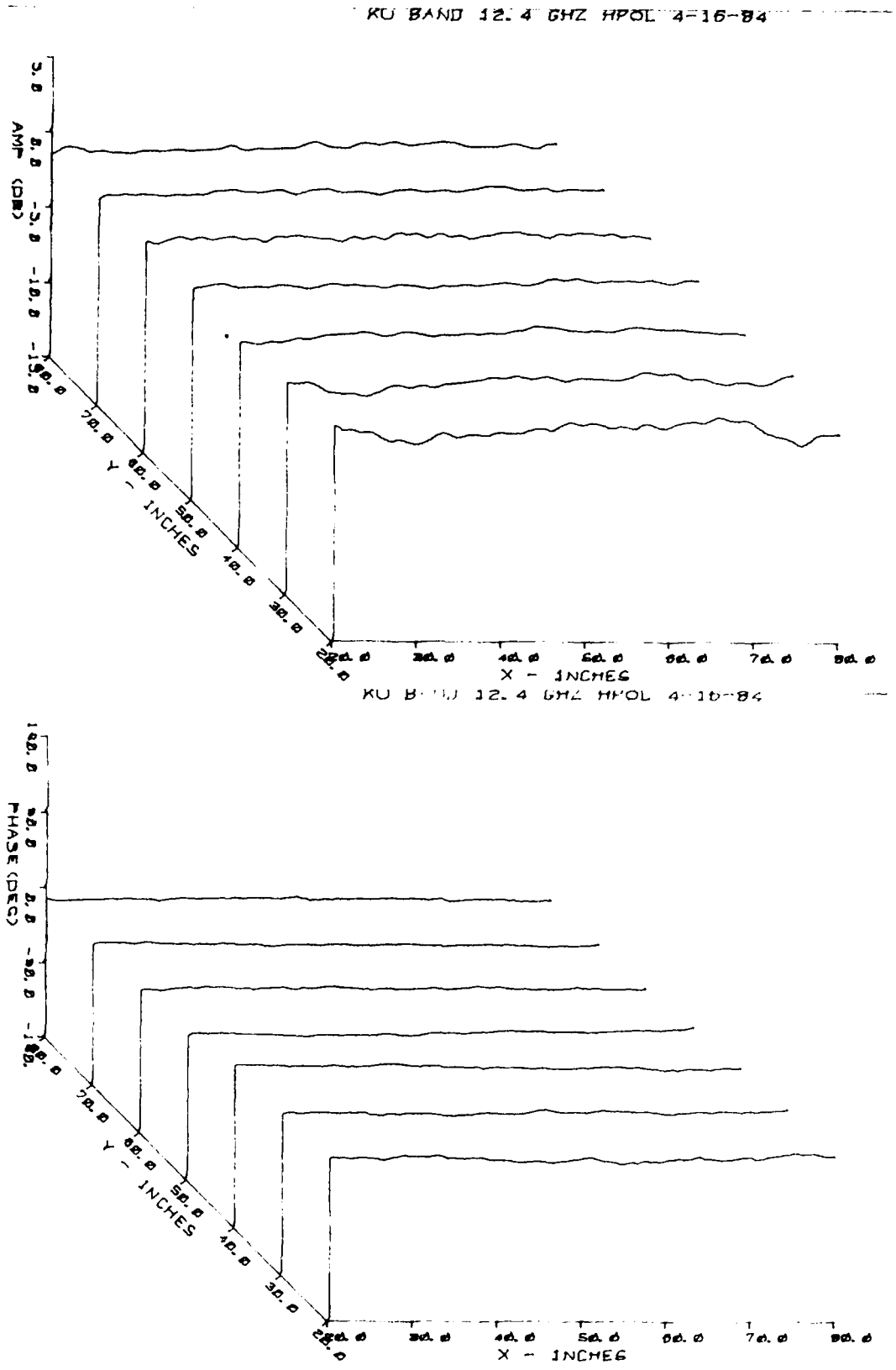


Figure A.35. 3D X-Plane Amplitude and Phase Field Probe Plot Taken at 12.4 GHz, H-Polarization, Using the Horn Probe

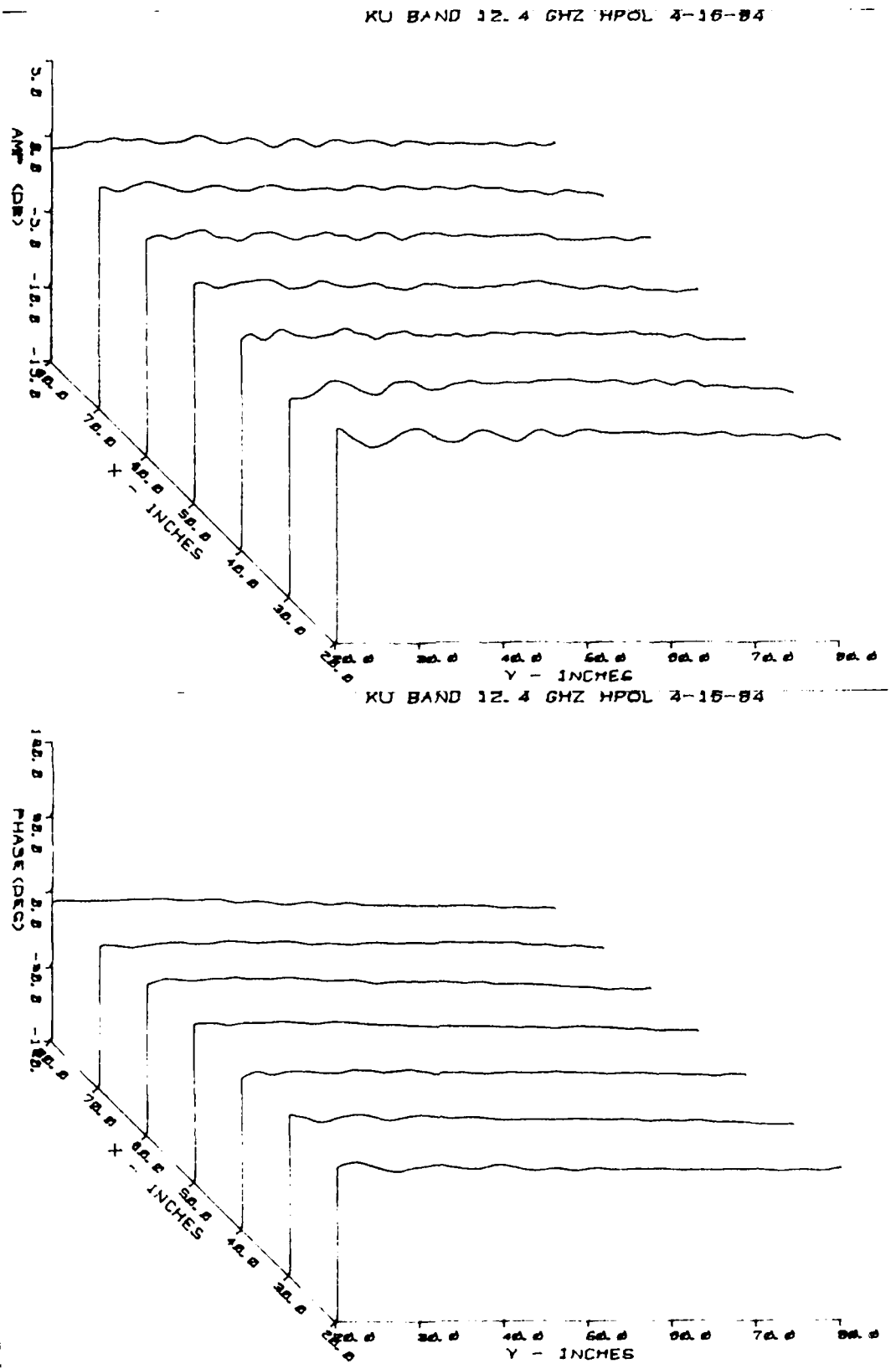


Figure A.36. 3D Y-Plane Amplitude and Phase Field Probe Plot Taken at 12.4 GHz, H-Polarization, Using the Horn Probe

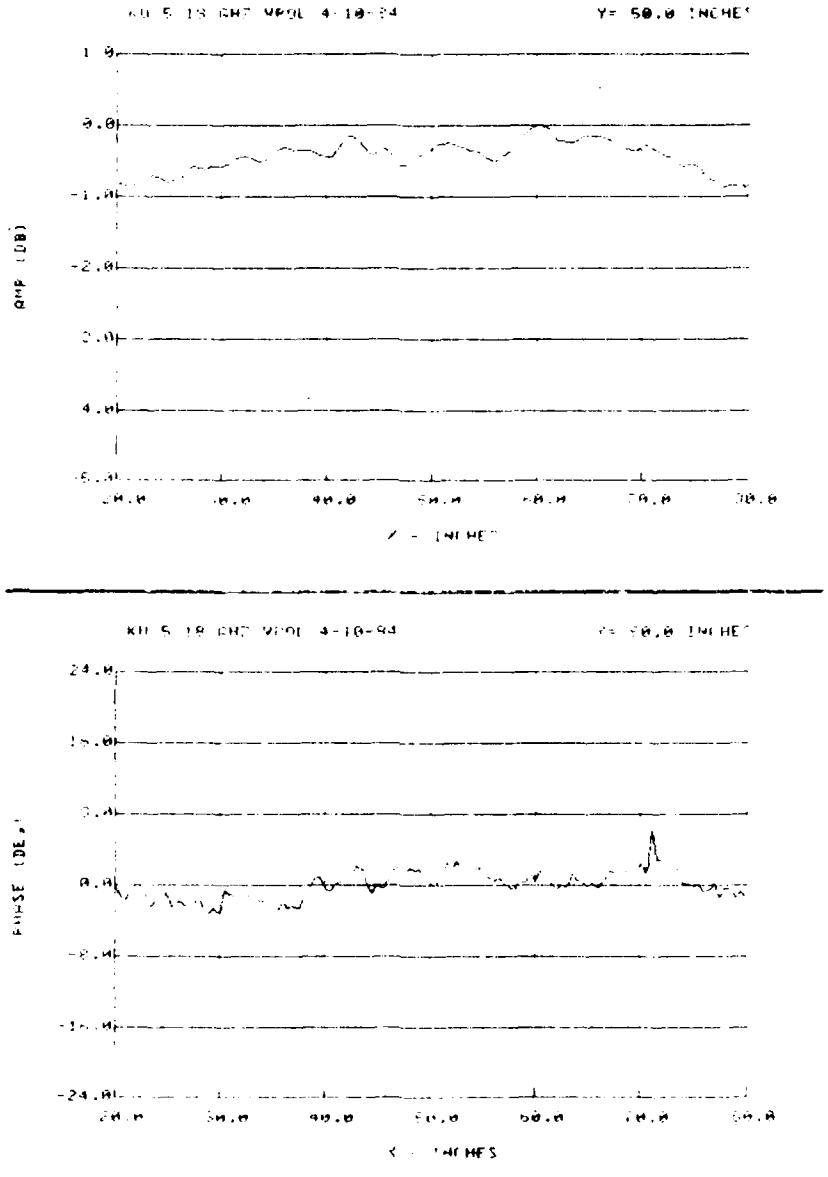
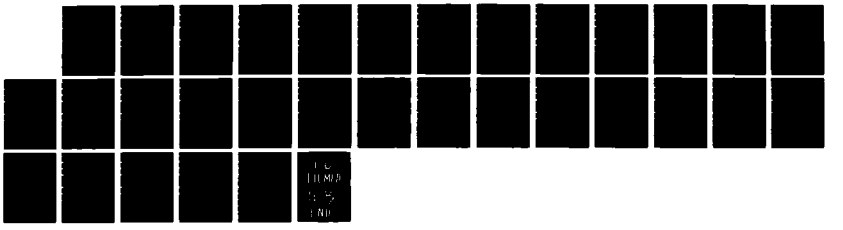
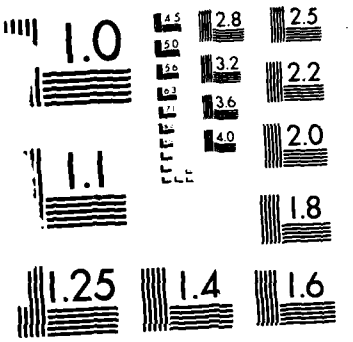


Figure A.37. X-Plane Amplitude and Phase Field Probe Plot Taken at 18.0 GHz, V-Polarization, Using the Horn Probe

AD-A165 275 EXPERIMENTAL VERIFICATION OF THE FAR FIELD CRITERIA FOR 2/2
AFWAL'S COMPACT R (U) AIR FORCE WRIGHT AERONAUTICAL
LABS WRIGHT-PATTERSON AFB OH H M CHIZEVER ET AL.
UNCLASSIFIED OCT 85 AFWAL-TR-85-1080 F/G 20/14 NL





MICROCOPY RESOLUTION TEST CHART
NATIONAL BUREAU OF STANDARDS-1963-A

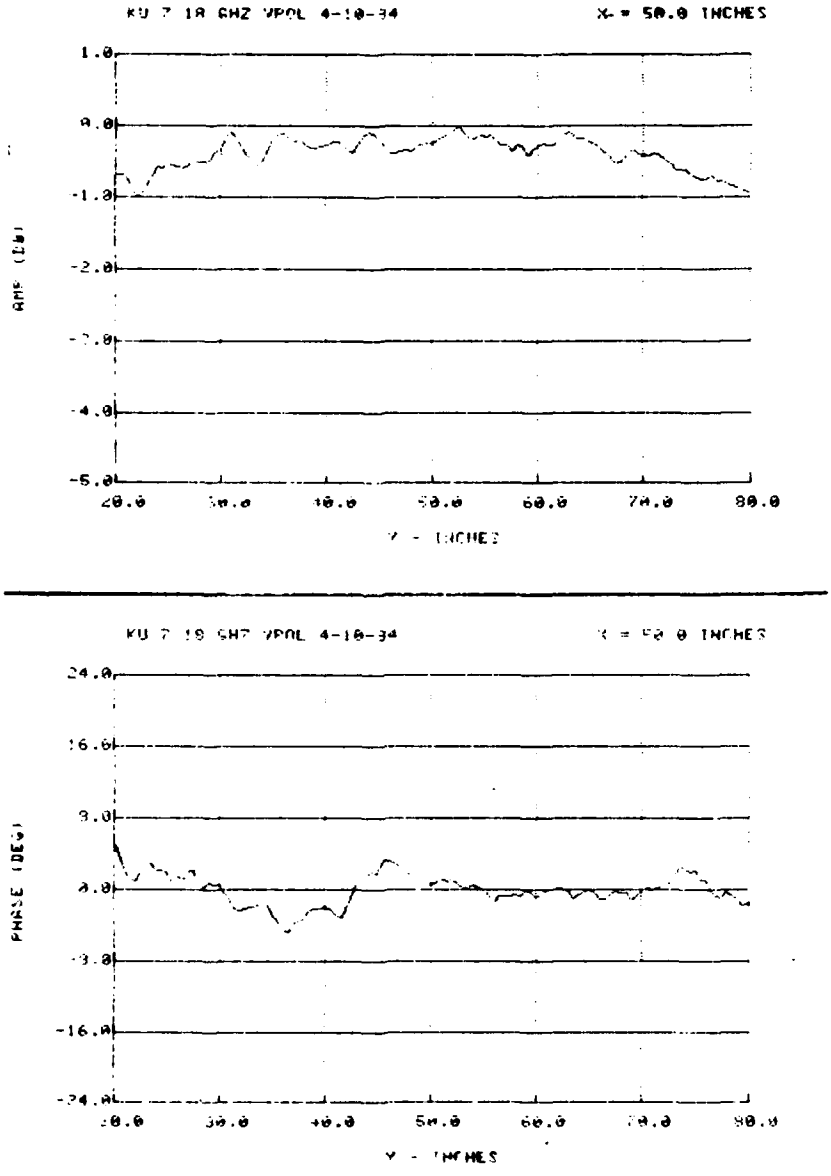


Figure A.38. Y-Plane Amplitude and Phase Field Probe Plot taken at 18.0 GHz, V-Polarization, Using the Horn Probe

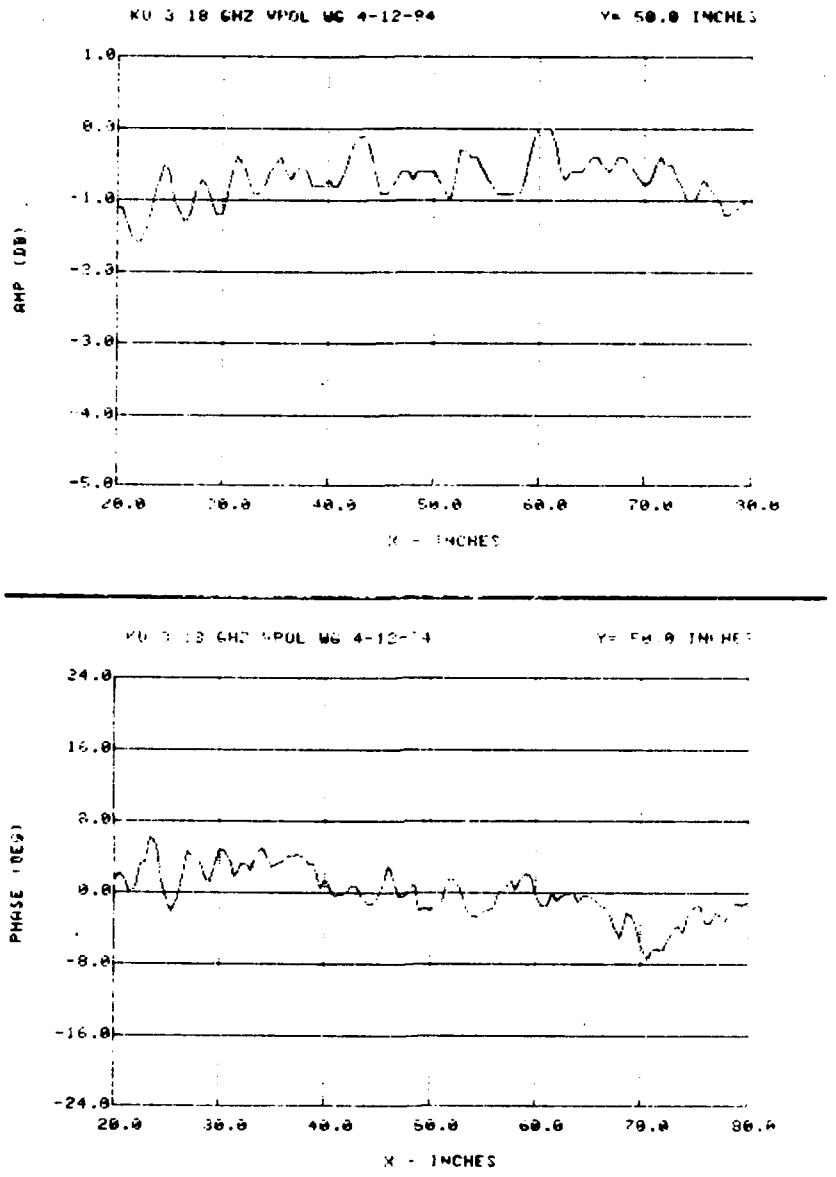


Figure A.39. X-Plane Amplitude and Phase Field Probe Plot Taken at 18.0 GHz, V-Polarization, Using the Waveguide Probe

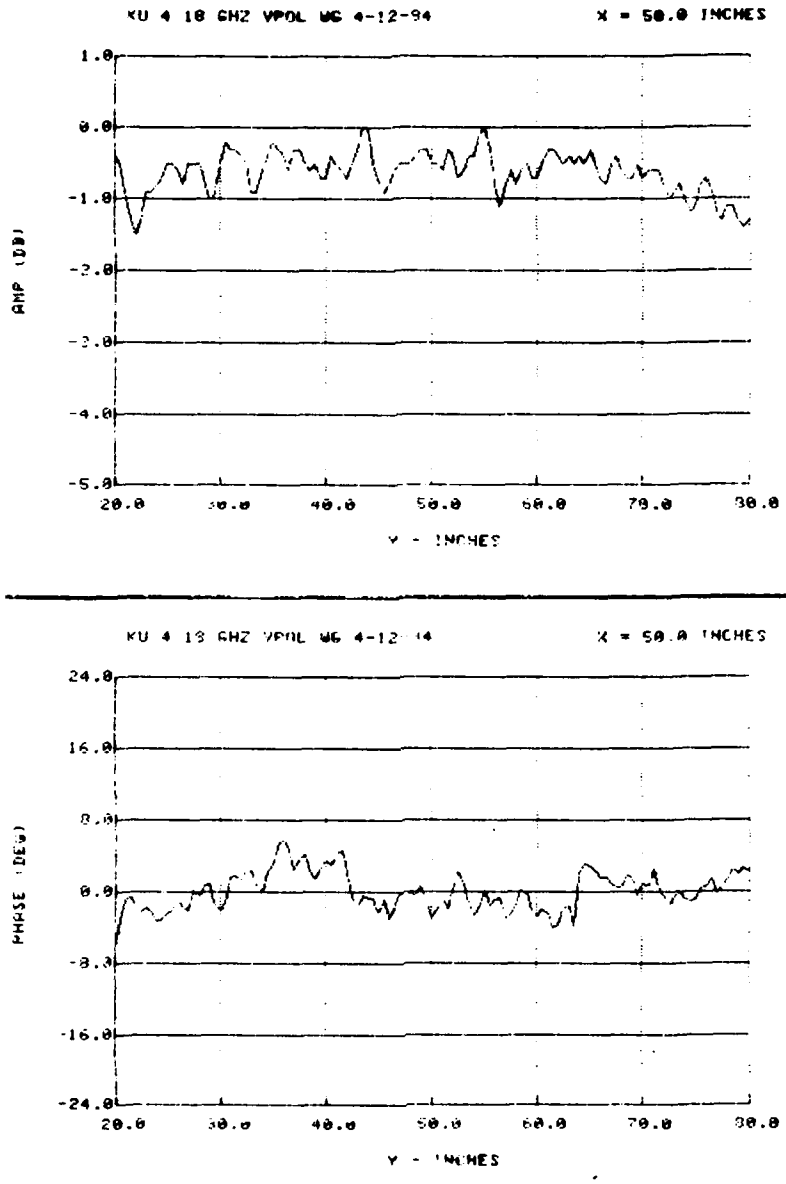


Figure A.40. Y-Plane Amplitude and Phase Field Probe Plot Taken at 18.0 GHz, V-Polarization, Using the Waveguide Probe

UNCLASSIFIED

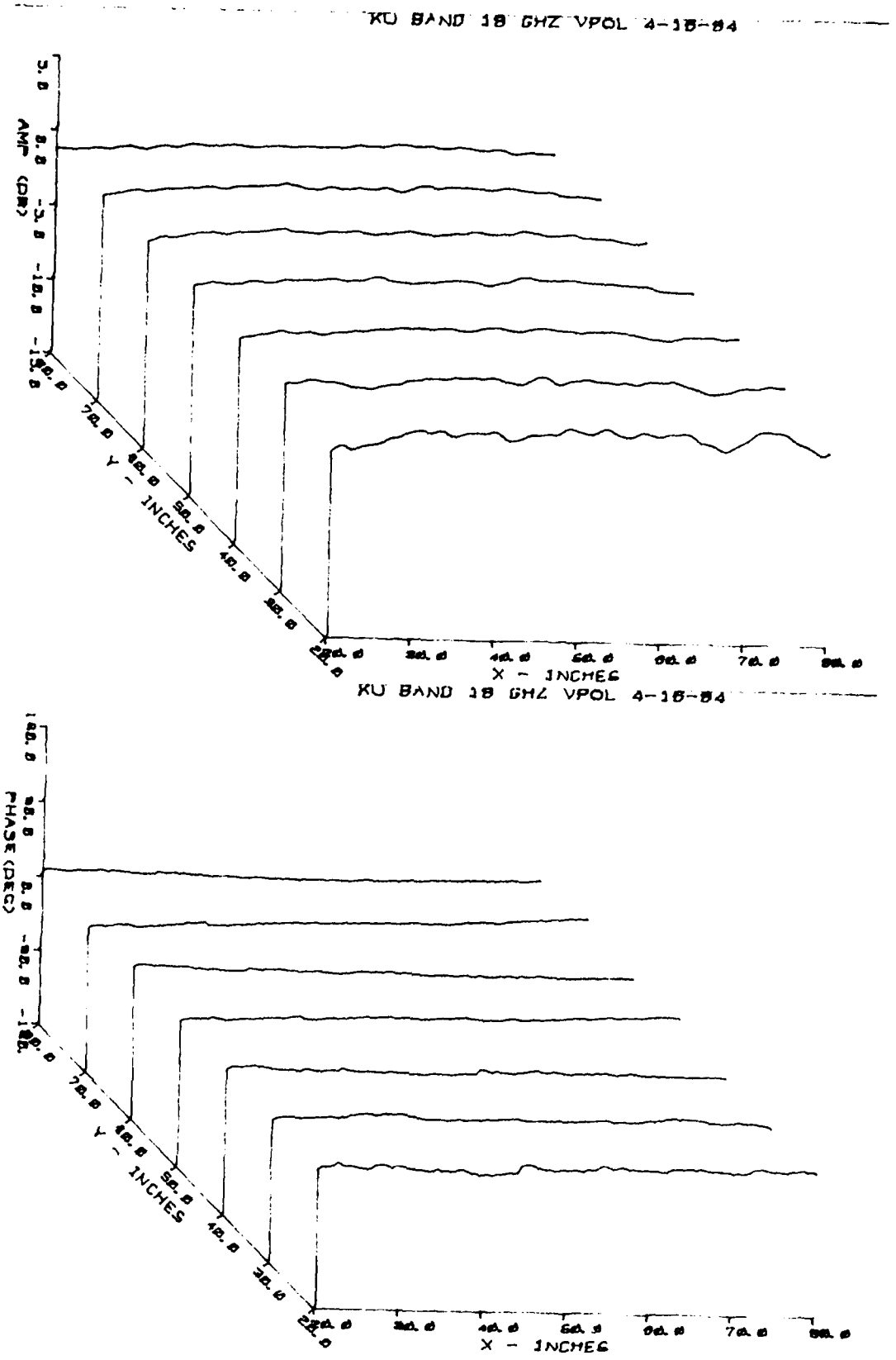


Figure A.41. 3D X-Plane Amplitude and Phase Field Probe Plot Taken at 18.0 GHz, V-Polarization, Using the Horn Probe

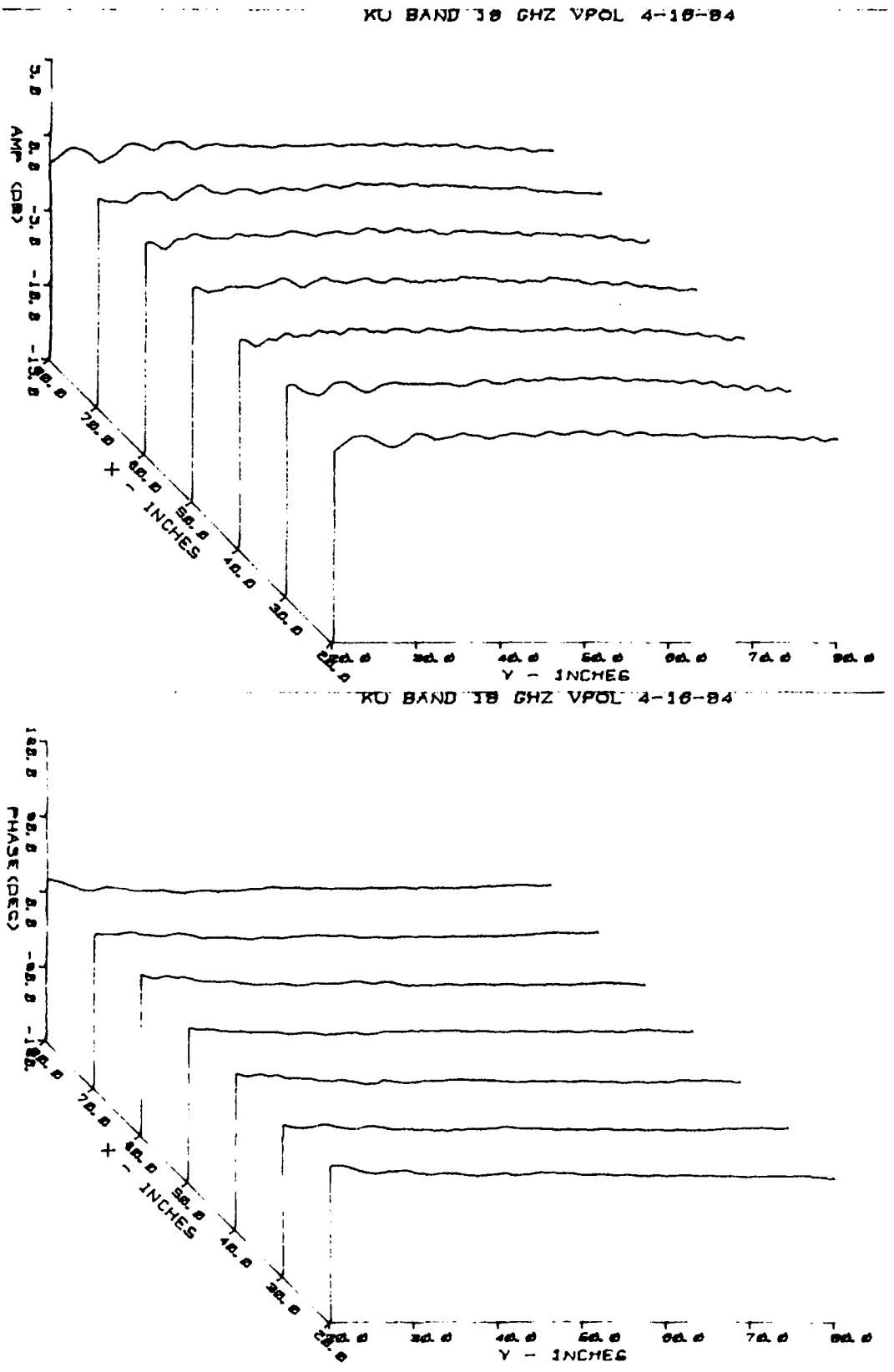


Figure A.42. 3D Y-Plane Amplitude and Phase Field Probe Plot Taken at 18.0 GHz, V-Polarization, Using the Horn Probe

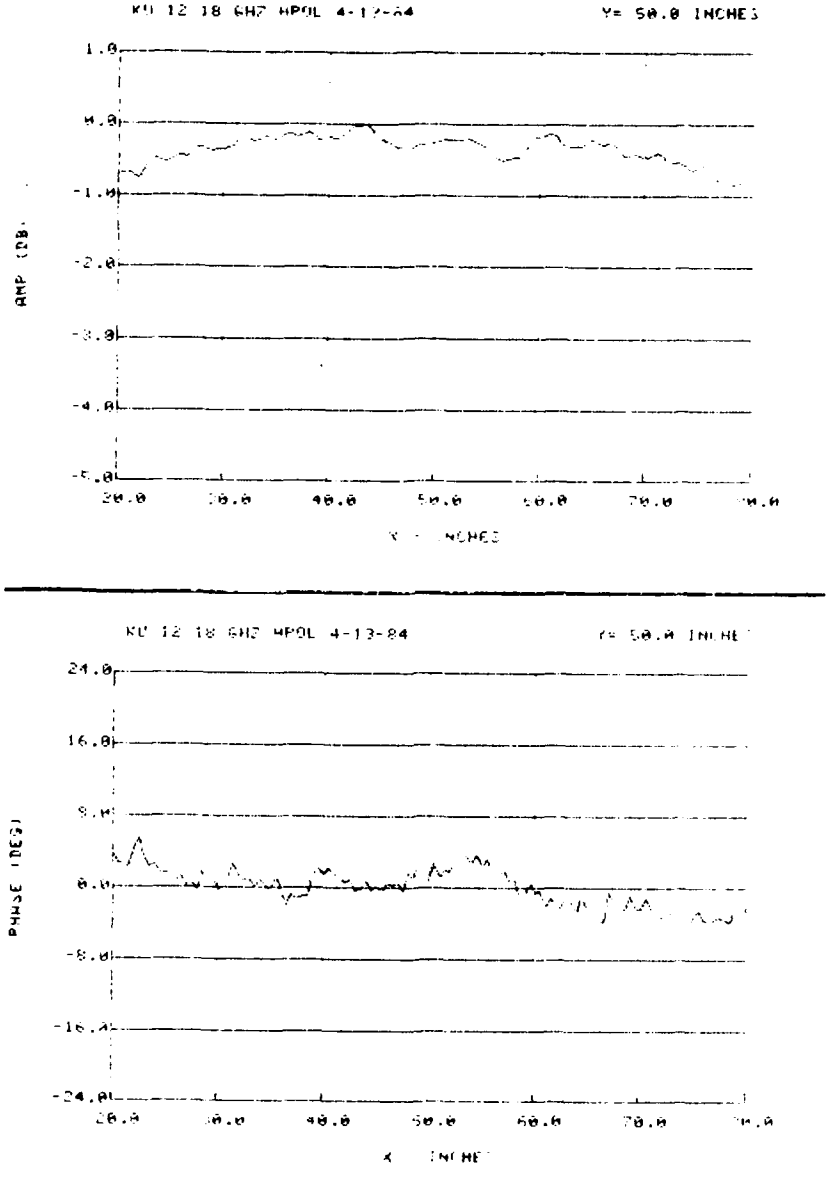


Figure A.43. X-Plane Amplitude and Phase Field Probe Plot Taken at 18.0 GHz, H-Polarization, Using the Horn Probe

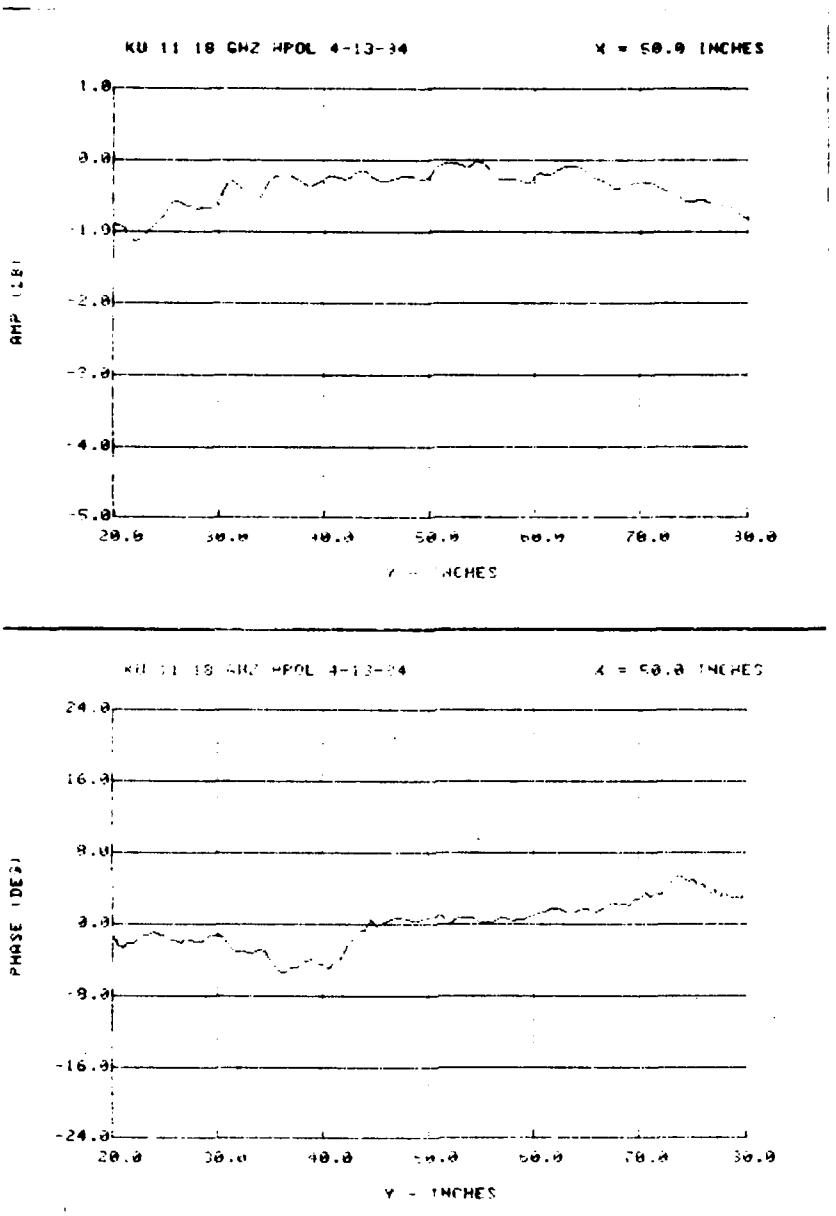


Figure A.44. Y-Plane Amplitude and Phase Field Probe Plot Taken at 18.0 GHz, H-Polarization, Using the Horn Probe

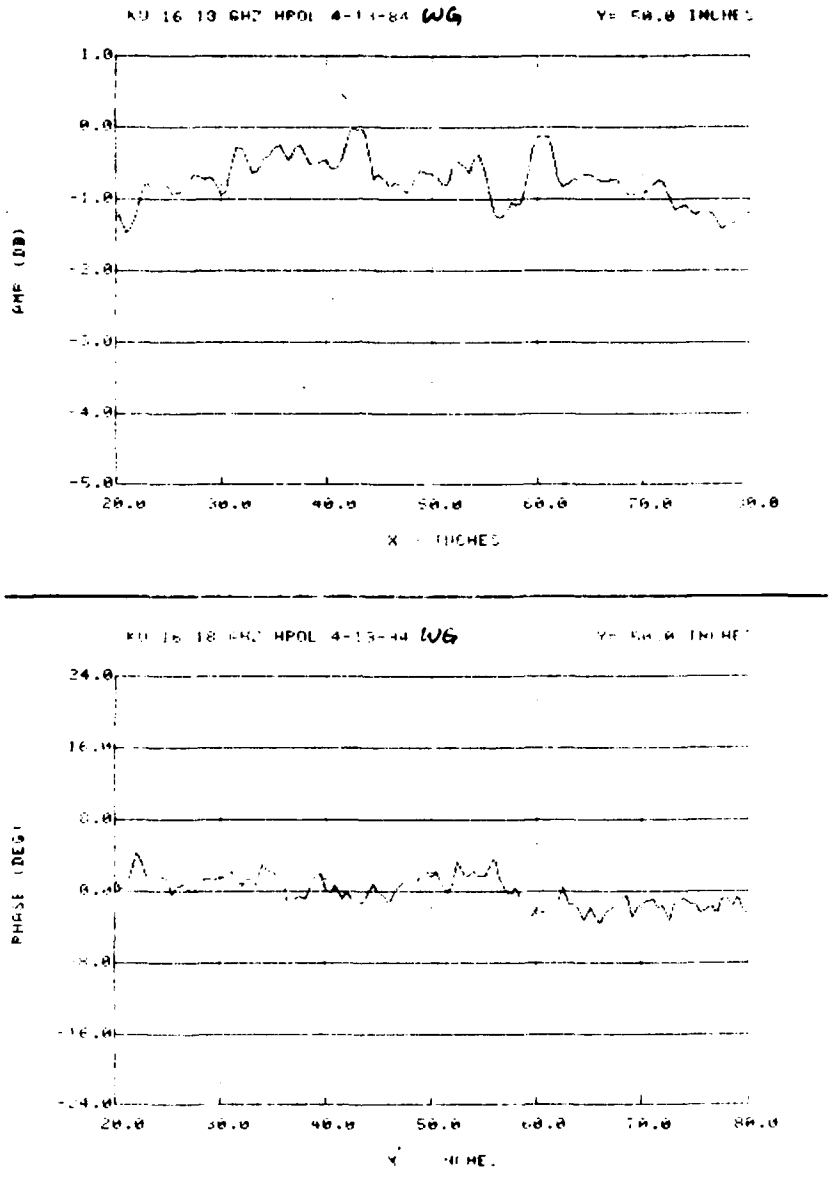


Figure A.45. X-Plane Amplitude and Phase Field Probe Plot Taken at 18.0 GHz, H-Polarization, Using the Waveguide Probe

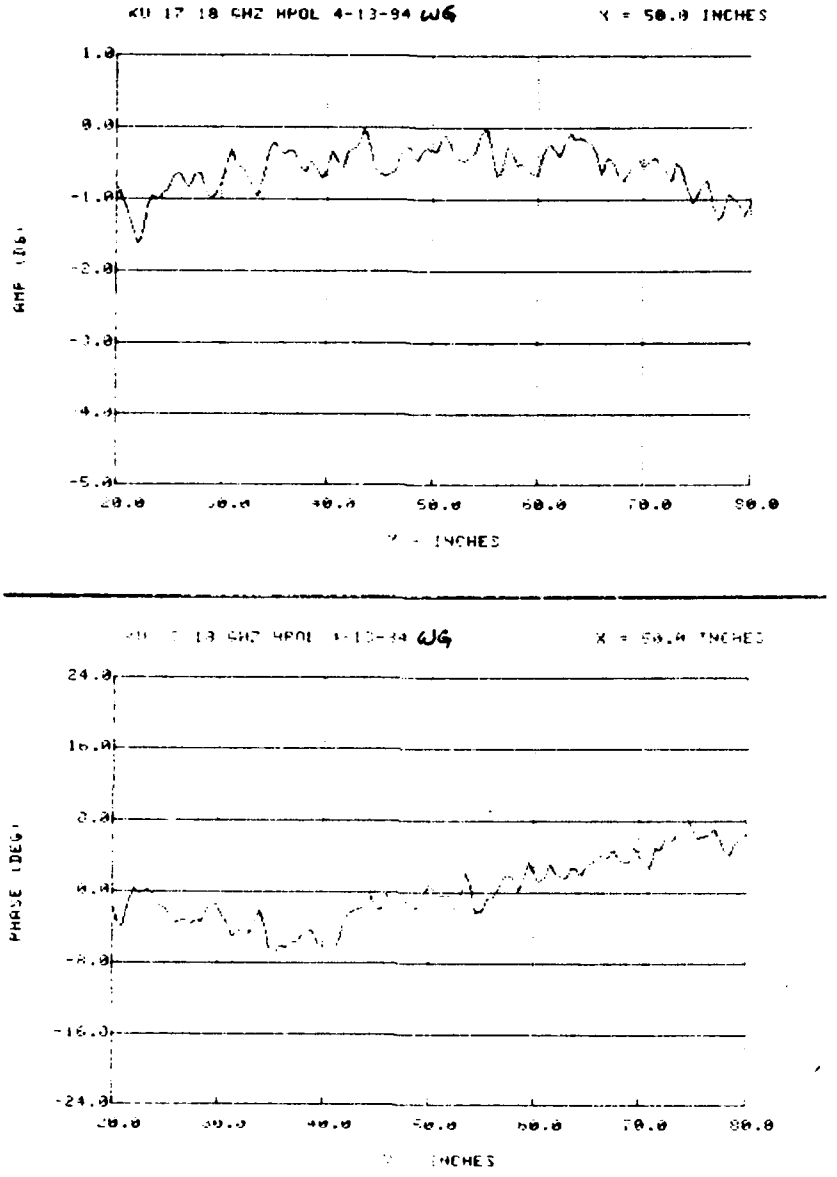


Figure A.46. Y-Plane Amplitude and Phase Field Probe Plot Taken at 18.0 GHz, H-Polarization, Using the Waveguide Probe

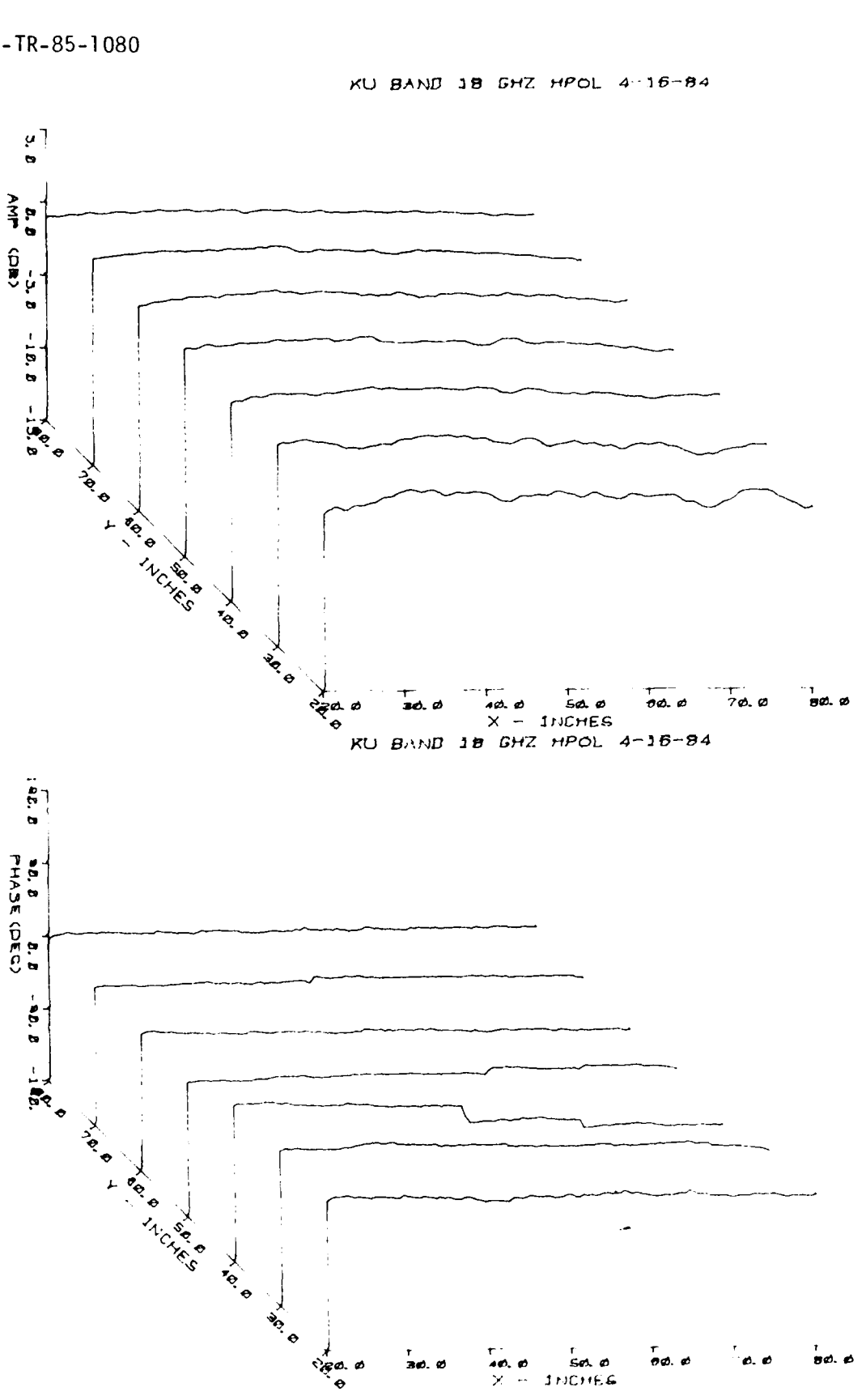


Figure A.47. 3D X-Plane Amplitude and Phase Field Probe Plot Taken at 18.0 GHz, H-Polarization, Using the Horn Probe

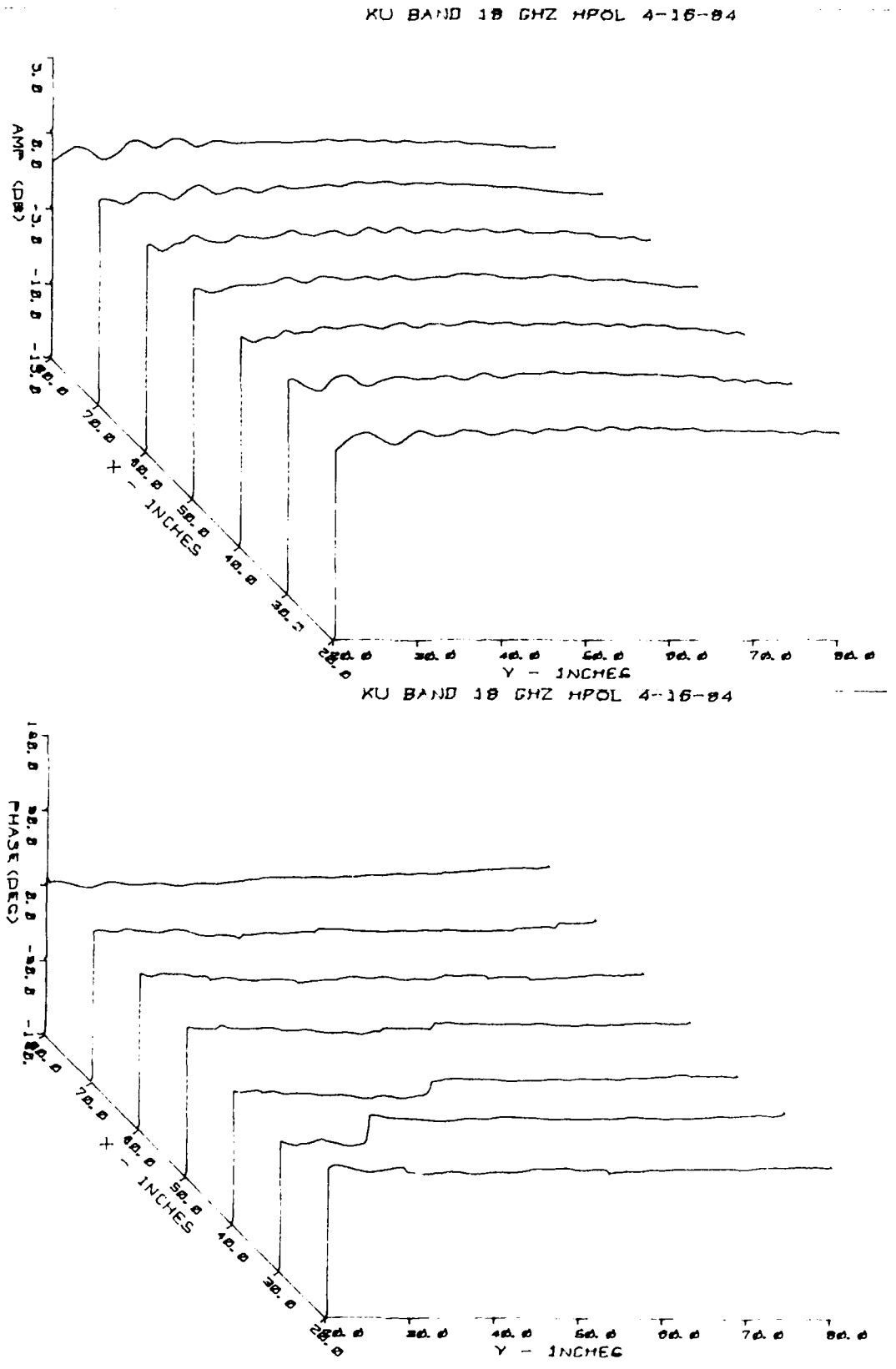


Figure A.48. 3D Y-Plane Amplitude and Phase Field Probe Plot Taken at 18.0 GHz, H-Polarization, Using the Horn Probe

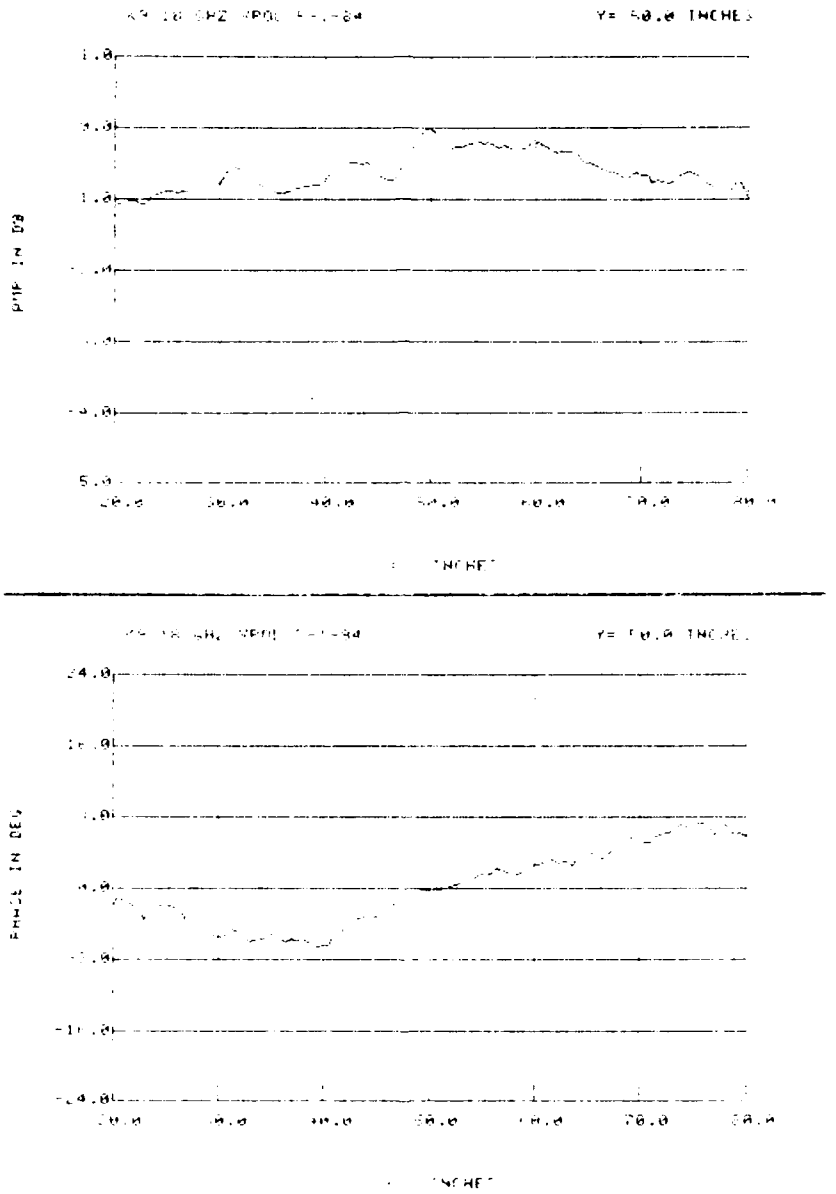


Figure A.49. X-Plane Amplitude and Phase Field Probe Plot Taken at 18.0 GHz, H-Polarization, Using the Horn Probe

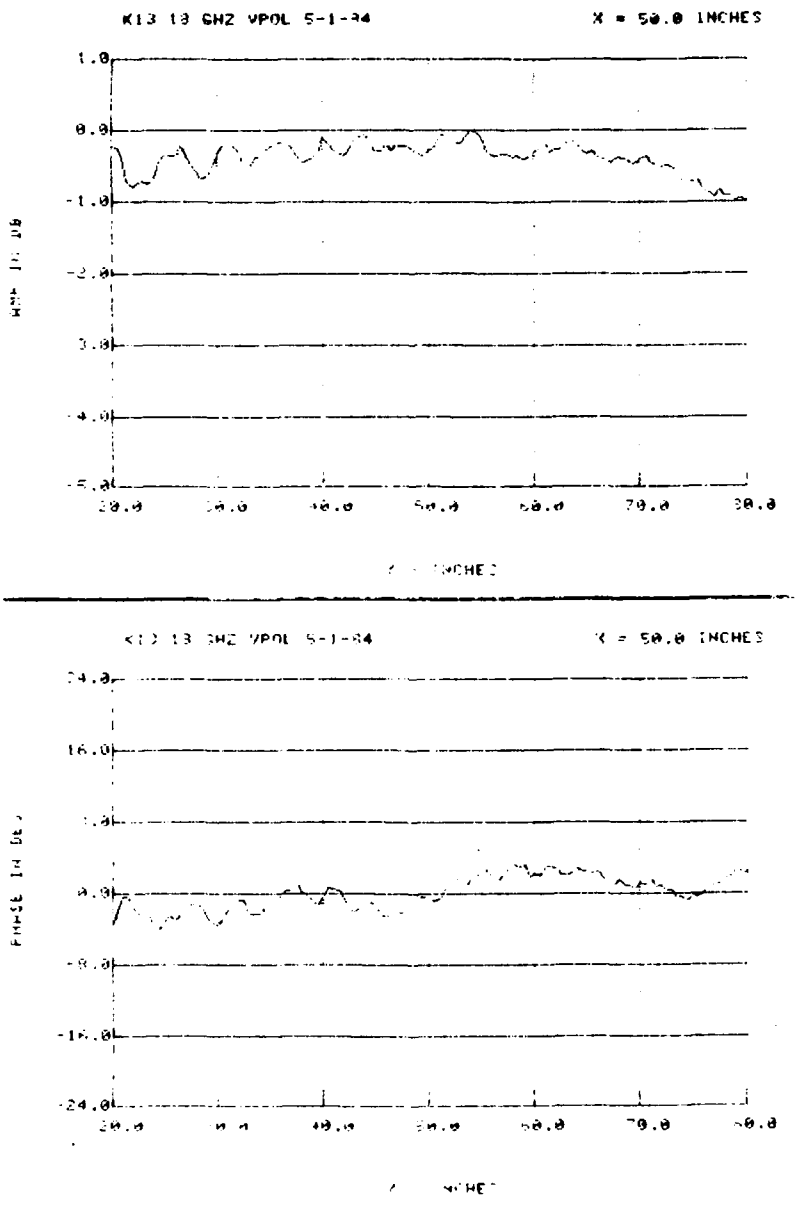


Figure A.50. Y-Plane Amplitude and Phase Field Probe Plot Taken at 18.0 GHz, V-Polarization, Using the Horn Probe

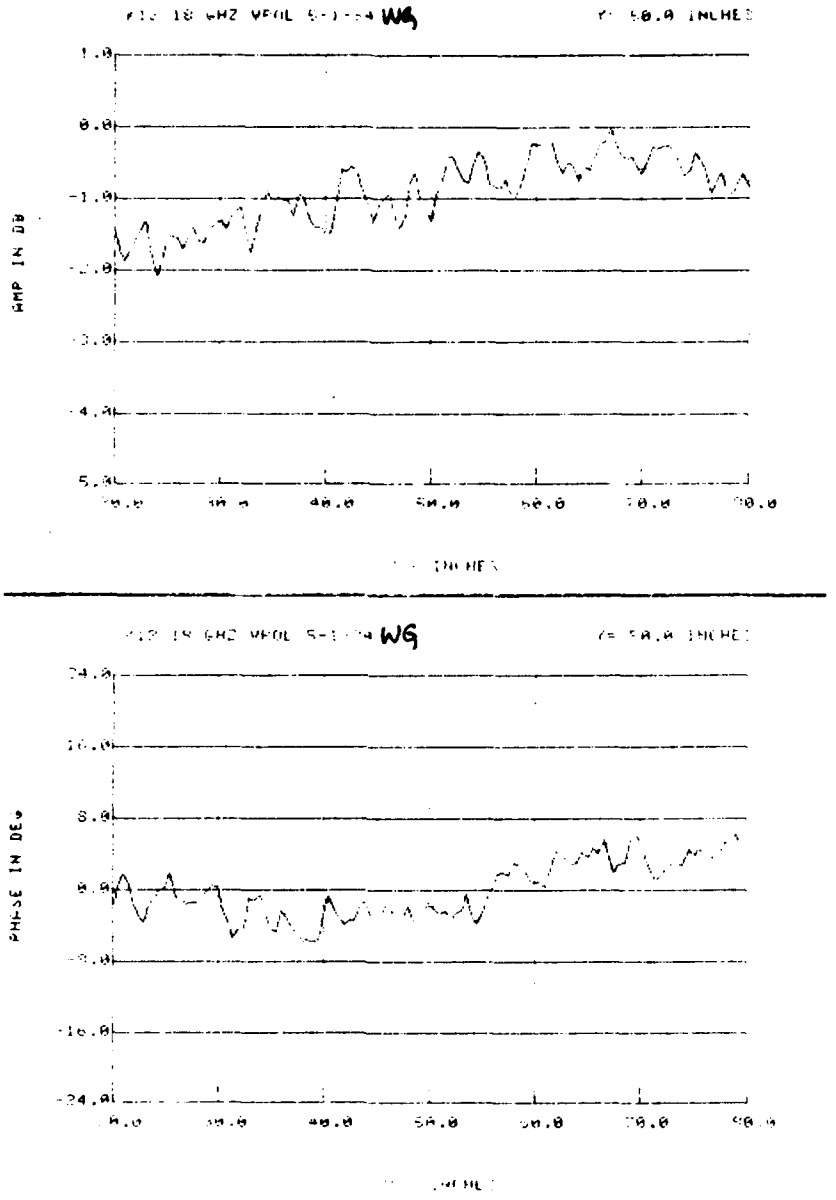


Figure A.51. X-Plane Amplitude and Phase Field Probe Plot Taken at 18.0 GHz, V-Polarization, Using the Waveguide Probe

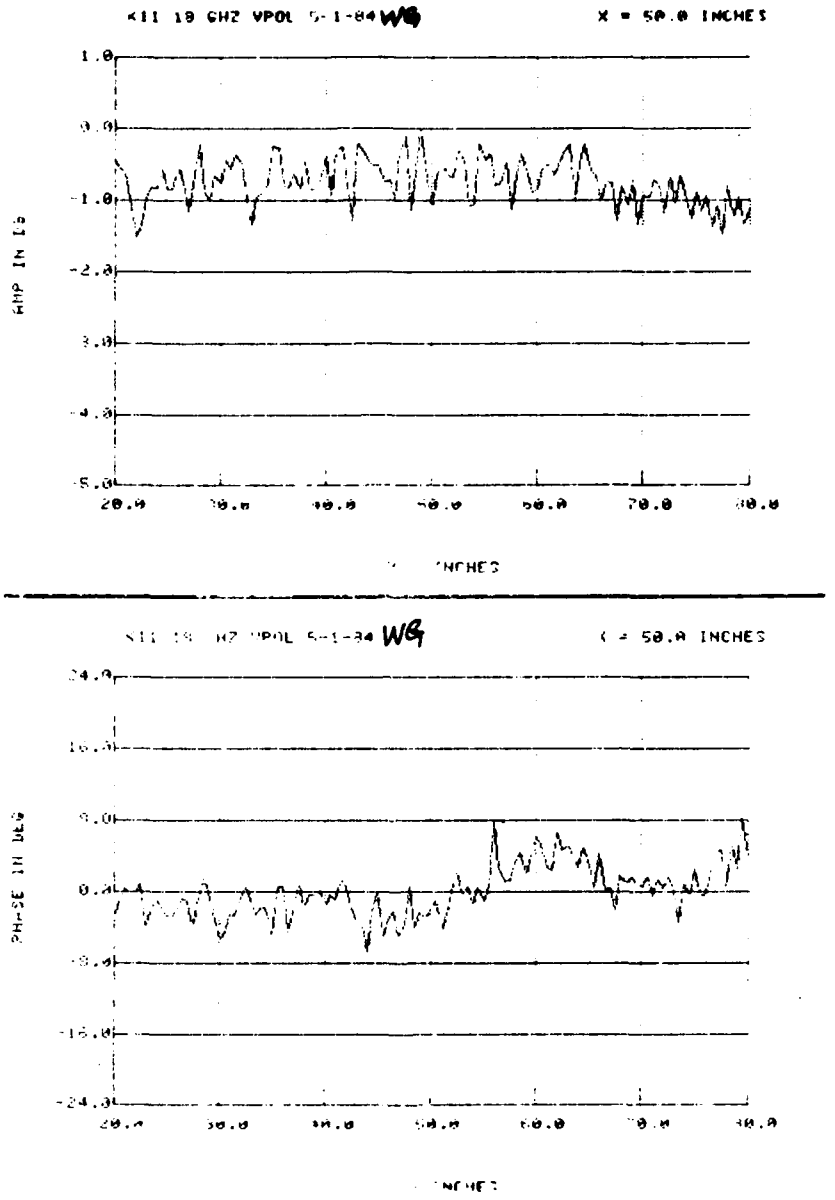


Figure A.52. Y-Plane Amplitude and Phase Field Probe Plot Taken at 18.0 GHz, V-Polarization, Using the Waveguide Probe

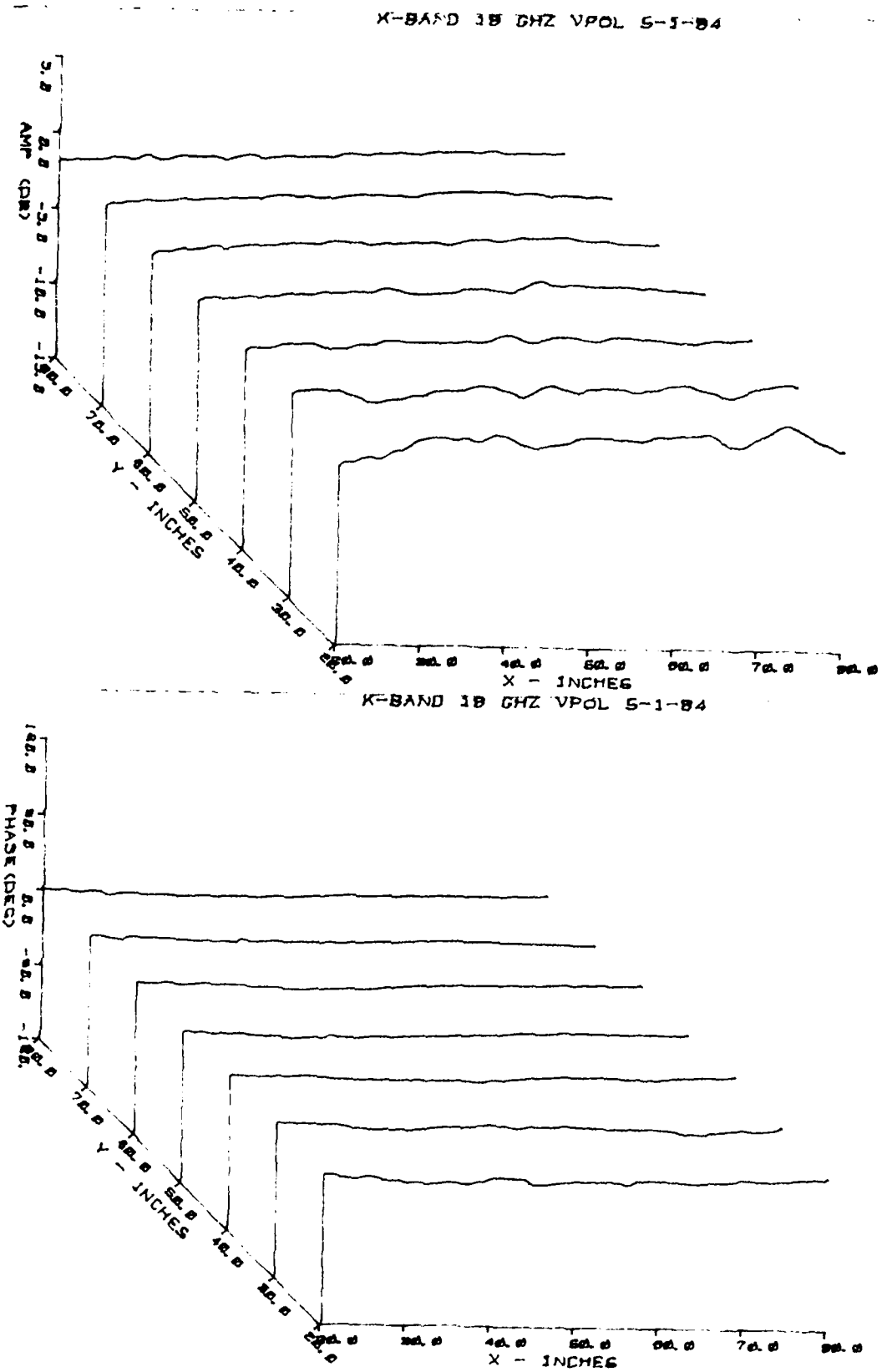


Figure A.53. 3D X-Plane Amplitude and Phase Field Probe Plot Taken at 18.0 GHz, V-Polarization, Using the Horn Probe

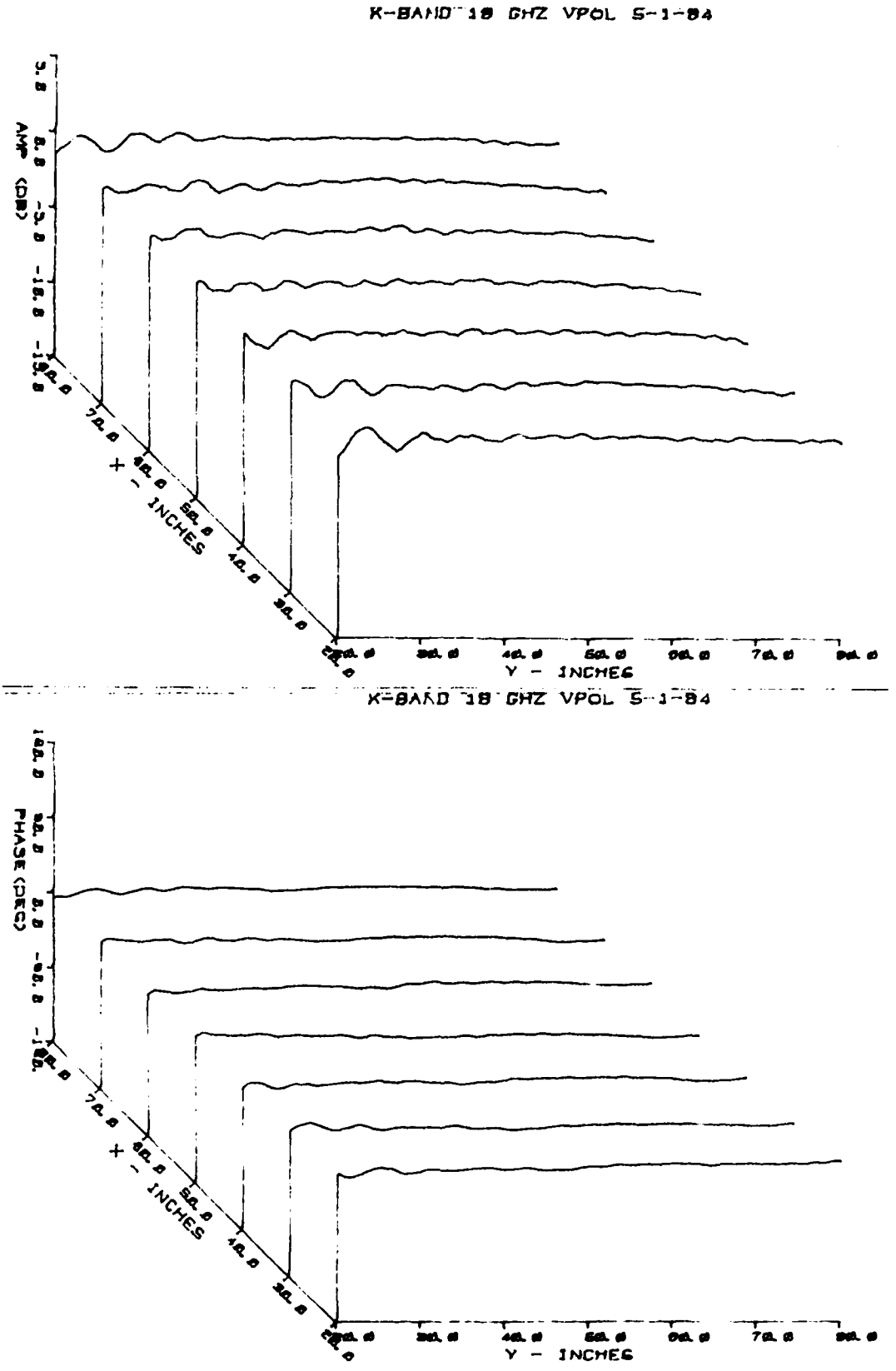


Figure A.54. 3D Y-Plane Amplitude and Phase Field Probe Plot Taken at 18.0 GHz, V-Polarization, Using the Horn Probe

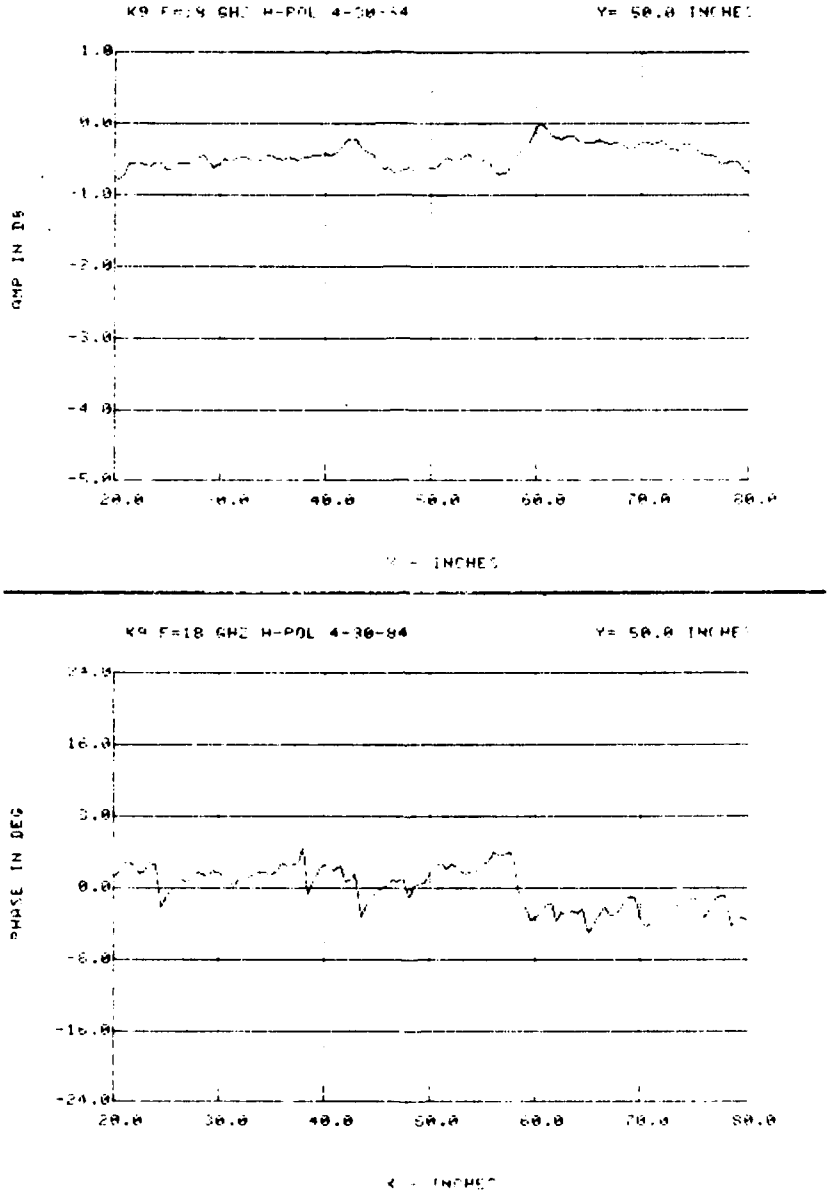


Figure A.55. X-Plane Amplitude and Phase Field Probe Plot Taken at 18.0 GHz, H-Polarization, Using the Horn Probe

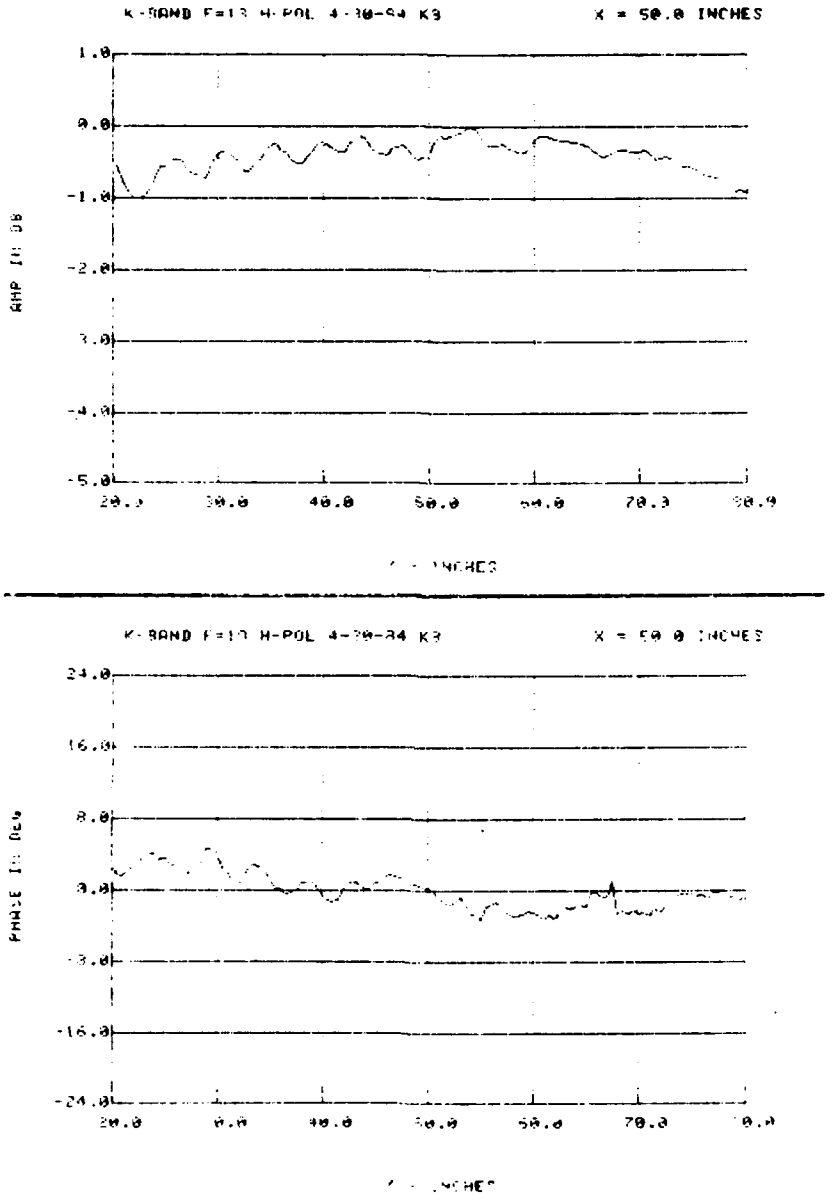


Figure A.56. Y-Plane Amplitude and Phase Field Probe Plot Taken at 18.0 GHz, H-Polarization, Using the Horn Probe

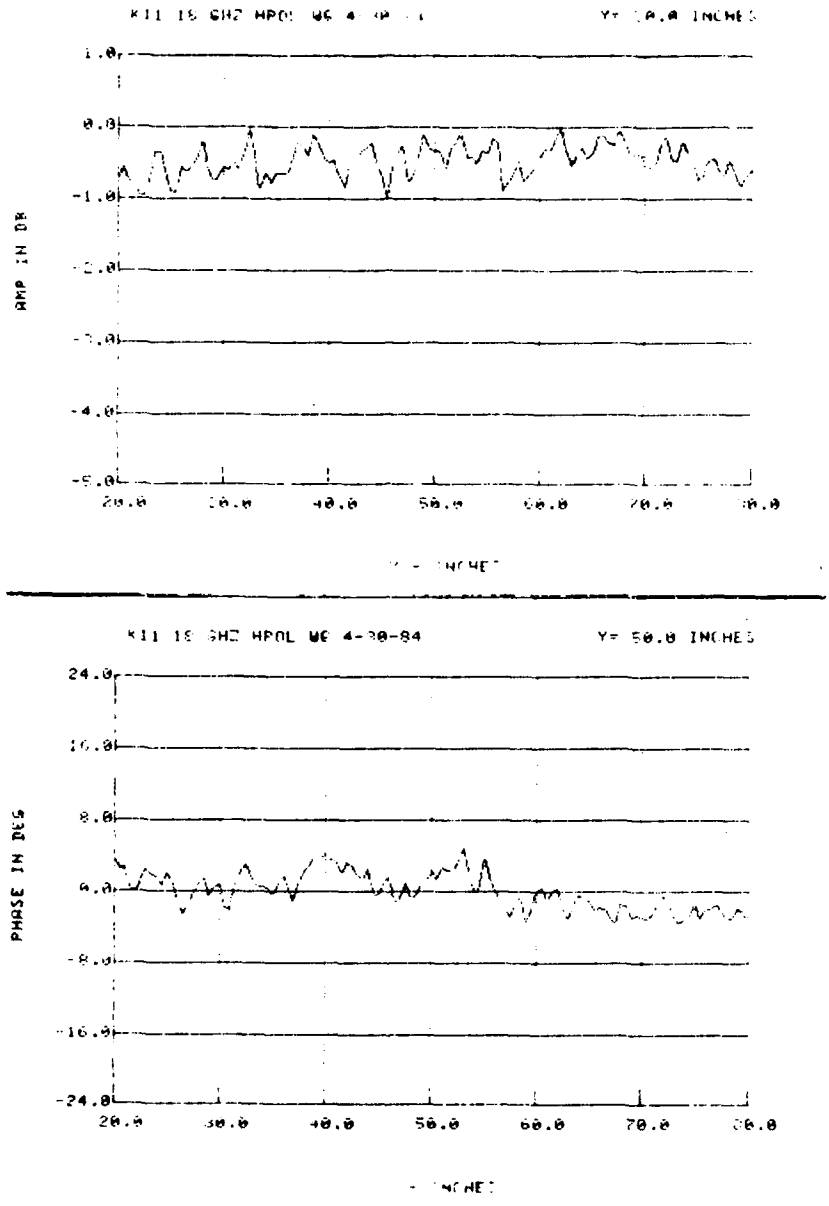


Figure A.57. X-Plane Amplitude and Phase Field Probe Plot Taken at 18.0 GHz, H-Polarization, Using the Waveguide Probe

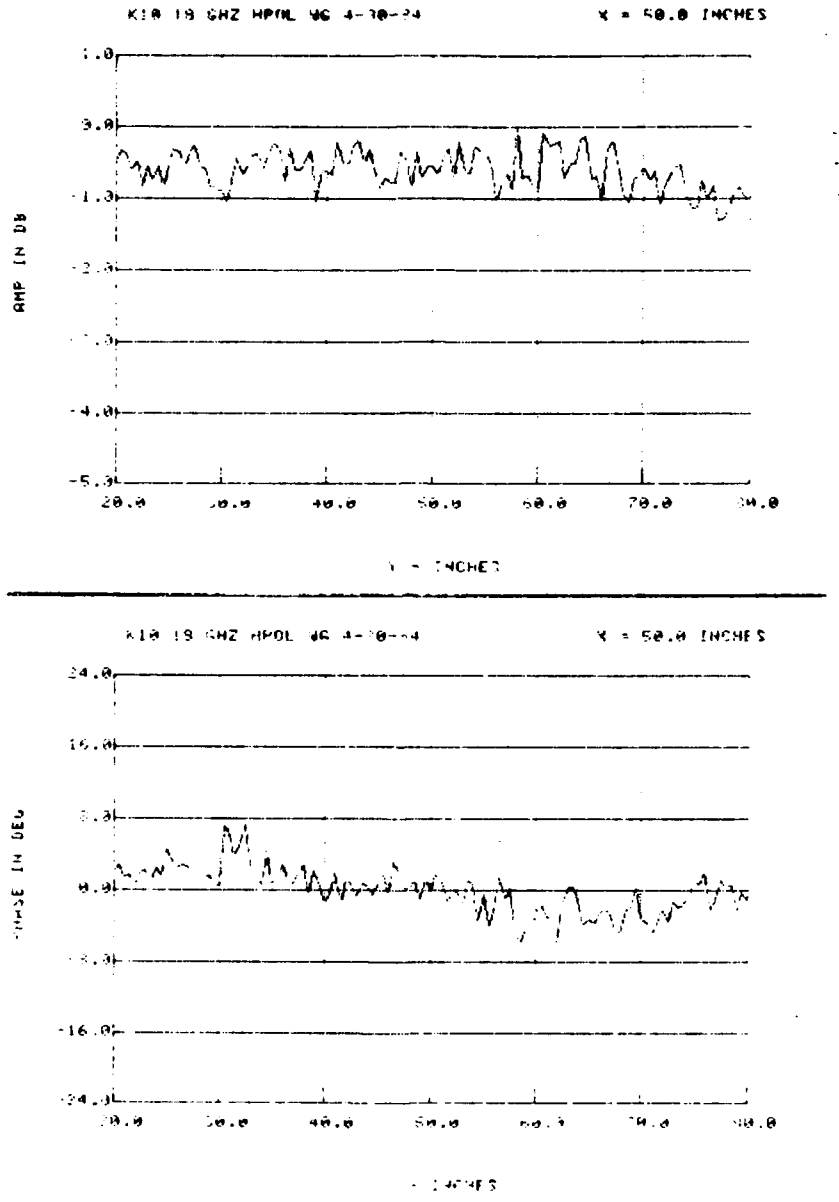


Figure A.58. Y-Plane Amplitude and Phase Field Probe Plot Taken at 18.0 GHz, H-Polarization, Using the Waveguide Probe

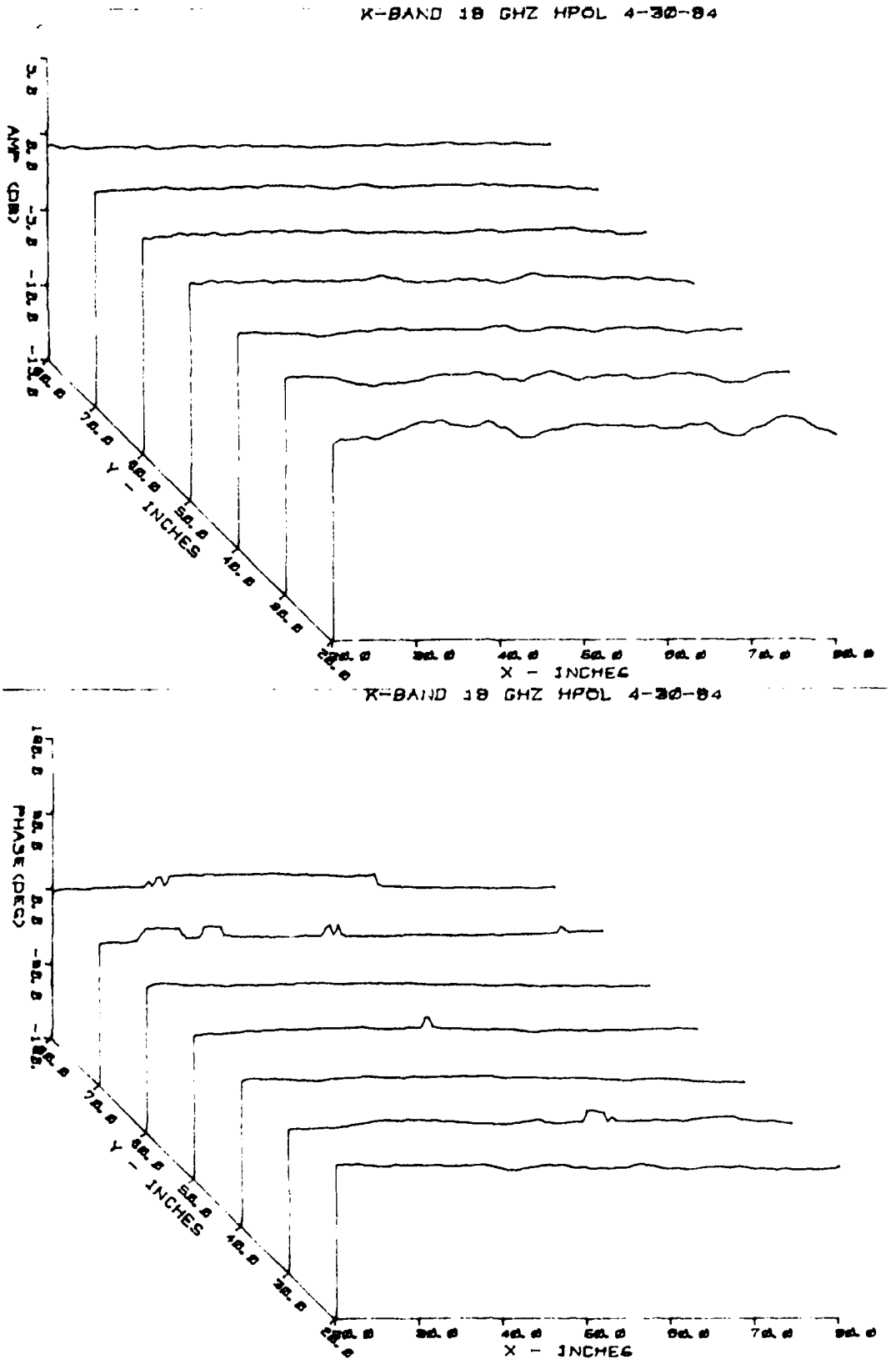


Figure A.59. 3D X-Plane Amplitude and Phase Field Probe Plot Taken at 18.0 GHz. H-Polarization, Using the Horn Probe

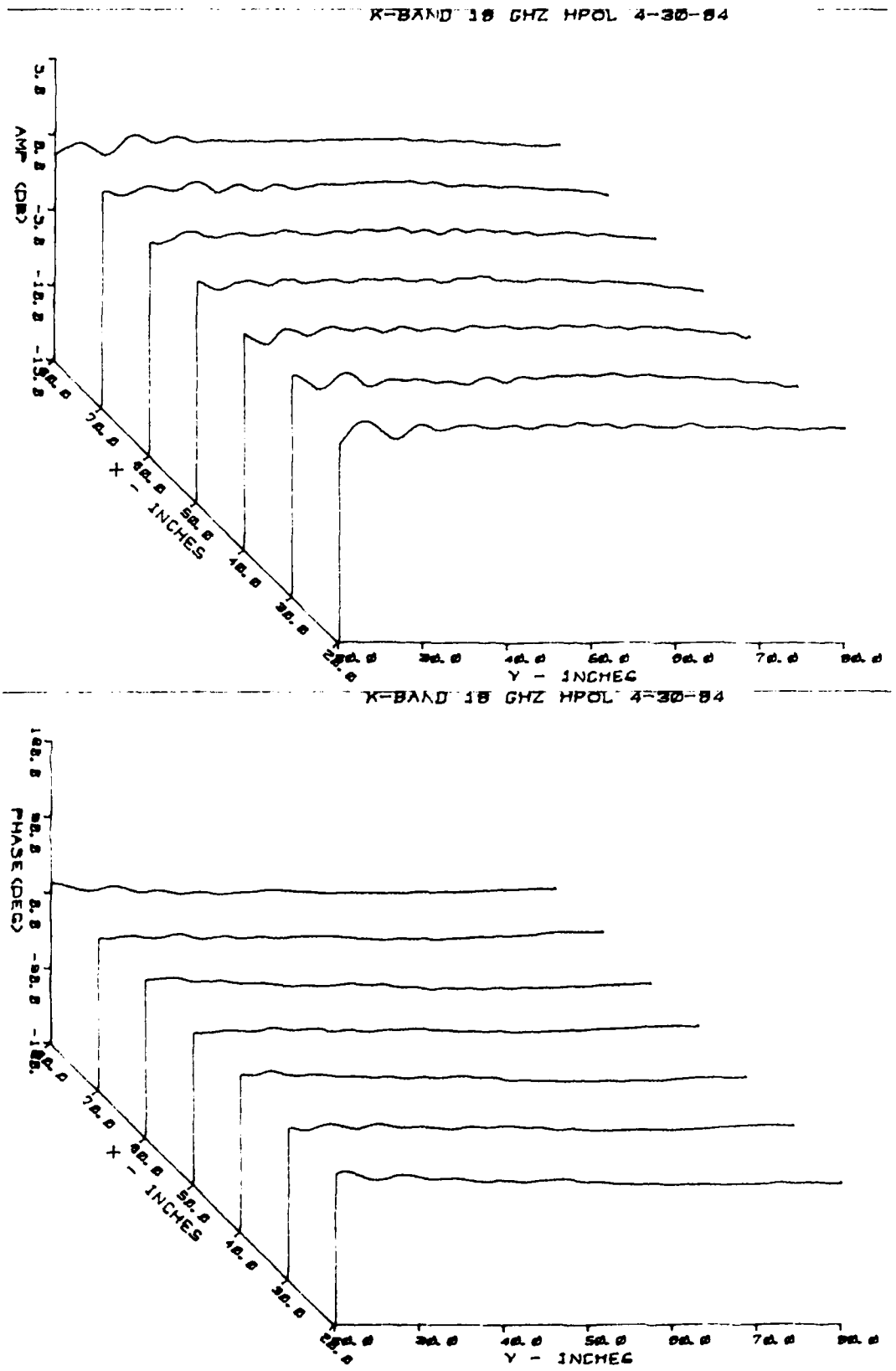


Figure A.60. 3D X-Plane Amplitude and Phase Field Probe Plot Taken at 18.0 GHz, H-Polarization, Using the Horn Probe

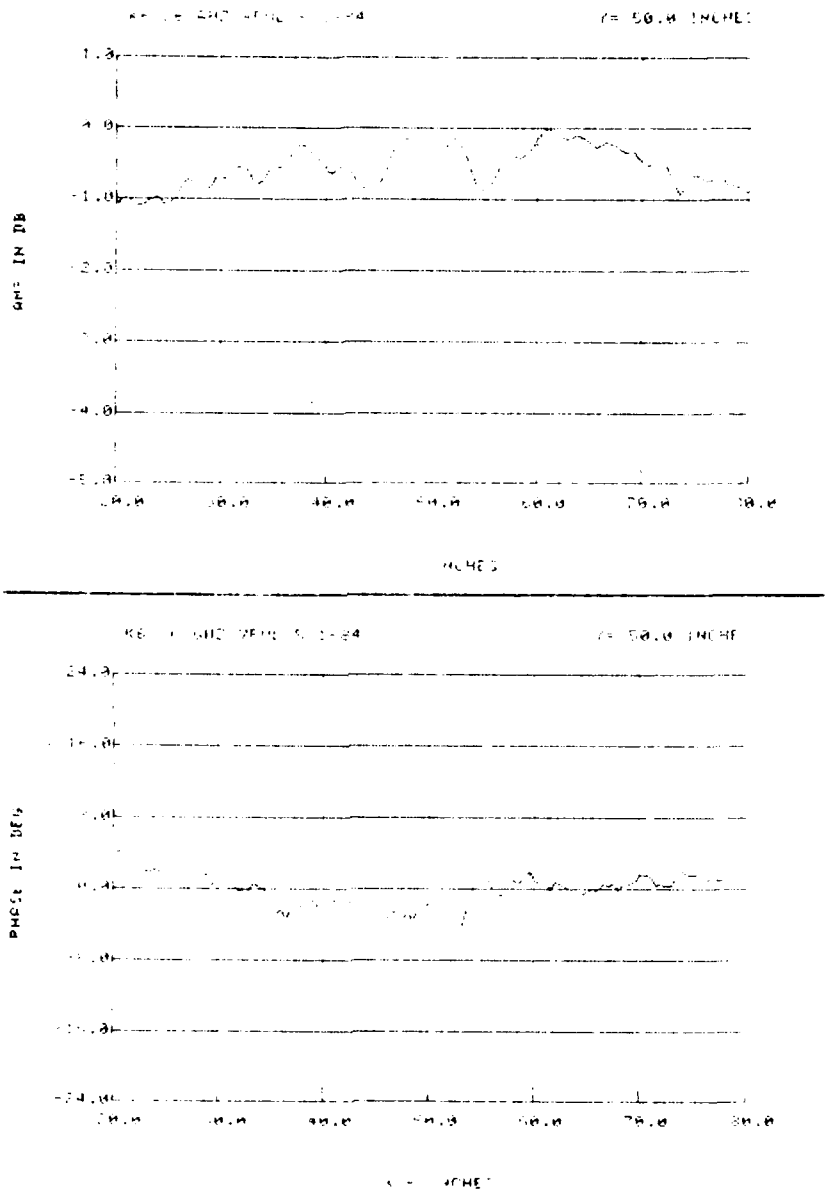


Figure A.61. X-Plane Amplitude and Phase Field Probe Plot Taken at 26.0 GHz, V-Polarization, Using the Horn Probe

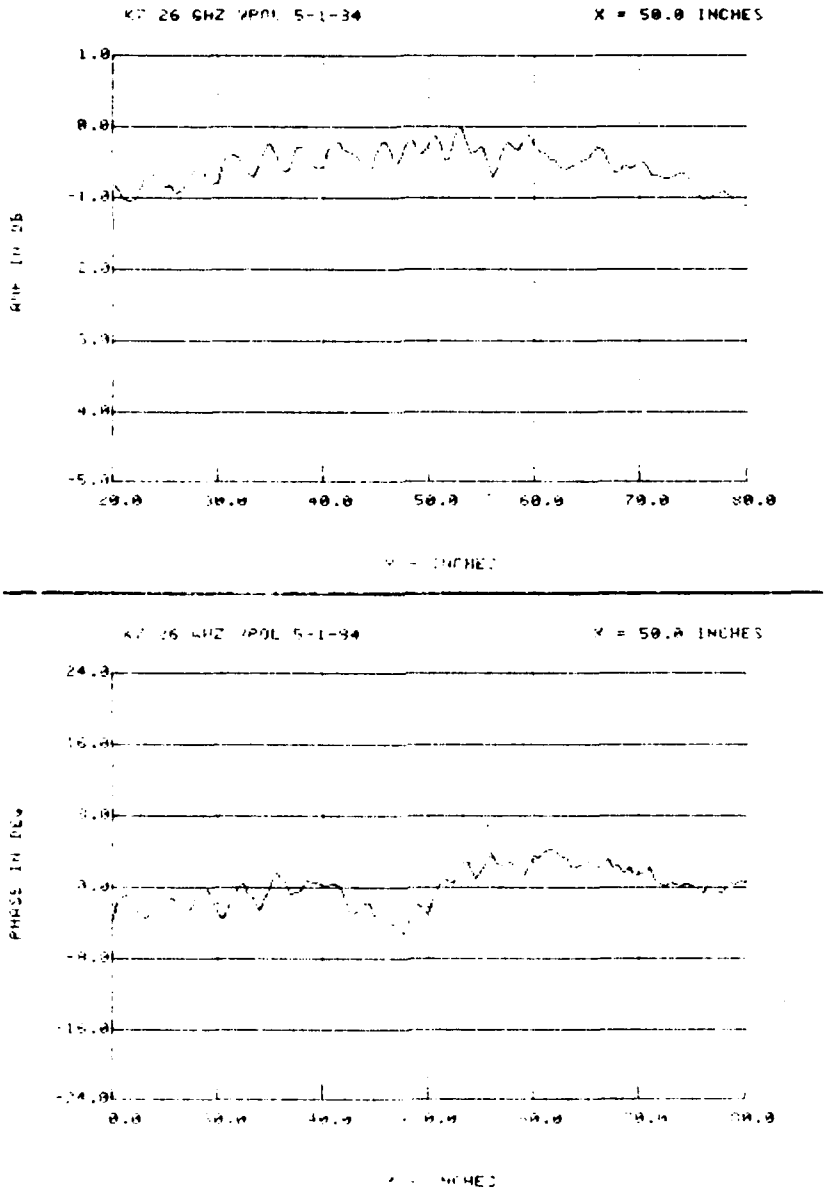


Figure A.62. Y-Plane Amplitude and Phase Field Probe Plot Taken at 26.0 GHz, V-Polarization, Using the Horn Probe

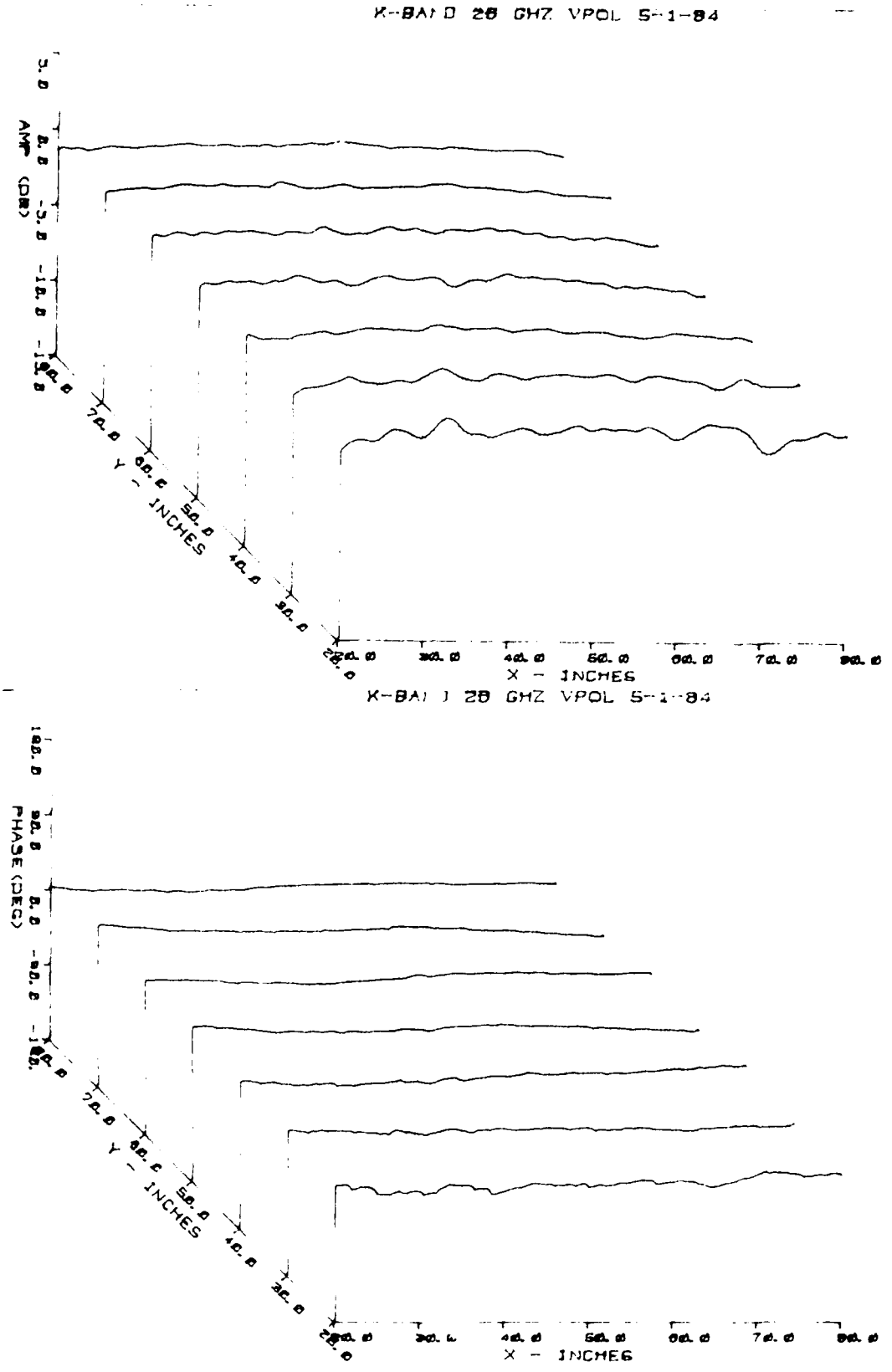


Figure A.63. 3D X-Plane Amplitude and Phase Field Probe Plot Taken at 26.0 GHz, V-Polarization, Using the Horn Probe

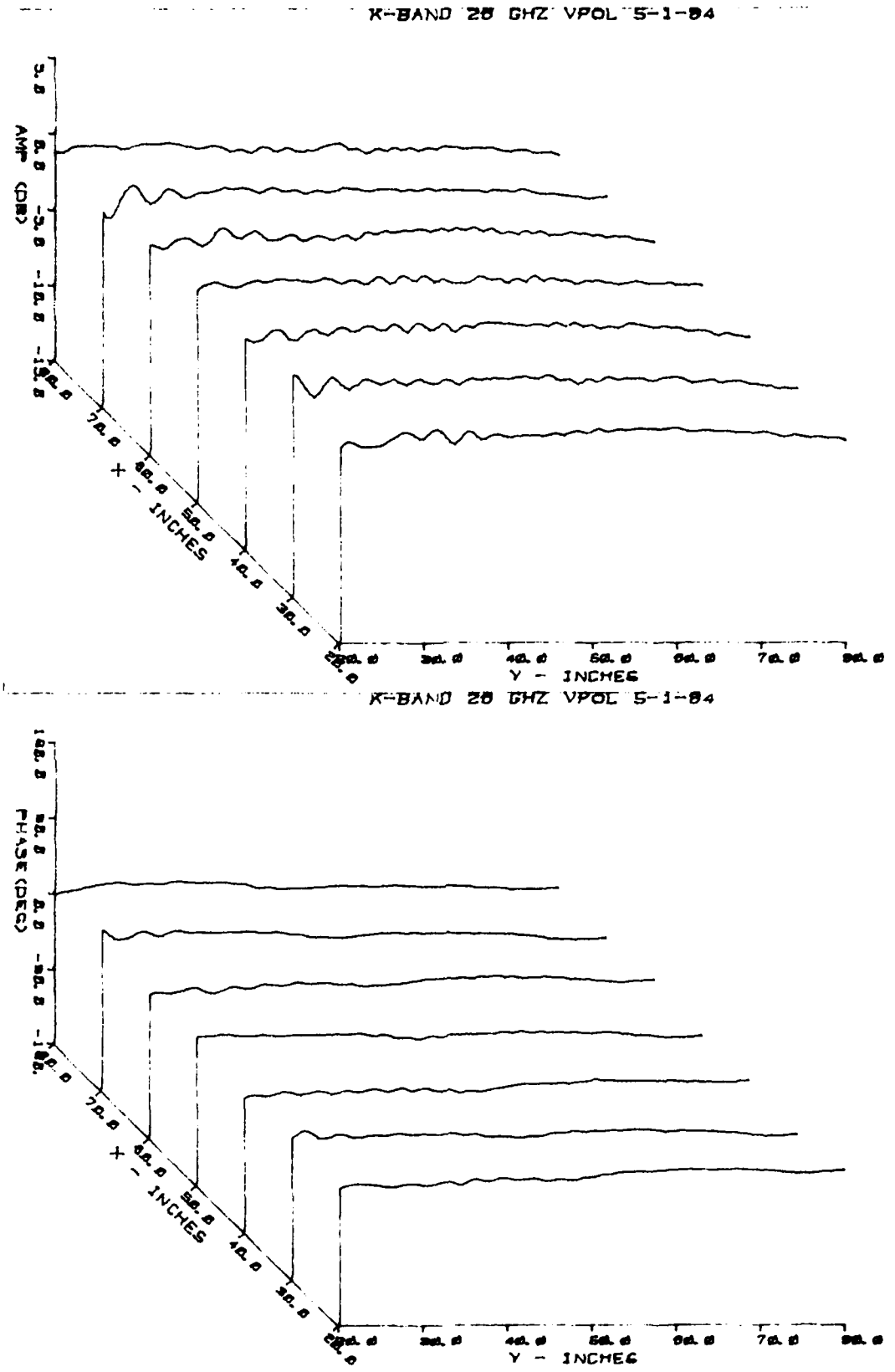


Figure A.64. 3D Y-Plane Amplitude and Phase Field Probe Plot Taken at 26.0 GHz, V-Polarization, Using the Horn Probe

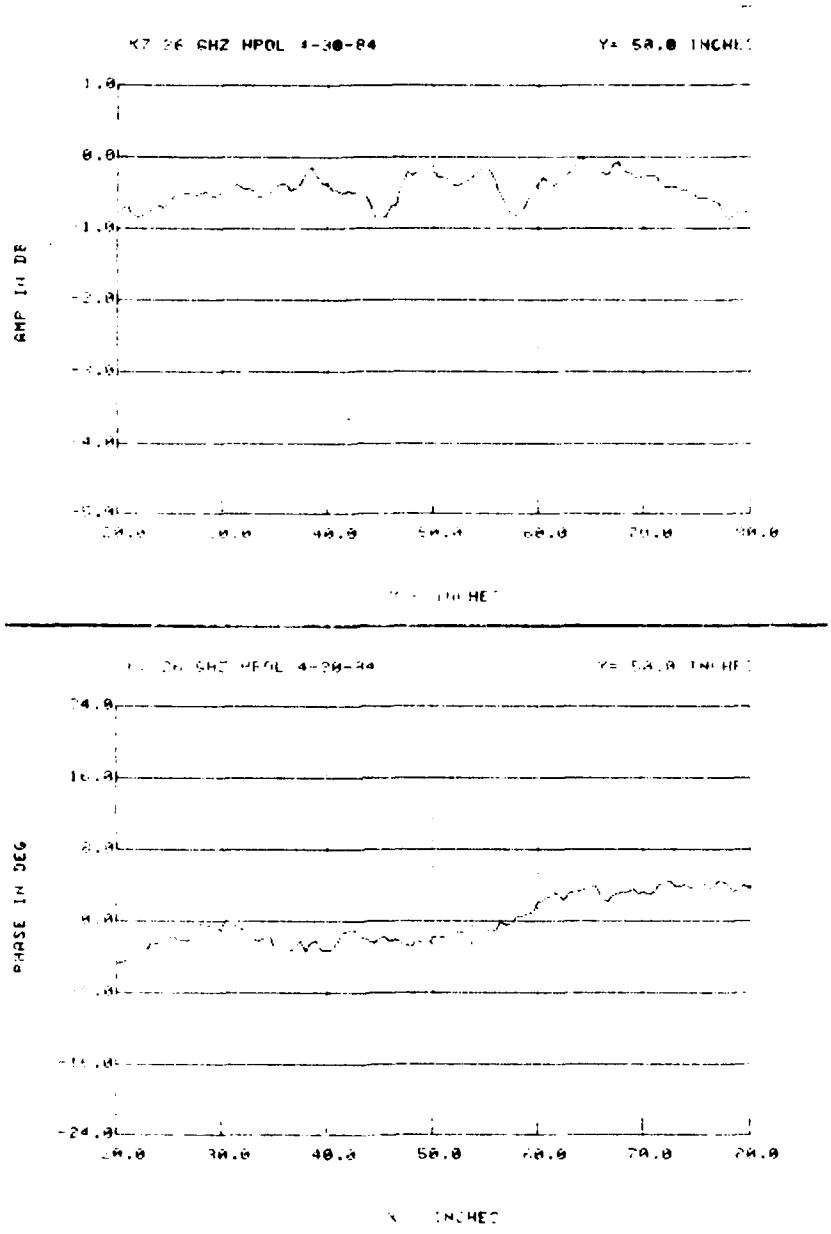


Figure A.65. X-Plane Amplitude and Phase Field Probe Plot Taken at 26.0 GHz, H-Polarization, Using the Horn Probe

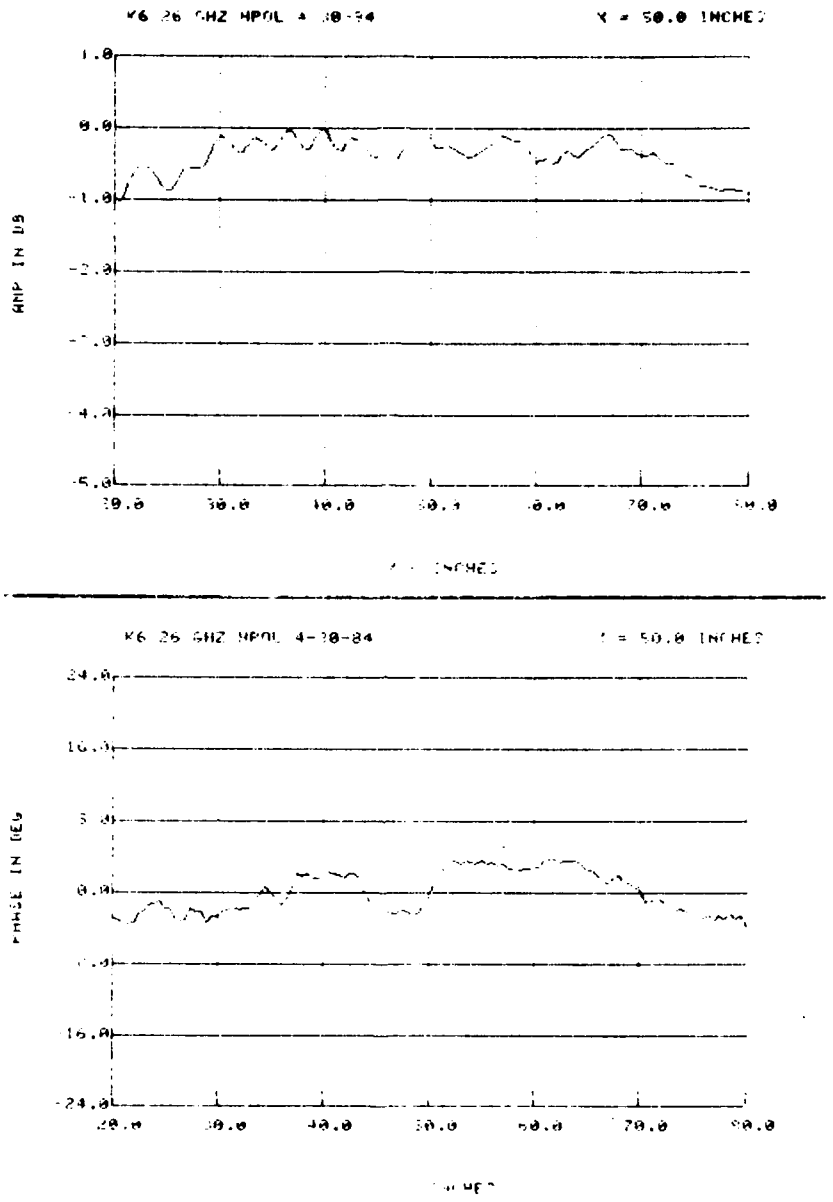


Figure A.66. Y-Plane Amplitude and Phase Field Probe Plot Taken at 26.0 GHz, H-Polarization, Using the Horn Probe

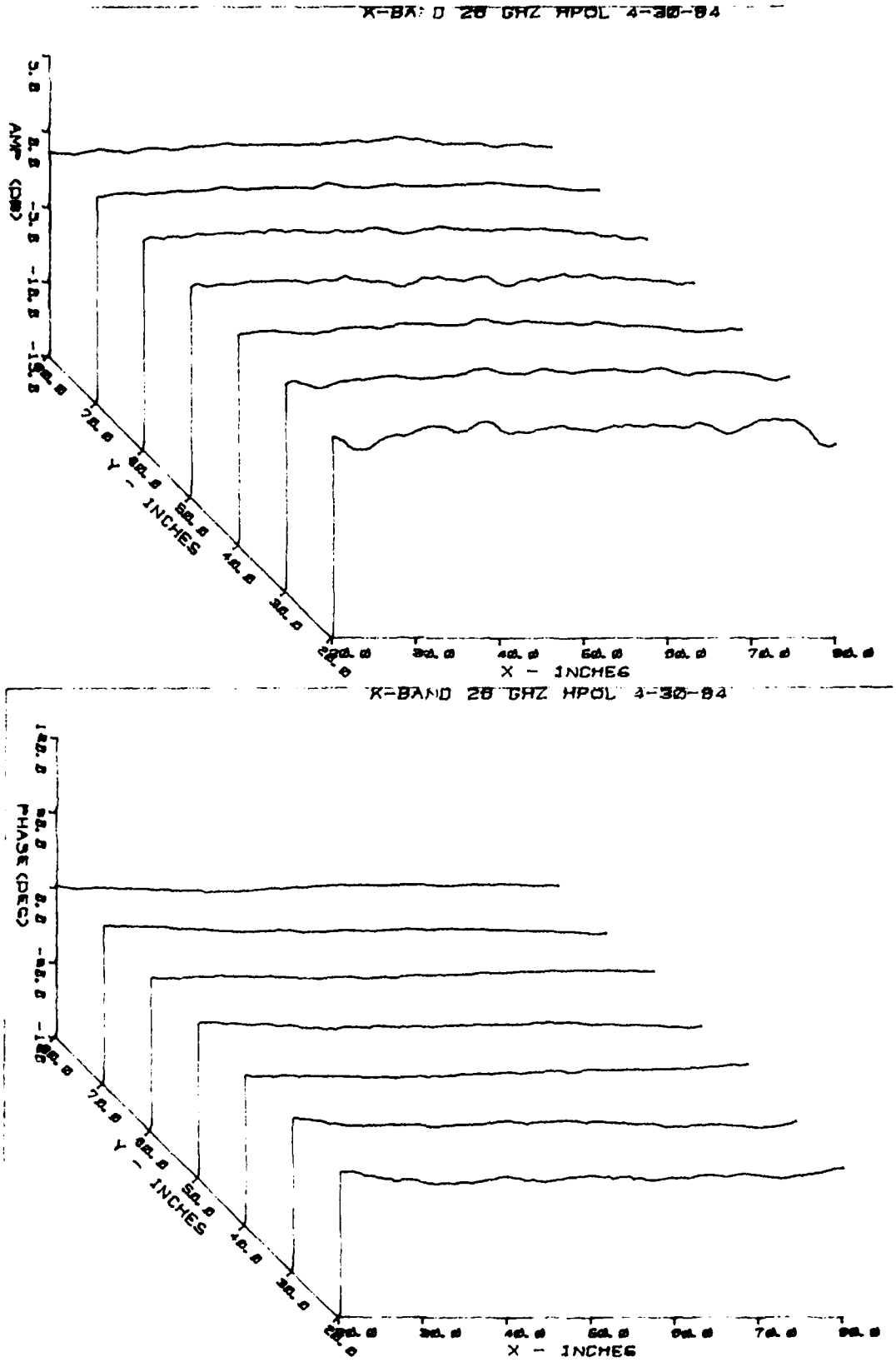


Figure A.67. 3D X-Plane Amplitude and Phase Field Probe Plot Taken at 26.0 GHz, H-Polarization, Using the Horn Probe

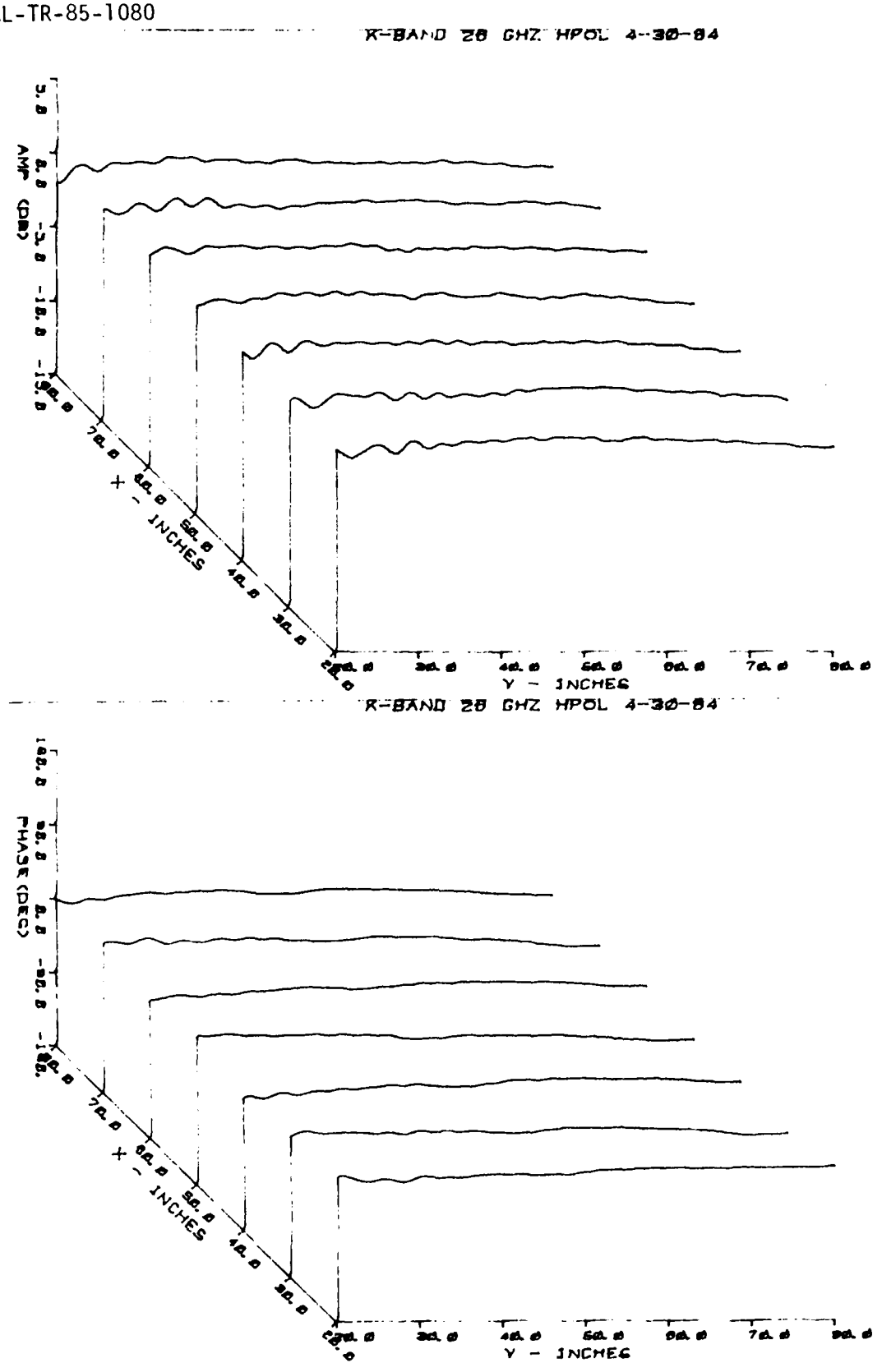


Figure A.68. 3D Y-Plane Amplitude and Phase Field Probe Plot Taken at 26.0 GHz, H-Polarization, Using the Horn Probe

U.S.Government Printing Office: 1986 — 646-067/40703

DTIC

FILMED

4-86

END